NASA - GEORGE C. MARSHALL SPACE FLIGHT CENTER

Technical Memorandum X-53565

January 13, 1967

THE INFLUENTIAL ASPECTS OF ATMOSPHERIC DISTURBANCES ON SPACE VEHICLE DESIGN USING STATISTICAL APPROACHES FOR ANALYSIS

by

Robert S. Ryan and Alberta W. King

DYNAMICS ANALYSIS BRANCH
DYNAMICS AND FLIGHT MECHANICS DIVISION
AERO-ASTRODYNAMICS LABORATORY
RESEARCH AND DEVELOPMENT OPERATIONS

NASA - GEORGE C. MARSHALL SPACE FLIGHT CENTER

Technical Memorandum X-53565

January 13, 1967

THE INFLUENTIAL ASPECTS OF ATMOSPHERIC DISTURBANCES ON SPACE VEHICLE DESIGN USING STATISTICAL APPROACHES FOR ANALYSIS

by

Robert S. Ryan and Alberta W. King

DYNAMICS ANALYSIS BRANCH
DYNAMICS AND FLIGHT MECHANICS DIVISION
AERO-ASTRODYNAMICS LABORATORY
RESEARCH AND DEVELOPMENT OPERATIONS

TECHNICAL MEMORANDUM X-53565

THE INFLUENTIAL ASPECTS OF ATMOSPHERIC DISTURBANCES ON SPACE VEHICLE DESIGN USING STATISTICAL APPROACHES FOR ANALYSIS

by

Robert S. Ryan and Alberta W. King

George C. Marshall Space Flight Center

Huntsville, Alabama

ABSTRACT

The influential aspects of various wind profile disturbances on the dynamic response of the vehicle are considered. Particular emphasis is given to separating the influence of wind shears, turbulence and quasi-steady wind speed on the dynamic response during the boost phase of flight. Four hundred and seven individual detailed (Jimsphere) wind profiles are the primary wind inputs, although the MSFC synthetic profile is also discussed. The time response to each profile is run and a statistical analysis made. Severe profiles are ranked in terms of the bending moment at two vehicle stations for the Saturn V vehicle. The influence of results on vehicle design and flight operational procedures is determined.

NASA - GEORGE C. MARSHALL SPACE FLIGHT CENTER

TABLE OF CONTENTS

LIST OF ILLUSTRATIONS

LIST OF ILLUSTRATIONS (Continued)

LIST OF ILLUSTRATIONS (Continued)

LIST OF ILLUSTRATIONS (Continued)

LIST OF ILLUSTRATIONS (Continued)

TECHNICAL MEMORANDUM X-53565

THE INFLUENTIAL ASPECTS OF ATMOSPHERIC DISTURBANCES ON SPACE VEHICLE DESIGN USING STATISTICAL APPROACHES FOR ANALYSIS

SUMMARY

The influential aspects of various wind profile disturbances on the dynamic response of the vehicle are considered. Particular emphasis is given to separating the influence of wind shears, turbulence and quasi-steady wind speed on the dynamic response during the boost phase of flight. Four hundred and seven individual detailed (Jimsphere) wind profiles are the primary wind inputs, although the MSFC synthetic profile is also discussed. The time response to each profile is run and a statistical analysis made. Severe profiles are ranked in terms of the bending moment at two vehicle stations for the Saturn V vehicle. The influence of results on vehicle design and flight operational procedures is determined.

I. INTRODUCTION

Launch vehicle design and flight operation procedures are dictated by many exterior disturbances and flight constraints. A major disturbance occurs for launch vehicles in space shots because, in general, they experience maximum dynamic pressure during an altitude of high wind velocity and turbulence. Thus, inflight atmospheric winds become a major consideration in vehicle design and operation. The problems to be considered because of these disturbances are (1) structural design, (2) control system design, (3) slosh baffle design, and (4) operational procedures such as wind restrictions, trajectory biasing, and prelaunch monitoring.

These definitions are complicated by the unpredictability of the vehicle characteristics, which requires statistical design studies based on a 3σ variation of appropriate parameters. Statistics of the wind input increase the study efforts as attempts are made to define the wind components (speed, shear, gust) and their influence. Previously, the MSFC synthetic wind profile has been used for this definition. Although it is a simple input to use, there is a shortage of real information on the effects of various wind components on vehicle response. In some cases, misleading information has been obtained through misuse of the approach. For example, the use of load relief using body-fixed

accelerometers showed a 20 percent reduction in bending moment when control system gains were programmed using the synthetic profile. Using many individual winds produced only a 7 percent reduction in moment for the same system. In attempts to overcome these problems many approaches have been used for wind definitions, vehicle models, and analysis. Although each of these have added information to overall vehicle response and wind interaction, they lack continuity and a clear base.

This study attempts to eliminate these basic shortcomings by using (1) an adequate vehicle model, (2) consistent wind inputs and turbulence definition, (3) accurate procedures for analysis, and (4) consistent criteria for evaluation of effects.

This study satisfies the vehicle model requirement by using a detailed mathematical model of the total vehicle dynamics including bending dynamics and propellant oscillations. To satisfy the wind field requirements, the individual wind profiles have been separated into low frequency components (magnitude) and high frequency components (turbulence). This results in three profiles, the unfiltered, filtered, and turbulence, for use in studying vehicle responses.

Solutions of the vehicle responses were obtained using the following three procedures: (1) numerical integration of the equations of motion, (2) analog computer solution, and (3) generalized harmonic analysis for the turbulence portion. Vehicle response is evaluated in terms of vehicle response parameters, angle of attack, engine deflection, bending moment, and unit compressive load.

The analysis shows that turbulence has a significant influence on the bending moment in areas where this moment is dominated by bending dynamics.

II. SIMULATION

A. Vehicle Model

A complete simulation of a launch vehicle during atmospheric flight requires the simultaneous generation of the trajectory, wind inputs, and vehicle dynamics. Since this much detailed simulation requires large amounts of computer time or excessive analog equipment, a complete simulation is impractical for general parameter studies. A simpler and more accurate approach can be used if it is assumed that the vehicle dynamics due to wind disturbances do not alter the trajectory. This assumption is good for the yaw plane. Under these conditions, the origin of the coordinate system is chosen to be at the undisturbed

vehicle center of gravity and its orientation along the tangent to the trajectory pointing in the direction of the nominal thrust vector. The translation of the coordinate system is eliminated by replacing it with an equivalent gravitational field. The slow rotation of the coordinate system following the trajectory is negligible. Since the vehicle is symmetrical, no cross-coupling between pitch and yaw planes is present; thus, the assumed yaw plane analysis is applicable (Figure 1).

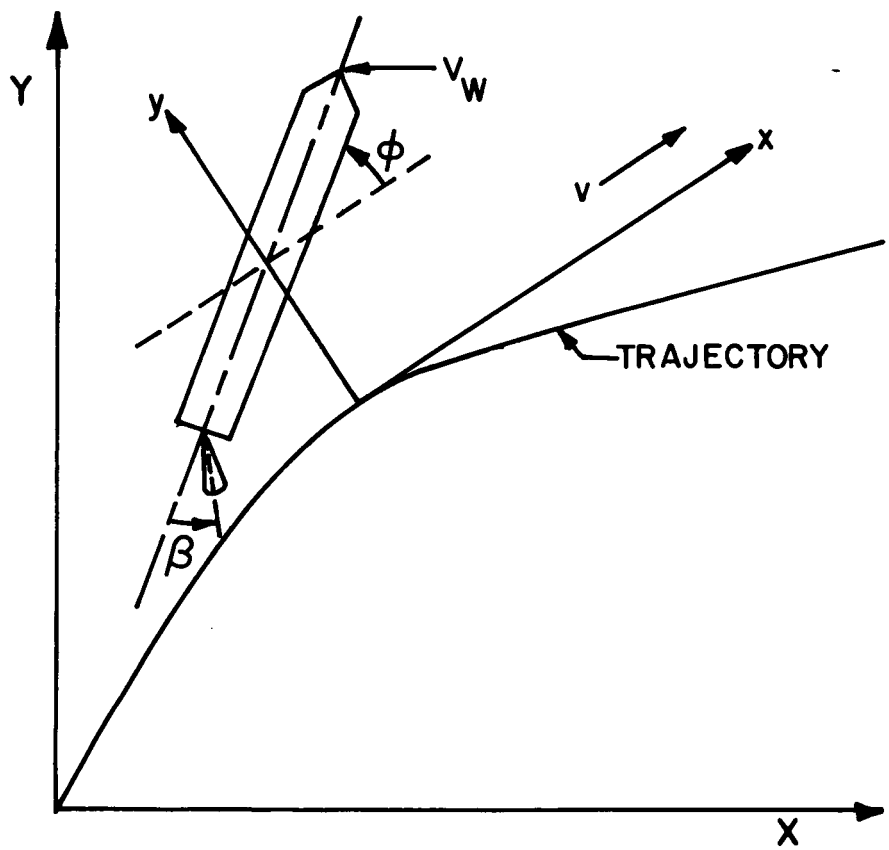

Figure 1. Coordinate System

Acting on the vehicle are aerodynamic, thrust, and control forces. The aerodynamic forces measured or calculated along the longitudinal vehicle axis, are quasi-steady, based on normal force distribution, and are considered to vary linearly with the local angle of attack. Because gust penetration and lift growth effects are small for Saturn V, they are neglected. The thrust force is provided by five liquid propellant engines, four of which swivel to provide the lateral control force, which is discussed in Section V.

The liquid propellant dynamics are represented by an equivalent mechanical model consisting of an assembly of springs, dashpots, masses, and inertial discs arranged in such a way as to represent dynamic behavior of the sloshing liquid (Figure 2). This model exactly duplicates the forces and moments determined from the hydrodynamical solution, and accurately reproduces the oscillating fluid insofar as the assumptions made for the hydrodynamic solutions are valid for an incompressible irrotational fluid with only small disturbances allowed. The effects of sloshing on bending (and vice versa), which are assumed to act through the slosh mass attack point and spring, should be accurate as long as local loads are of no concern.

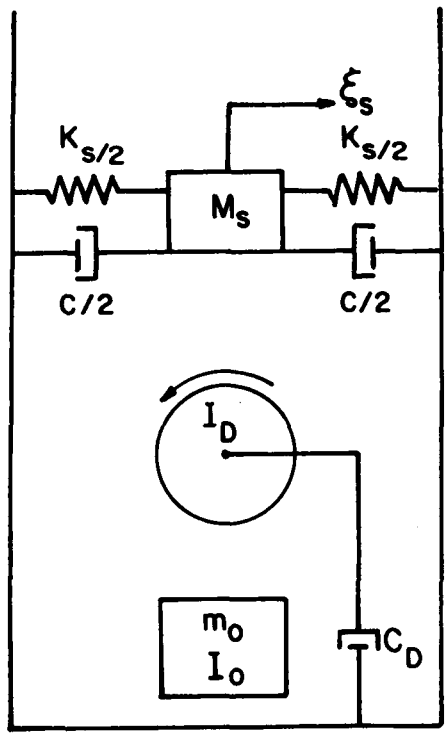

$$\omega_s^2 = \frac{\xi_n}{a_f}\,\bar{g}\,\tanh \xi_n \frac{h_f}{a_f}$$

$$M_s = \frac{2 \tanh \xi_n \frac{h_f}{a_f}}{\xi_n \frac{h_f}{a_f}\left(\xi_n^2 - 1\right)} M_f$$

Figure 2. Slosh Model

The bending effects of the launch vehicle structure are approximated by the superposition of several free-free normal mode shapes by

$$y(x,t) = \sum_{j=1}^{n} \eta_j(t)\, Y_j(x), \qquad (1)$$

which defines the displacement of the vehicle centerline (Figure 3). The normal modes are computed with the swiveling engine masses removed, but the liquid propellant mass is included. Control of the vehicle is maintained by swiveling the engines, using a hydraulic actuator for positioning. The actuator position is determined from a control law formulated to produce desired response and stability characteristics. The control law results from a proper choice of gains attached to the output signal from various control sensors, whose signals are summed and fed directly to the actuators (Figure 4).

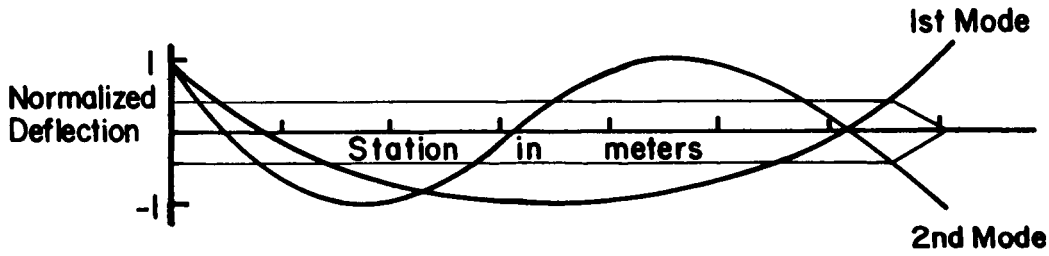

Figure 3. Bending Mode Deflection Curves

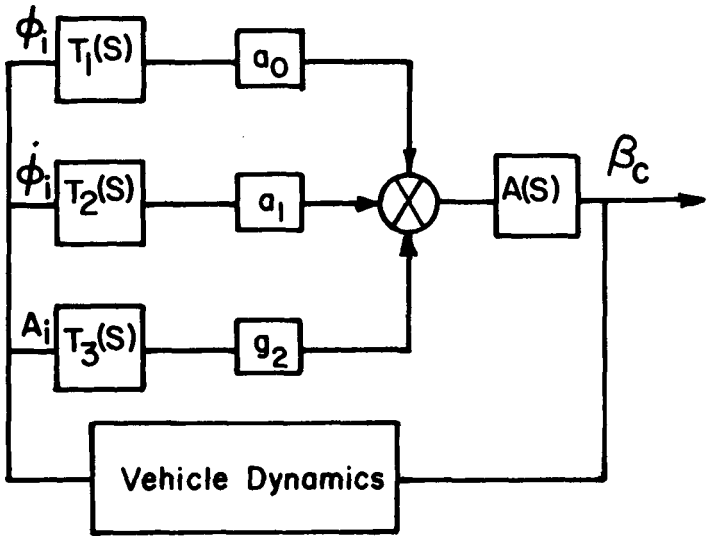

Figure 4. Block Diagram of Control System

The control system used in this analysis is defined by a control law, β_c, in the following manner:

$$\beta_c = a_o\, T_1(s)\, A(s)\, \varphi_i + a_1\, T_2(s)\, A(s)\, \dot{\varphi}_R + g_2\, T_3(s)\, A(s)\, A_i, \qquad (2)$$

where

φ_i is the indicated position error

$\dot{\varphi}_R$ is the indicated position rate, and

A_i is the indicated normal acceleration.

The symbols a_o, a_1, and g_2, represent the control gains for these sensors. The $T_i(s)$ $(i = 1, 2, 3)$ are transfer functions which describe the characteristics of various networks designed for stability purposes, and A(s) is the transfer function which describes the engine actuator characteristics. The transfer functions used in this study are as follows:

Gyro = 1

Rate = $1/(1 + B_1 s + B_2 s^2)$

Accelerometer = $1/(1 + 20s)$.

Both an attitude-only and a body-fixed accelerometer system are studied. The attitude-only system occurs when g_2 is set equal to zero in the control system equation and appropriate networks $T_1(s)$ and $T_2(s)$ inserted. Varying g_2 allows other systems to be studied.

Based on the assumptions given above for the coordinate system, forces, propellant and bending dynamics, and control system, the equations of motion are derived for the Saturn V launch vehicle (Figure 5).

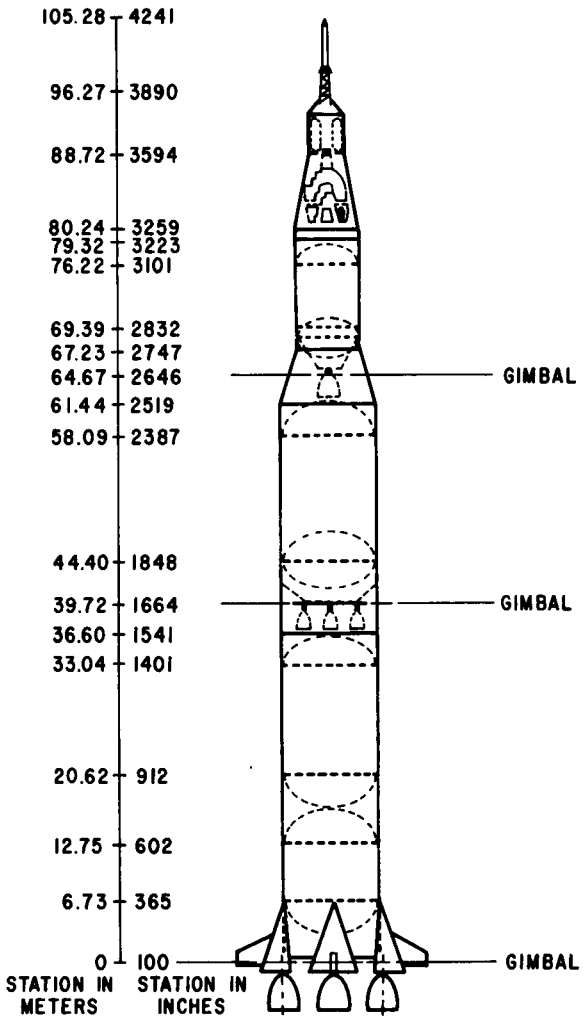

Figure 5. Saturn V Vehicle Configuration

The model used in this analysis includes the following:

(1) rigid body translation (y)

(2) rigid body rotation (φ)

(3) engine compliance mode (β_E)

(4) sensor dynamics ($\dot{\varphi}_R$, A_i)

(5) three propellant oscillation modes (tanks) (ξ_s)

(6) two elastic body modes (η_i)

(7) control (β_c).

The differential equations describing the system are listed in the appendix.

B. Load Indicator

The total load due to all forces acting on the vehicle structure is a direct output of the simulation. This load indicator can be calculated directly during simulation as either the lateral bending moment or unit compressive and tension loads. A direct calculation of the load indicator in this fashion insures correct phasing of all interacting responses and the vehicle control system. The bending moment or unit compressive load results from inertial forces, aerodynamic forces, and engine side forces, and can be used as the load indicator. The bending moment equation is

$$M_B(x) = \bar{M}'_\alpha(x)\,\alpha(t) + \bar{M}'_\beta(x)\,\beta(t) + \bar{M}'_{\ddot{y}}(x)\,\ddot{y}(t) + \bar{M}'_{\ddot{\varphi}}(x)\,\ddot{\varphi}(t) + \bar{M}'_{\dot{\varphi}}(x)\,\dot{\varphi}(t)$$

$$+ \sum_{j=1}^{n} \bar{M}'_{\eta_j}(x)\;\eta_j(t) + \sum_{j=1}^{n} \bar{M}'_{\dot{\eta}_j}(x)\,\dot{\eta}_j(t) + \sum_{j=1}^{n} \bar{M}'_{\ddot{\eta}_j}(x)\,\ddot{\eta}_j(t)$$

$$+ \sum_{s=1}^{3} \bar{M}'_{\ddot{\xi}_s}(x)\,\ddot{\xi}_s(t). \qquad (3)$$

If terms of small magnitude, η_j, $\dot{\eta}_j$, $\dot{\varphi}$, are neglected and if substitution is made for translational and rotational acceleration in terms of their source, this equation can be simplified [1]. Since the

major causes of these accelerations are aerodynamic and control forces, the translational acceleration can be expressed as

$$\ddot{y} = \ddot{y}_{aero} + \ddot{y}_{control} = \frac{\partial \ddot{y}}{\partial \alpha}\alpha + \frac{\partial \ddot{y}}{\partial \beta}\beta. \tag{4}$$

A similar expression for the rotational acceleration is

$$\ddot{\varphi} = \ddot{\varphi}_{aero} + \ddot{\varphi}_{control} = \frac{\partial \ddot{\varphi}}{\partial \alpha}\alpha + \frac{\partial \ddot{\varphi}}{\partial \beta}\beta. \tag{5}$$

Substituting these expressions into the bending moment equation results in a simplified expression:

$$M_B(x) = \overbrace{M'_\alpha(x)\ \alpha(t) + M'_\beta(x)\ \beta(t)}^{\text{Rigid}} + \overbrace{\sum_{j=1}^{n} M'_{\ddot{\eta}_j}(x)\ \ddot{\eta}_j(t)}^{\text{Bending Dynamics}}$$

$$+ \overbrace{\sum_{s=1}^{m} M'_{\ddot{\xi}_s}(x)\ \ddot{\xi}_s(t)}^{\text{Sloshing Dynamics}} . \tag{6}$$

In this form, various effects of the bending moment can be completely separated. A typical set of the bending moment coefficients is shown in Figures 6 and 7.

The total unit compressive load, N_c, is a more comprehensive load indicator. The equation for the total load at an unpressurized section is as follows:

$$N_c(x) = \frac{F(t)\ \bar{m}(x,t)}{m(t)\ \pi D(x)} + \frac{X(x,t)}{\pi D(x)}\left(1 - \frac{\bar{m}(x,t)}{m(t)}\right) + \frac{4M_B(x,t)}{\pi D^2(x)}, \tag{7}$$

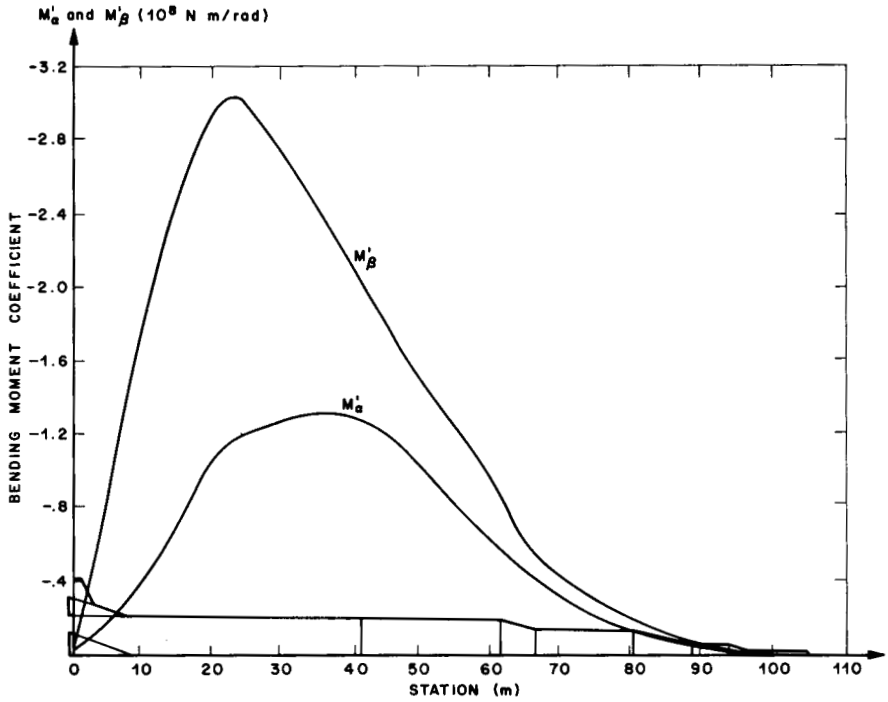

Figure 6. Rigid Body Bending Moment Coefficient vs Vehicle Station

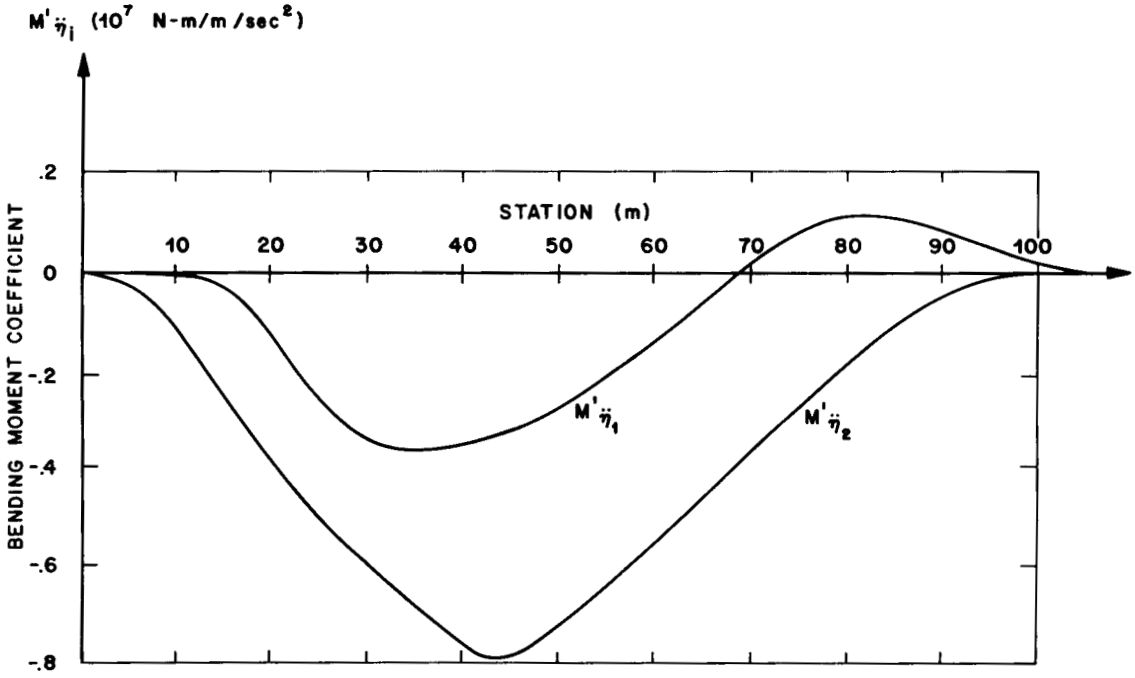

Figure 7. Elastic Body Bending Moment Coefficients vs Vehicle Station

where

F/m is the longitudinal acceleration,

$\bar{m}$ is the mass supported above the station of concern,

X is the aerodynamic drag,

M_B is the vehicle bending moment, and

D(x) is the local vehicle diameter.

Both the bending moment and the total load separate the various effects that create the vehicle loads, and thereby give insight into the details.

III. WIND INPUTS

Wind inputs used in the analysis were (1) an ensemble of 407 individual detailed profiles, (2) spectrum of wind turbulence, and (3) discrete synthetic profiles.

A. Measured Profiles

The individual wind profiles used in this study were measured at the Eastern Test Range, Florida, by the FPS-16 radar/Jimsphere method [2]. Four hundred and seven wind profile measurements taken over a period of a year were distributed fairly evenly throughout the entire period. Therefore, the data should not exhibit a seasonal or monthly bias.

Since this study is concerned with the relative influence between small scale motions (turbulence) and base scale wind effects (wind magnitude and shear), it is of interest to know the accuracy and resolution of the data. The RMS errors, determined by comparing simultaneous tracks of the same balloon for wind speed, are approximately 0.2 to 0.3 meters per second, and about one degree in wind direction. The RMS amplitudes of the small scale motions associated with individual profiles range up to about thirty times this magnitude [3,4]. The method chosen to reduce the data used a first degree equation to smooth the position coordinates. Average wind speeds were computed for approximately 50-meter layers and printed out at 25-meter altitude intervals, thus providing information on the small scale motion as well as the gross motion.

The measured wind profiles used in this report are adequate for most large space vehicle design and operational studies. The problem is incorporating the winds in the vehicle response studies and interpreting the data. To compute the responses of a space vehicle to a slowly changing wind field (quasi-steady-state) as it ascends through the atmosphere is a well-documented and reasonably straightforward procedure for the rigid body, and the problem is not too complicated for elastic vehicles. In the real case, where an elastic vehicle with several degrees of freedom must be considered and the total wind profile may be thought of as being composed of a quasi-steady-state with superimposed turbulence, the problem of computing vehicle responses becomes more difficult. In performing flight simulations, one of the major problems is how to treat the small scale motions (turbulence).

An attempt has been made to define gusts (turbulence) in a meaningful way by separating a detailed wind velocity profile into two profiles on the basis of frequency content. The basic profile represents the total wind field, the filtered profile represents the quasi-steady-state wind speeds, and the difference between these two represents gust or turbulence. The wind content to be filtered out of the total wind profile is determined by considering the relationships between the rawinsonde and the FPS-16 radar/Jimsphere profiles plus frequency response characteristics of the vehicle to be used (in our case, the Saturn V). The statistical properties of the gust profile, such as normality and stationarity, were also considered. A filter function is defined so that the resulting filtered profile approximates the rawinsonde-measured profile. The filter function used in this study is shown in Figure 8 as a function of gust wave length [5].

The separated gust or turbulence profile contains frequencies that cover the whole frequency spectrum of the elastic vehicle. The statistical distribution of the gusts is approximately Gaussian, enhancing interpretation of the vehicle responses, and also providing a basis for assessing the influence of gusts on the vehicle which are not measured by the rawinsonde method.

If the quasi-steady-state is defined as the wind profile approximating the rawinsonde-measured profile, the small scale motions are still nonstationary with altitude [6] because the variance of the small scale motions, as computed over limited altitude intervals, changes by a significant magnitude within the same velocity profile.

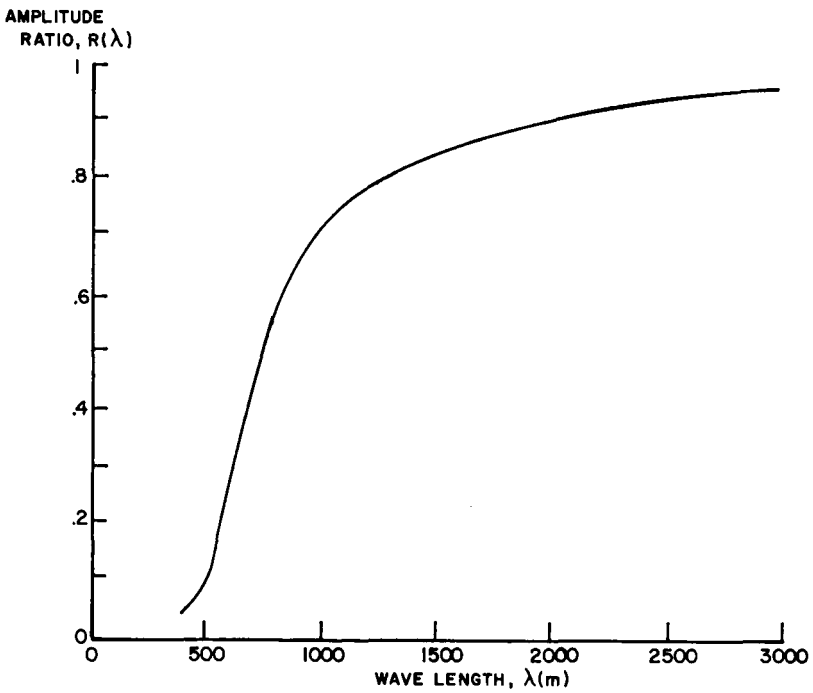

Figure 8. Approximate Response Function for Rawinsonde (GMD-18) System Based on Standard Rawinsonde Reduction Technique

Since the characteristics of the small scale motions vary with altitude, synoptic conditions, etc., a spectrum of the small scale motions over the entire altitude to, say, 14 kilometers may not be representative of the spectrum over a subinterval of this altitude range. Since, in designing and operating space vehicles, the peak responses are of the most interest, it is desirable to define a spectrum of small scale motions which could be superimposed on the quasi-steady-state wind profile to produce a peak vehicle response equivalent to that obtained from the total wind profile.

An attempt was made to define a spectrum of the small scale motions which could be superimposed on the quasi-steady-state profile to give the same variance and peak responses as the total profile. The spectrum was computed from approximately 400 detailed wind profile measurements by computing the spectra associated with each profile, then determining the probabilities of spectral density as a function of frequency. Thus, the spectra represent envelopes of spectral density for the given probability level.

For a linear system the peak responses due to the small scale motions will be given approximately by 3σ, where σ is the standard deviation of the output parameter. This 3σ value of the response is then added to the quasi-steady-state value of the response to obtain the total response.

Spectra associated with the scalar wind speed profiles were computed and used in this analysis. The following is a plot of the spectrum used (Figure 9). This spectrum, which was computed by determining

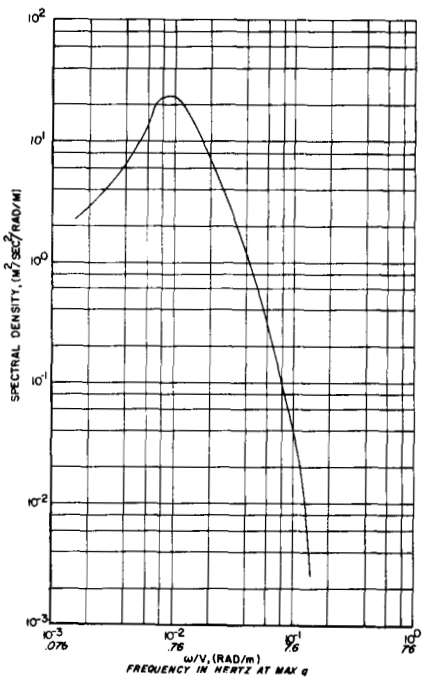

Figure 9. Spectral Density for Maximum Dynamic Pressure Region

the average spectral density as a function of frequency, has been transferred from wave numbers to frequency in vehicle flight time near the maximum dynamic pressure region. The spectrum associated with each profile was computed over the entire altitude range of the data and used as input in computing vehicle responses.

B. Synthetic Profiles

A synthetic profile is one which is representative of any measured profile or statistically designed profile and is usually determined from quasi-steady-state wind speeds, wind shears, and gusts which are combined to represent physically reasonable conditions to insure a high probability of success when the vehicle is launched.

They are constructed by defining the quasi-steady-state wind profile envelope that is not exceeded more than, for example, 5 percent of the time during some reference period, then defining a wind buildup rate whose envelope is not exceeded more than, say, 1 percent of the time, and combining these in a suitable way [6]. Gusts are then combined with the steady-state wind speed envelope. An idealized quasi-steady-state wind speed envelope representing the 95 percent probability of occurrence using a monthly reference period is shown in Figure 10, where the gust (Figure 11) is superimposed to represent the small scale motions. Synthetic wind profiles were constructed using a 95 percent wind speed and a 99 percent wind shear value. Envelopes of the 99 percent wind shear for various scales of distance are shown in Figure 12. To construct the synthetic profile with gust, the 95 percent wind magnitude is used with a 99 percent gust and a shear reduced by 15 percent. These profiles were used as an additional wind input (see Figure 13).

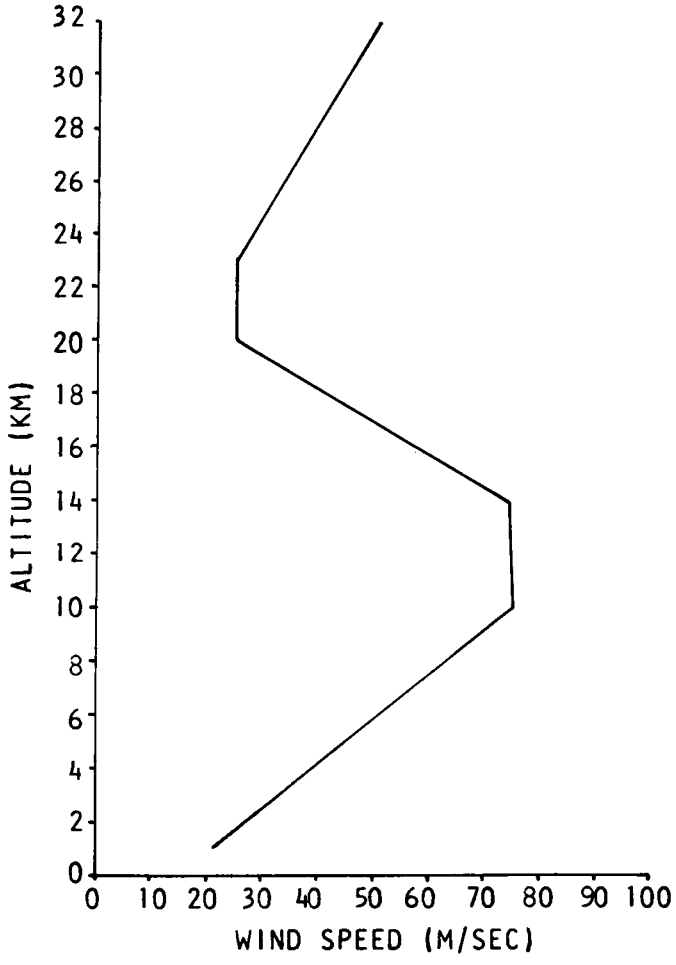

Figure 10. Wind Speed Envelope vs Altitude

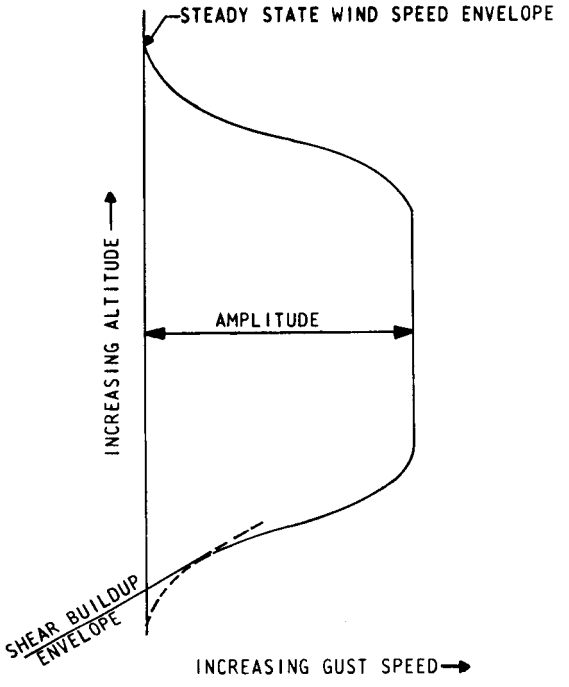

Figure 11. Wind Gust

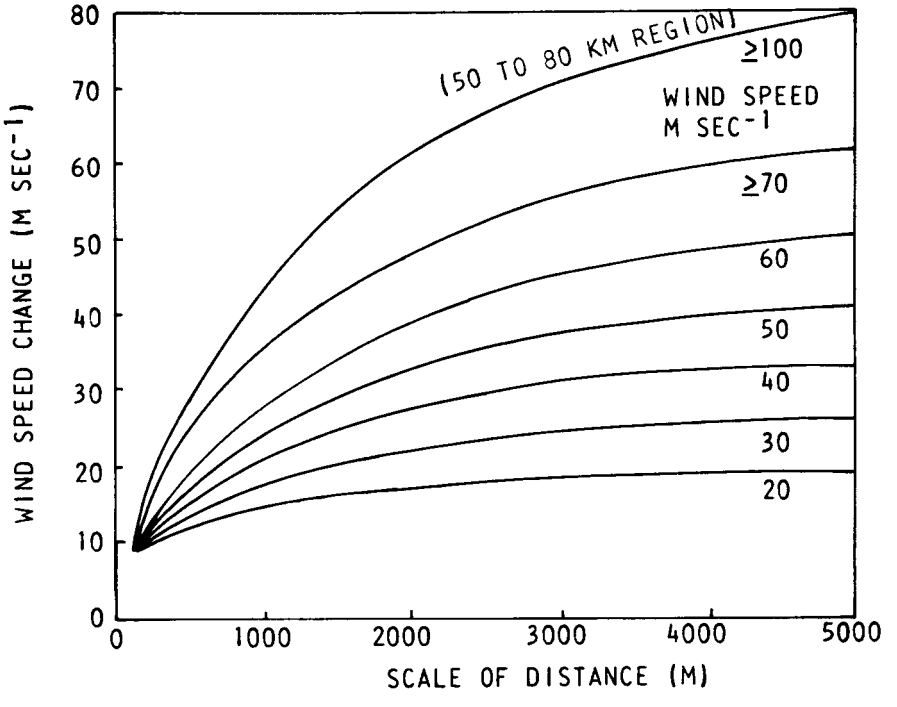

Figure 12. Envelope of Wind Speed Change

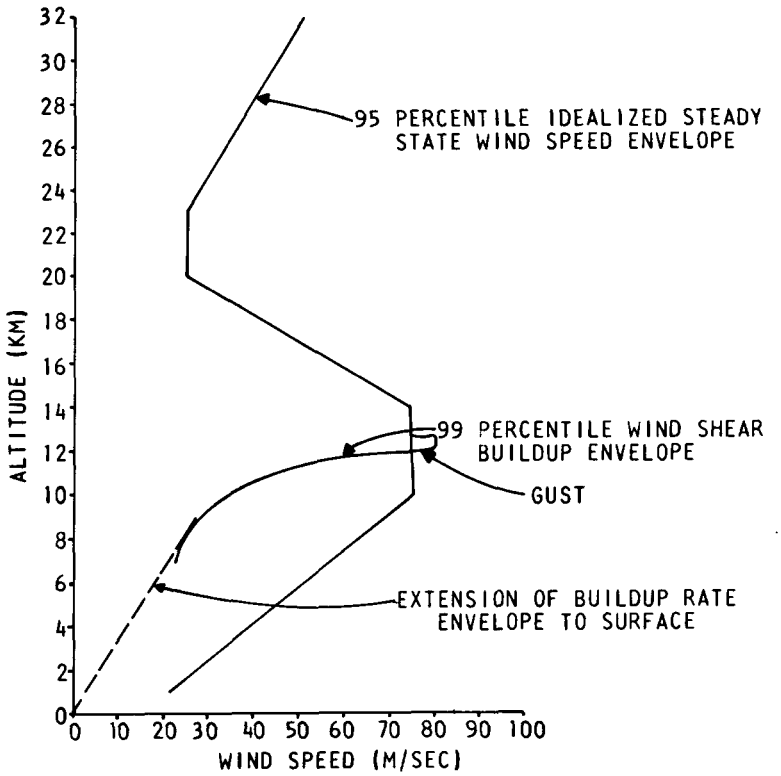

Figure 13. Synthetic Wind Profile with Gust

IV. PROCEDURES FOR ANALYSIS

Three approaches used for determining vehicle responses for atmospheric disturbances are (1) numerical integration of equations of motion on a digital computer, (2) integration of equations of motion on an analog computer, (3) generalized harmonic analysis using the spectrum of turbulence. The digital approach, because of its high accuracy, is used as a check against the analog computer. However, because of the large amount of machine time for each wind profile (40 minutes on the IBM 7094), only a few cases could be run economically. The GPS high speed analog computer is chosen as the basic method of evaluating the responses of many profiles because of the speed of output per trajectory run. The various computer capabilities are illustrated in Figure 14.

Four hundred and seven trajectory simulations of two minutes real time each can be made in about five minutes of computer time. By time transformation, the events on the computer take place up to 3000 times faster than real time. Since there is an integration factor of 3000 seconds with a maximum of 50 volts from the amplifiers in repetitive operation, theoretically up to 20 solutions could be obtained, during one

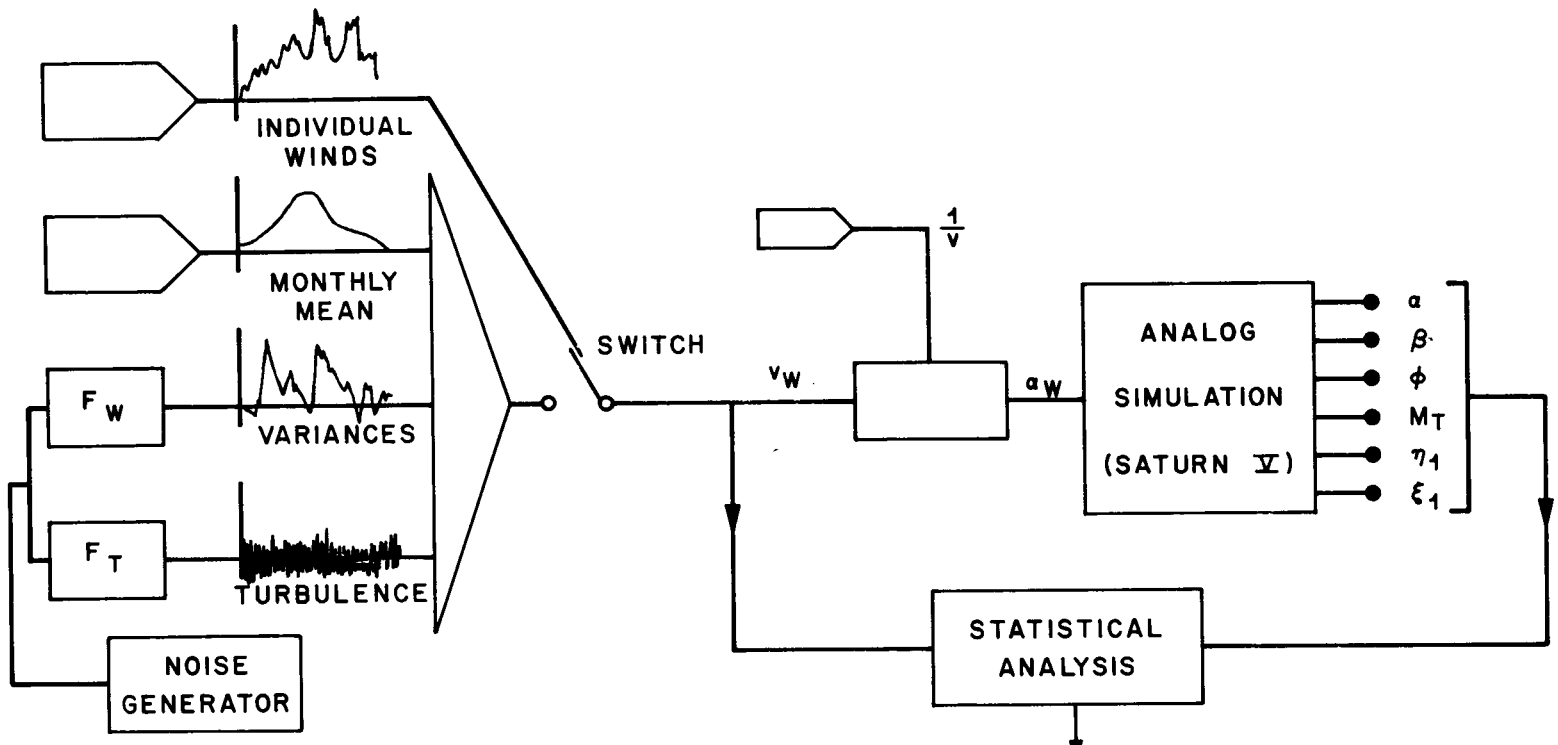

$$F_W = \frac{K_W V^{3/2}}{(S + \zeta_2 \Omega_W V)(S^2 + 2\zeta_1 \Omega_W V S + \Omega_W^2 V^2)}$$

$$F_T = \frac{K_T V^{3/2}}{S^2 + 2\zeta_T V S + \Omega_T^2 V^2}$$

Figure 14. Schematic for the Analog Simulation of Wind Profiles

second, from take-off to cutoff of the launch stage. Scaling of the problem resulted in a running speed of about .001 real time.

The computer is composed of 50 integrators, 50 summing amplifiers, 350 coefficient potentiometers, 20 quarter-square multipliers, 15 function generators, and 70 amplifiers. Tape units are available for feeding information into the computer, fully synchronized with the vehicle simulation. Each tape contains seven tracks and is used for wind inputs. Solutions may also be recorded on these tapes [7].

The vehicle responses were statistically analyzed using several aspects of the computer's capability. The probability of exceeding a certain response level was obtained by setting a value on the desired response function, then counting the number of times the actual vehicle response exceeded this value in flying through the whole ensemble of winds individually. To determine the probability, only one exceedance per profile was counted and the probability determined by dividing the number of exceedances by the number of wind profiles. Changing the setting of the response for the counter, another point on the probability curve can be obtained. This process is repeated until the complete curve is obtained. The computer has the capability of counting exceedances on four variables simultaneously. The probability was determined for all vehicle responses for the unfiltered, filtered, and turbulence wind ensembles.

Statistical probability as a function of magnitude is determined by simulating the flight of the vehicle through all of the measured winds and counting the number of profiles in which the response exceeds a preset value. Establishment of the probability levels for any selected response parameter allows a ranking of the severity of the wind profiles. For detailed analysis, particularly interesting wind profiles may be captured on a recorder with closed-loop tape. By placing the computer in a repetitive mode of operation, this wind profile and its responses can be analyzed in any desired detail.

Additional statistical information can be obtained by computing the mean and variance of the ensemble at various flight times by sampling each profile and the resulting response at a specific flight time and computing the variance and mean from the relationships:

$$\bar{X} = \frac{1}{n} \sum_{i=1}^{n} X_i \tag{8}$$

$$\sigma^2 = \frac{1}{n - 1} \sum_{i=1}^{n} (X_i - \bar{X})^2. \tag{9}$$

Thus, the variance and mean can be plotted versus flight time.

Generalized harmonic analysis allows the statistical qualities of a vehicle response to be computed directly if certain restrictions, such as normality of the input force, are met. If one considers that the equations representing the dynamics of the vehicle are linear and that the coefficients are frozen over a certain altitude band, these conditions can basically be met. These conditions can be satisfied only for the wind turbulence. The output spectrum for this approach is

$$S_x(\omega) = |T_i(i\omega)|^2 S_{in}(\omega). \tag{10}$$

This expression shows that the spectral density $S_x(\omega)$ of the output of a linear dynamic system is equal to the product of the square of the modulus of its transfer function and the spectral density of the input. Other statistical quantities, exceedances and probability, can be calculated directly from the variance and standard deviation. These statistical values are computed for all vehicle responses for the spectrum of the wind turbulence. The 3σ standard deviation values of the responses were compared with results obtained from the turbulence ensemble (see table 1).

V. PARAMETERS FOR ASSESSMENT

The interpretation of a space vehicle's response to atmospheric disturbances is very complicated because of the interaction of the various components of the wind (magnitude, shear, gust), vehicle dynamics (rigid body, elastic body, propellant oscillations), and control system. The assessment of the various aspects of this interaction depends upon a choice of vehicle parameters and proper separation of the wind component influences versus vehicle dynamics and control. This is accomplished by appraisal of the various parameters necessary for evaluation of different types of space vehicles.

The evaluation of vehicle response to atmospheric disturbances cannot be generalized to one vehicle parameter. Neither can it be reduced to a few general studies. The many factors involved must be interpreted in terms of the current phases of the vehicle design. These various areas are categorized as (1) preliminary design, (2) final structural design, (3) guidance and control system design and optimization (preliminary and final), and (4) operational procedures.

In each of these design areas, two problems arise which must be correctly evaluated. The first deals with the consideration of the statistics of the predictability of the total vehicle characteristics, such as aerodynamic forces, structural weight characteristics, and thrust, and is not discussed in this paper. The second concerns the type of vehicle being studied. One type of vehicle is a highly accelerating, small vehicle that has, in general, a marginal control force availability. This control force arises from jet tab and air vanes. A typical vehicle in this class is the Pershing. Because of the high longitudinal acceleration and other structural design constraints, vehicles of this type have no structural load problem. In fact, the vehicle has more than an adequate structural margin for any anticipated wind loading. The overriding constraint placed on the vehicle is, therefore, from the control mechanism. The parameters for evaluating vehicle response to atmospheric disturbances naturally follow as deflection and deflection rates of the control devices.

Another type of vehicle, represented by Saturn V, goes to the opposite extreme. In this case, although adequate control force is available, the man-rating of the structural integrity, along with the optimization of all aspects of the vehicle design to maximum payload, forces the designer to consider as a primary concern the influence of wind on structural loads. These loads should be treated as unit compressive and tension loads. If shear forces are of significance, these must also be evaluated. Thus, consideration of optimizing the control system in terms of these structural loads forces the control system design engineer to consider all aspects of the vehicle design (control and structural) in a system analysis so that vehicle structural constraints are not violated. Vehicles optimized using this system approach have more operational flexibility because more severe trajectories can be flown without endangering the mission, and at the same time, more launch days are available since wind restrictions are not necessary.

Another type of vehicle is a combination of the above two, in that both a limited control force and restricted structural capability are available. The Saturn I typifies this group. In this case, a more detailed evaluation is necessary, since engine deflection, engine deflection rate, and the unit compressive and tension load must be monitored. Operational procedures become more complex since, in

general, wind biased trajectories must be flown. Also, a more comprehensive prelaunch wind monitoring and vehicle response to these winds must be conducted. Final flight decisions must be made in terms of these simulations and previously acquired knowledge of vehicle structural integrity, total dynamics, and wind statistics. In general, the influence of wind on design can be evaluated in light of the basic parameters presented. Two other areas of concern must be examined for final design assurance: The first is associated with the amplitude of propellant oscillation in a tank. In this case, oscillations must be controlled so that amplitudes do not cause an early cutoff (in case propellant level is used as criteria). Second, in achieving desired responses, stability margins of various vehicle modes may be deteriorated. In all cases, a trade-off must be made between desired response and desired stability boundaries. This trade-off can be made in terms of mission, probability of occurrences, etc.

One additional design problem arises in setting of abort limits for safety of the astronaut. In this case, the vehicle response to malfunctions must be studied for various wind inputs. The parameters for evaluation must become the output of the emergency detection sensors, such as rate gyros. The parameters necessary to evaluate a vehicle response is, therefore, a function of the design problem and the vehicle type. This study is not concerned with all these problems, but will concentrate on the structural sizing and control system optimization.

VI. FUNDAMENTALS

Although the vehicle reacts to a disturbance as a total system, simplifications can be made in representing the dynamics, if the elastic body frequencies are high. In this case, basic understanding and preliminary design values can be obtained by treating the rigid and elastic body separately.

A. Rigid Body

The representation of the vehicle response as a rigid body has basic application in preliminary design. Using this representation, in conjunction with 3σ variations of the vehicle parameters and a synthetic profile, allows the determination of basic response characteristics and preliminary sizing of the structure. This same simulation affords insight into the interaction of vehicle dynamics and control law so that guidelines for control system design can be determined.

The effect of the control law on response can be illustrated by the rigid body equations of motion:

$$\ddot{y} + K_1\varphi + K_2\alpha + K_3\beta = 0 \tag{11}$$

$$\ddot{\varphi} + c_1\alpha + c_2\beta = 0 \tag{12}$$

$$\alpha = \varphi - \frac{\dot{y}}{V} + \frac{V_w}{V} \tag{13}$$

$$M_B(x) = M'_\alpha(x)\ \alpha(t) + M'_\beta(x)\ \beta(t) \tag{14}$$

$$\beta = a_o\varphi + a_1\dot{\varphi} + b_o\alpha. \tag{15}$$

Since the control law written in this form is fairly general, it is representative of several systems. For example, the output of a body-fixed accelerometer can be expressed for rigid body motion in terms of the source of sensed accelerations, (α, β), as

$$A_i = \frac{\partial A_i}{\partial \alpha}\,\alpha + \frac{\partial A_i}{\partial \beta}\,\beta. \tag{16}$$

This produces the same control law with only a modification of gains.

The solution to this set of equations is obtained by using frozen coefficients (a conservative assumption, in general) for a representative wind input which is the slow build-up wind (quasi-steady wind profile) or ramp. The characteristic equation of the system, in terms of vehicle parameters, is used to obtain these solutions.

$$S\left\{S^3 + S^2\left[a_1c_2 - \frac{b_oK_3}{V} - \frac{K_2}{V}\right] + S\left[c_2(a_o + b_o) + c_1 - \frac{a_1}{V}(c_2K_2 - c_1K_3)\right]\right.$$

$$\left. - \frac{1}{V}\left[-c_1K_1 + a_o(c_2K_2 - c_1K_3) - b_oc_2K_1\right]\right\} = 0. \tag{17}$$

A simpler form in terms of the roots

$$S_1 = 0 \tag{18}$$

$$S_2 = A_1 \tag{19}$$

$$S_{3,4} = \sigma \pm i\omega \tag{20}$$

is

$$S\left\{S^3 + S^2(-A_1 - 2\sigma) + S(2A_1\sigma + \sigma^2 + \omega^2) + \left[-A_1(\sigma^2 + \omega^2)\right]\right\} = 0. \tag{21}$$

Equating coefficients of powers of S between equations allows the expression of the roots in terms of vehicle parameters and control system gains. A logical choice is to express the control system gains a_o and a_1, and the drift foot A_1 as a function of control system gain b_o, control frequency ω_c, and control damping ζ_c; that is,

$$a_o = \frac{-\lambda\omega_c^2 B_1 + 2B_3 c_2 \zeta_c \omega_c + \lambda B_3 - c_2 B_2 \omega_c^2}{-2\lambda c_2 \zeta_c \omega_c - \lambda^2 - c_2^2 \omega_c^2} \tag{22}$$

$$a_1 = \frac{c_2 B_3 - 2\lambda B_1 \zeta_c \omega_c + B_2 \lambda - B_1 c_2 \omega_c^2}{-2\lambda c_2 \zeta_c \omega_c - \lambda^2 - c_2^2 \omega_c^2} \tag{23}$$

$$A_1 = \frac{\lambda c_2 B_2 + B_1 \lambda^2 + c_2^2 B_3}{2\lambda c_2 \zeta_c \omega_c - \lambda^2 - c^2 \omega_c^2} \tag{24}$$

where

$$B_1 = 2\zeta_c \omega_c + \frac{K_2 + b_o K_3}{V} \tag{25}$$

$$B_2 = -c_1 + \omega_c^2 - c_2 b_o \tag{26}$$

$$B_3 = -\frac{K_1}{V}(c_1 + b_o c_2) \tag{27}$$

$$\lambda = \frac{1}{V}(c_2 K_2 - c_1 K_3) \tag{28}$$

$$\sigma = -\zeta_c \omega_c \tag{29}$$

$$\omega_c^2 = \sigma^2 + \omega^2. \tag{30}$$

Typical plots of A_1, a_o, and a_1 for the maximum dynamic pressure region of the Saturn V space vehicle are shown on figures 15, 16, and 17. The drift root A_1 is stable for zero b_o, but moves toward instability as b_o increases. The b_o value that produces A_1 equal to zero is the well known drift minimum condition. Further increase of b_o initially moves A_1 toward instability; however, the effect asymptotically approaches the limiting value of A_1 determined by the straight line where $b_o = -c_1/c_2$. These results show that the basic influence on the drift root is determined by the angle-of-attack gain, b_o.

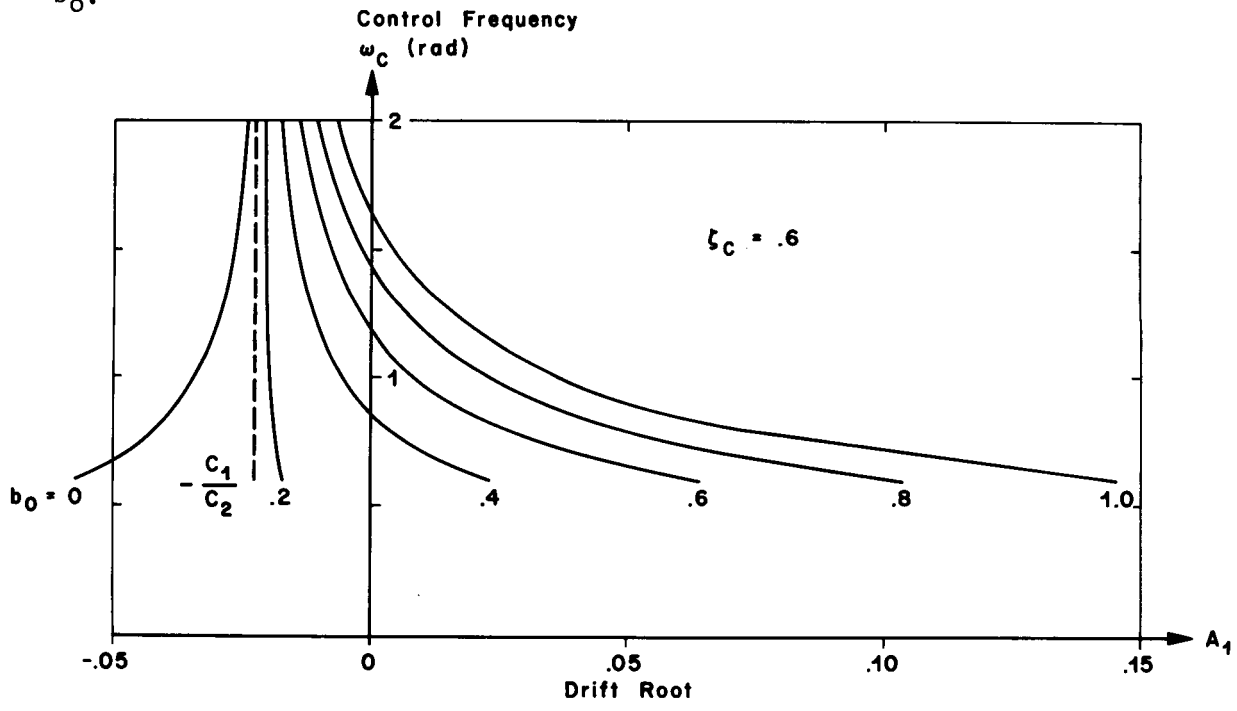

Figure 15. A_1 as a Function of Control System Gain, b_o, Control Frequency, ω_c, and Damping, ζ_c.

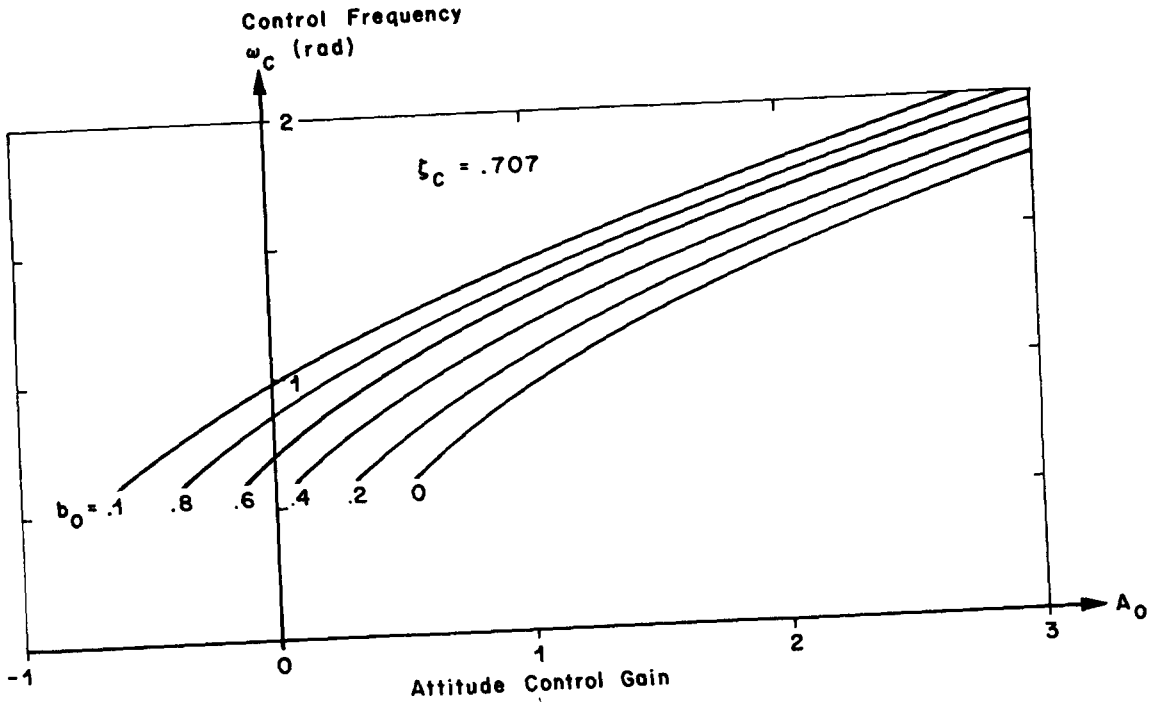

Figure 16. a_o as a Function of Control System Gain, b_o, Control Frequency, ω_c, and Damping, ζ_c

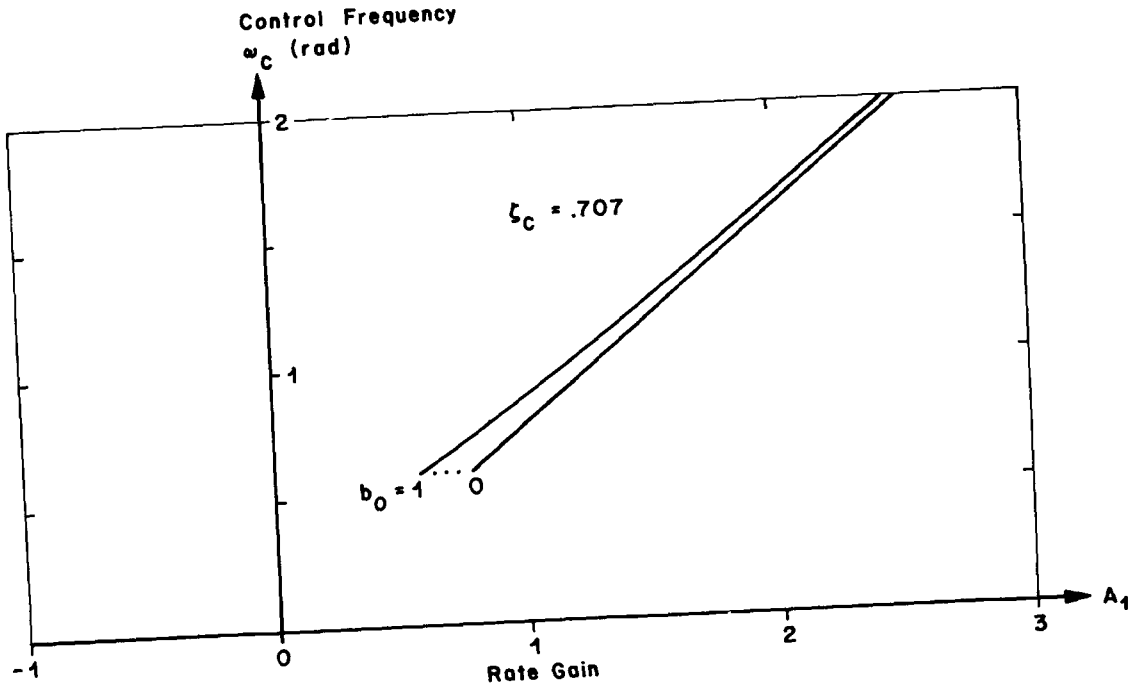

Figure 17. a_1 as a Function of Control System Gain, b_o, Control Frequency, ω_c, and Damping, ζ_c

The only apparent effect on the control gain, a_1, is the damping, ζ_c, and the control frequency, ω_c. The control gain, a_o, increases as b_o decreases for a constant frequency ω_c. Increasing ω_c increases a_o for a constant angle of attack gain b_o. The solution to the set of differential equations can be formulated in terms of these roots and the system parameters. Only one solution will be formulated, the response to a ramp wind Kt. This is sufficient, since, for the equations used, the time derivative of the ramp produces the response to a step. The solutions are not valid for A_1 = zero, since at this point, a singularity is introduced into the equations:

$$\varphi(t) = \frac{K(c_1 + c_2 b_o)}{A_1(\sigma^2 + \omega^2)} \left\{ 1 + \frac{(\sigma^2 + \omega^2)^{1/2} e^{\sigma t} \sin(\omega t - \psi_1)}{\omega[A_1^2 - 2\sigma A_1 + \sigma^2 + \omega^2]^{1/2}} \right. \tag{31}$$

$$\left. - \frac{(\sigma^2 + \omega^2) e^{A_1 t}}{A_1^2 - 2\sigma A_1 + \sigma^2 + \omega^2} \right\}$$

where

$$\psi_1 = \tan^{-1} \frac{\omega}{\sigma} + \tan^{-1} \frac{\omega}{\sigma - A_1} \tag{32}$$

$$y(t) = \frac{V}{2} t^2 - \left\{ a_1(c_2K_2 - c_1K_3) - V(\sigma^2 + \omega^2 - 2A_1\sigma) \right\} t$$

$$- \frac{\left\{ \left[(a_o + a_1\sigma)(c_2K_2 - c_1K_3) - K_1(b_o c_2 + c_1) + (\sigma^2 + \omega^2) \right.\right.}{\omega(\sigma^2 + \omega^2)^{3/2} (A_1^2 - 2\sigma A_1 + \sigma^2 + \omega^2)^{1/2}} \cdot$$

$$\left.\left. (K_2 + b_o K_3) \right]^2 + \omega^2 \left[2\sigma(K_2 + b_o K_3) + a_1(c_2K_2 - c_1K_3) \right]^2 \right\}^{1/2}$$

$$\frac{}{\omega(\sigma^2 + \omega^2)^{3/2} (A_1^2 - 2\sigma A_1 + \sigma^2 + \omega^2)^{1/2}} e^{\sigma t} \sin(\omega t - \psi_2)$$

$$+ \frac{(K_2 + K_3 b_o)A_1 + a_1(c_2K_2 - c_1K_3) - V(\sigma^2 + \omega^2)}{A_1^2(A_1^2 - 2\sigma A_1 + \sigma^2 + \omega^2)} e^{A_1 t}, \tag{33}$$

where

$$\psi_2 = \tan^{-1}\frac{\omega}{\sigma} + \tan^{-1}\frac{\omega}{\sigma - A_1} + \tan^{-1}\frac{-\omega[2\sigma(K_2 + K_3 b_o) + a_1(c_2K_2 - c_1K_3)]}{(a_o + a_1\sigma)(c_2K_2 - c_1K_3) - K_1(b_oc_2 + c_1) + (\sigma^2 + \omega^2)(K_2 + K_3b_o)}, \tag{34}$$

$$\alpha(t) = -\frac{a_oc_2}{A_1(\sigma^2 + \omega^2)} - \frac{1}{\omega[(\sigma^2 + \omega^2)(A_1^2 - 2\sigma A_1 + \sigma^2 + \omega^2)]^{1\ 2}}\left\{[\sigma^2 + a_1c_2\sigma + a_oc_2 - \omega^2]^2 + \omega^2[2\sigma + a_1c_2]^2\right\}^{1/2} e^{\sigma t}\sin(\omega t - \psi_3) + \frac{A_1^2 + a_1c_1A_1 + a_oc_2}{A_1(A_1^2 - 2\sigma A_1 + \sigma^2 + \omega^2)} e^{A_1 t}, \tag{35}$$

where

$$\psi_3 = \tan^{-1}\frac{\omega}{\sigma} + \tan^{-1}\frac{\omega}{\sigma - A_1} + \tan^{-1}\frac{-\omega(2\sigma + a_1c_2)}{\sigma^2 + a_1c_2\sigma + a_oc_2 + \omega^2}, \tag{36}$$

$$\beta(t) = \frac{a_oc_1}{A_1(\sigma^2 + \omega^2)} + \frac{\left\{[a_oc_1 + a_1c_1\sigma - b_o\sigma^2 + b_o\omega^2]^2 + \omega^2[2b_o\sigma - a_oc_1]^2\right\}^{1/2}}{\omega[(\sigma^2 + \omega^2)(A_1^2 - 2A_1\sigma + \sigma^2 + \omega^2)]^{1/2}} \cdot e^{\sigma t}\sin(\omega t - \psi_4) + \frac{(b_oA_1^2 - a_1c_1A_1 - a_oc_2)}{A_1(A_1^2 - 2\sigma A_1 + \sigma^2 + \omega^2)} e^{A_1 t}, \tag{37}$$

where

$$\psi_4 = \tan^{-1}\frac{\omega}{\sigma} + \tan^{-1}\frac{\omega}{\sigma - A_1} + \tan^{-1}\frac{\omega(2b_o\sigma - a_1c_1)}{a_oc_1 + a_1c_1\sigma - b_o\sigma^2 + b_o\omega^2}\,. \tag{38}$$

The bending moment is

$$M_B(x) = M'_\alpha\alpha + M'_\beta\,\beta. \tag{39}$$

By defining

$$R(x) = M'_\alpha / M'_\beta$$

$$M_B(x) = M'_\beta(R(x)\,\alpha + \beta) \tag{40}$$

$$M_B(x) = \frac{a_o}{A_1(\sigma^2 + \omega^2)}(-R(x)\,c_2 + c_1) + \frac{e^{A_1t}}{A_1(A_1^2 - 2\sigma A_1 + \sigma^2 + \omega^2)}\Big\{A_1^2(R(x) - b_o)$$

$$+ a_1c_1A_1(R(x) - .1) + a_oc_2(R(x) - 1)\Big\}$$

$$+ \frac{e^{\sigma t}\sin(\omega t + \psi_5)}{\omega[(\sigma^2 + \omega^2)(A_1^2 - 2\sigma A_1 + \sigma^2 + \omega^2)]^{1/2}}\Big\{R^2(x)\,[(\sigma^2 + a_1c_2\sigma$$

$$+ a_0c_2 - \omega^2)^2 + \omega^2(2\sigma + a_1c_2)^2] + (a_0c_1 + a_1c_1\sigma - b_0\sigma^2 + b_0\omega^2)^2$$

$$+ \omega^2(2b_0\sigma - a_0c_1)^2 + 2R(x)\ [(\sigma^2 + a_1c_2\sigma + a_1c_2 - \omega^2)^2$$

$$+ \omega^2(2\sigma + a_1c_2)^2]^{1/2}\ [(a_0c_1 + a_1c_1\sigma - b_0\sigma^2 + b_0\omega^2)^2$$

$$+ \omega^2(2b_0\sigma - a_0c_1)^2]^{1/2}\ (\cos\psi_3 \cos\psi_4 + \sin\psi_3 \sin\psi_4)\Big\}^{1/2}, \quad (41)$$

where

$$\psi_5 = \tan^{-1}\Big[\Big\{R(x)\ [\sigma^2 + a_1c_2\sigma + a_0c_2 - \omega^2)^2 + \omega^2(2\sigma + a_1c_2)^2]^{1/2} \cos\psi_3$$

$$+ [(a_0c_1 + a_1c_1\sigma - b_0\sigma^2 + b_0\omega^2)^2 + \omega^2(2b_0\sigma - a_0c_1)^2]^{1/2} \cos\psi_4\Big\}\Big/$$

$$\Big\{R(x)\ [(\sigma^2 + a_1c_2\sigma + a_0c_2 - \omega^2)^2 + \omega^2(2\sigma + a_1c_2)^2]^{1/2} \sin\psi_3$$

$$+ [(a_0c_1 + a_1c_1\sigma - b_0\sigma^2 + b_0\omega^2)^2 + \omega^2(2b_0\sigma - a_0c_1)^2]^{1/2} \sin\psi_4\Big\}\Big]. \quad (42)$$

When plotted as a function of R(x), ψ_5 changes very little (see Figure 18). Writing the above equations as a function of R(x), σ, ω, A_1, yields

$$\gamma_1(\sigma,\omega,A_1)\ R(x) + \gamma_2(\sigma,\omega,A_1) + \frac{1}{A_1}\Big(\gamma_3(\sigma,\omega,A_1)\ R(x) + \gamma_4(\sigma,\omega,A_1)\Big)\ e^{A_1t}$$

$$+ \frac{1}{(\sigma^2 + \omega^2)^{1/2}}\ \Big\{\gamma_5(\sigma,\omega,A_1)\ R^2(x) + \gamma_6(\sigma,\omega,A_1)\ R(x) +$$

$$+ \gamma_7(\sigma,\omega,A_1)\Big\}^{1/2}\ e^{\sigma t} \sin(\omega t + \psi_5). \quad (43)$$

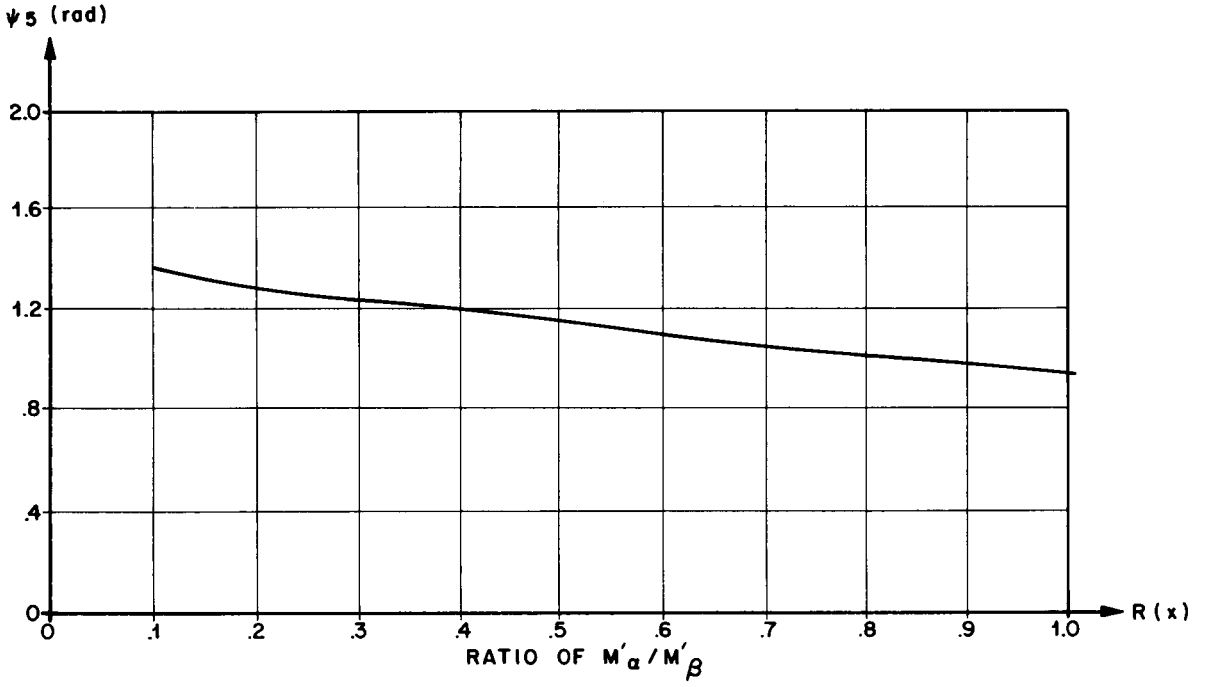

Figure 18. Phase Angle ψ_5 vs R(x)

By taking the special case of $\omega_c = 1.2$ and $\zeta_c = .707$, the bending moment for a step wind becomes, for gyro control ($A_1 = -0.031$),

$$M_B(x) = -K M'_\beta e^{-.0722} [0.051 R^2(x) + 0.12 R(x) + 0.09)^{1/2}] \sin (0.882t + \gamma)$$

$$+ K M'_\beta(x) (0.714 R(x) + 0.13) e^{-0.03t} , \qquad (44)$$

where

$$\gamma = \tan^{-1} \frac{0.22 R(x) + 0.3}{0.244 R(x) + 0.27} . \qquad (45)$$

For the drift minimum case ($A_1 = 0$), which was solved as a special case, the bending moment is

$$M_B(x) = -K\, M'_\beta(x)\, e^{-0.72t}\, [0.174\, R^2(x) + 0.428\, R(x) + 0.31)^{1/2}]\, \sin(0.882t + \gamma) + K\, M'_\beta(x)\, (0.64\, R(x) + 0.113), \quad (46)$$

where

$$\gamma = \tan^{-1} \frac{0.21\, R(x) + 0.452}{0.359\, R(x) + 0.332}\ . \quad (47)$$

Since for most of the stations of Saturn V vehicles, $R(x) \leqq 0.3$, β contributes the major part of the transient portion of the solution for the bending moment, while angle-of-attack has more influence on the quasi-steady-state portion. Changing of the drift root from negative to zero increases the amplitude caused by the transient solution, but decreases the part caused by the drift root. The choice then becomes one of the trade-off between the transient and steady-state solution. This choice can be related to changing the gains, since by increasing b_o, the drift root becomes more positive; this reduces quasi-steady-state loads, but increases transient loads even more. In general, for a rigid vehicle, an overall load reduction is possible by increasing b_o.

B. Elastic Body Influence

Simplifying the equations of motion allows an overall picture of the bending dynamics influence and uses much less computer time. For this purpose, the following premises were made in deriving the equations of motion of the vehicle:

(1) A space-fixed coordinate system was chosen with its origin at the center of gravity of the vehicle.

(2) The acceleration of the vehicle is replaced by an equivalent gravitational field (see section II).

(3) The bending modes were assumed to be uncoupled.

(4) The control system effect on bending frequency was assumed to be negligible, while the effect on bending mode damping was introduced as additional structural damping.

(5) The forces acting on the bending modes were assumed to be due to the rigid body α and β only.

(6) Time varying coefficients were used.

(7) Curve fits were used for the aerodynamic distributions.

(8) Gust penetration effects were assumed to be small.

(9) Both filtered and unfiltered winds were used as forcing function, as well as the synthetic profile.

The equations derived were the same as for rigid body calculations for rotation, translation, and angle of attack, plus the introduction of the bending equation which follows:

$$\ddot{\eta}_i + 2\omega_B (\zeta_{B_i} + \zeta_c) \eta_i + \omega_{B_i}^2 \eta_i + \bar{D}_{i\alpha} + \frac{F_s Y_{E_i}}{M_{B_i}} \beta = 0, \qquad (48)$$

$$i = 1 \rightarrow 4$$

where

$$\bar{D}_i = \frac{2Q D_i}{M_{B_i}} . \qquad (49)$$

With the addition of bending, the bending moment becomes

$$M_B = M'_\alpha \alpha + M'_\beta \beta + \sum_{j=1}^{4} M'_{\eta_j} \ddot{\eta}_j . \qquad (50)$$

To show the effect of the bending dynamics on the bending moment, the ratio of the bending moment due to bending dynamics to total bending moment was computed.

$$R = \frac{M_{B(total)} - M_{B(rigid)}}{M_{B(total)}} . \qquad (51)$$

This yields the following results, which show the influence of the elastic body dynamics on the bending moment for various types of control systems (Figure 19).

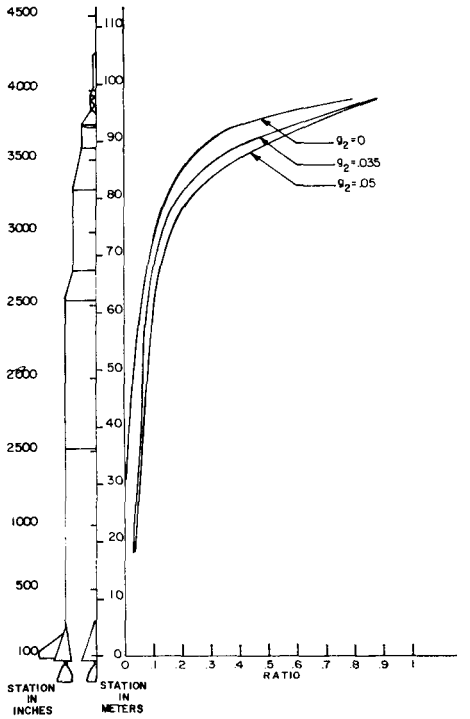

Figure 19. Ratio Influence of Bending Moment Due to Bending Dynamics to Total Bending Moment

It is clearly shown in this study that the bending dynamics portion of the bending mode becomes predominant at the forward end of the vehicle. The booster and second stage area show a negligible influence of bending dynamics. Also, any increase in accelerometer gains increases the bending dynamics effect. This system can be made equivalent to the alpha meter system discussed previously. In this case, the reduction in bending moment due to rigid body dynamics more than offsets the increase due to bending dynamics, producing a slight overall reduction in moment.

Some variance of the bending dynamics effect with flight time is caused by the aerodynamic forces acting on the vehicle. However, in all cases, the contribution of bending dynamics to the bending moment in the spacecraft is large; therefore, elastic body effects cannot be neglected in the vehicle analysis.

VII. RESULTS

A. Gross Effect of Ensemble Compared to Synthetic Profile

To obtain some insight into the general characteristics of the vehicle response to the wind ensemble, the response to each individual profile is superimposed on the response obtained by using a synthetic profile. Only one case for the synthetic profile is used; that is the wind peaking at 75 seconds flight time, which is in the region of maximum dynamic pressure. Figure 20, showing the wind velocity versus flight time for the unfiltered wind ensemble, clearly indicates that most of the individual wind profiles have a peak wind velocity less than the synthetic profile. The average wind velocity of the individual profiles falls below the wind velocity of the synthetic profile throughout the flight regime, except in the early part of flight (0 to 30 seconds). Since the synthetic profile was designed for a 95 percent "worst month" wind magnitude and 99 percent wind shear and gust, these results are expected. All of the vehicle responses show this same general behavior, with most of the responses of the individual profiles being concentrated below the response of the synthetic profile with gust. The exceptions are the bending mode displacements, angle of attack, and bending moment (Figures 20, 21, 22), which show a substantially higher response for the individual profiles during the first 30 seconds of flight than that obtained using a synthetic profile. This is due to the larger wind magnitudes of the individual profiles during the first 30 seconds of flight time. Since the flight time of major concern (maximum dynamic pressure) is outside this region, these differences are negligible. The statement can be made from this general approach that the synthetic profile should produce a slightly conservative design and should, in general, give a representative response.

A comparison of the filtered winds with the synthetic profile without gust shows the same trends (Figures 23, 24, 25). There are about two winds that peak above the synthetic profile peak wind value. The response follows the same pattern with only one or two winds creating peak responses equaling the response obtained from the synthetic profile without gust. The most noticeable change in response is from one wind that creates an engine deflection response 30 percent greater than that caused by the synthetic profile without gust.

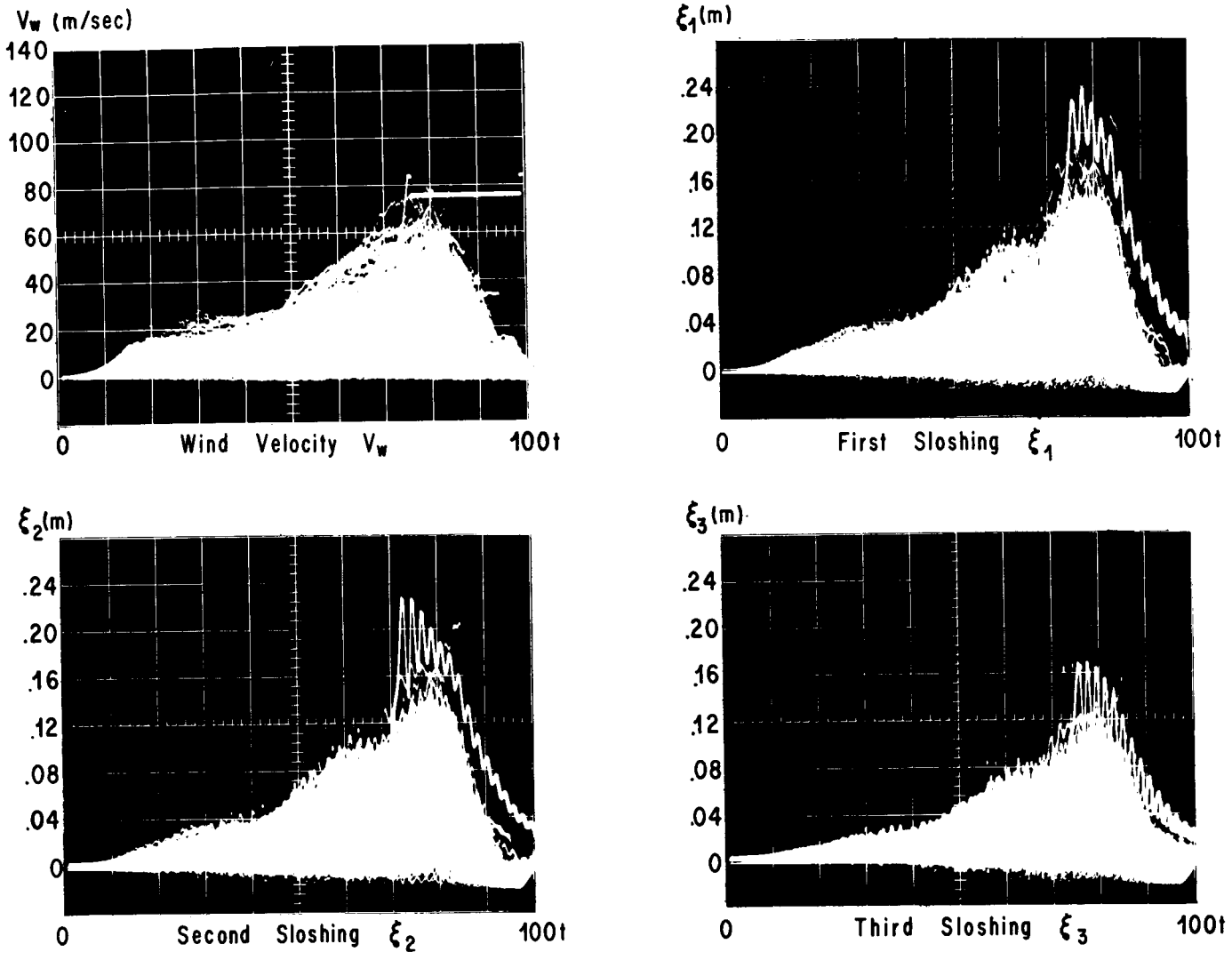

Figure 20. Synthetic Profile with Gust Compared with Wind Ensemble Filtered

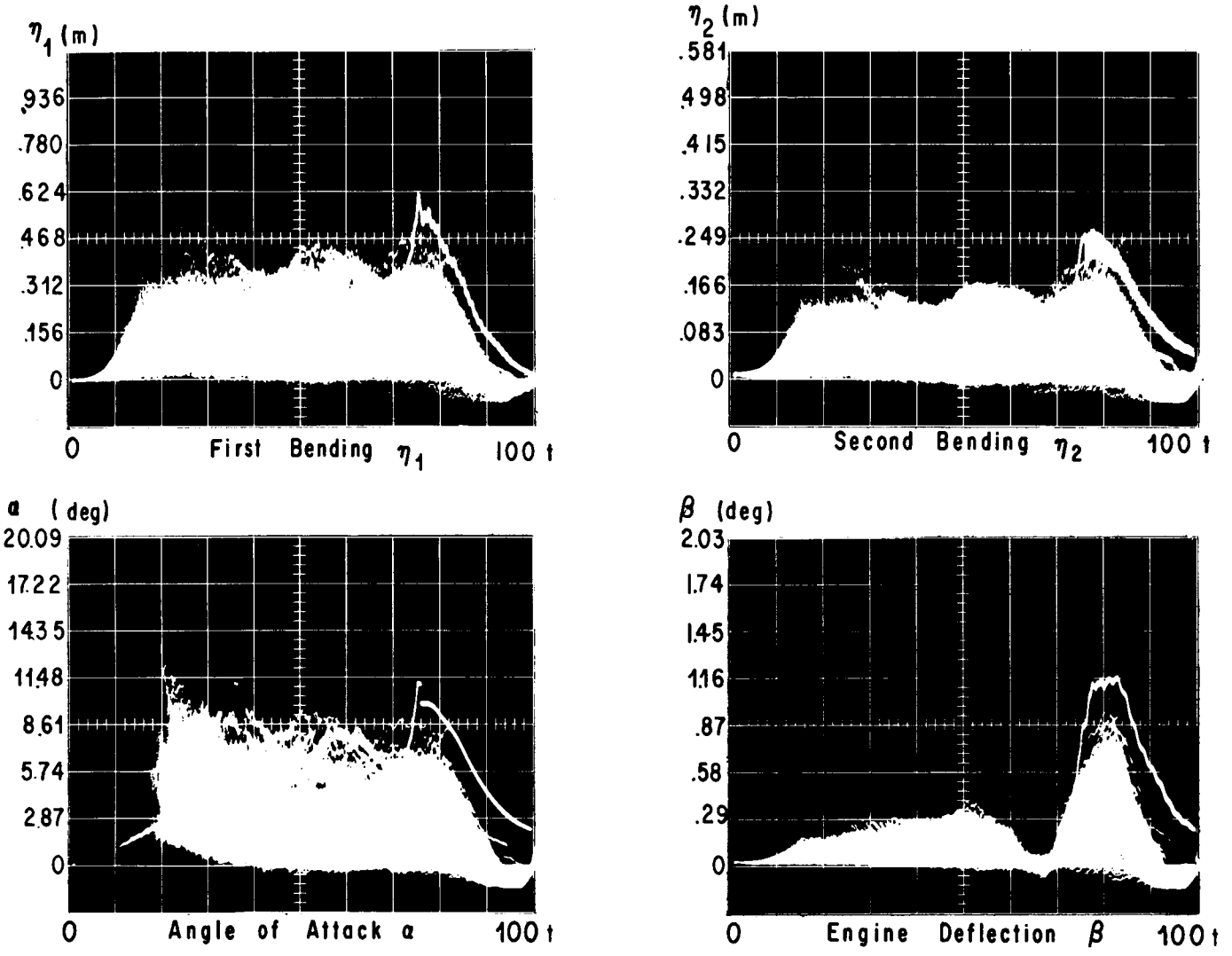

Figure 21. Synthetic Profile with Gust Compared with Wind Ensemble Unfiltered

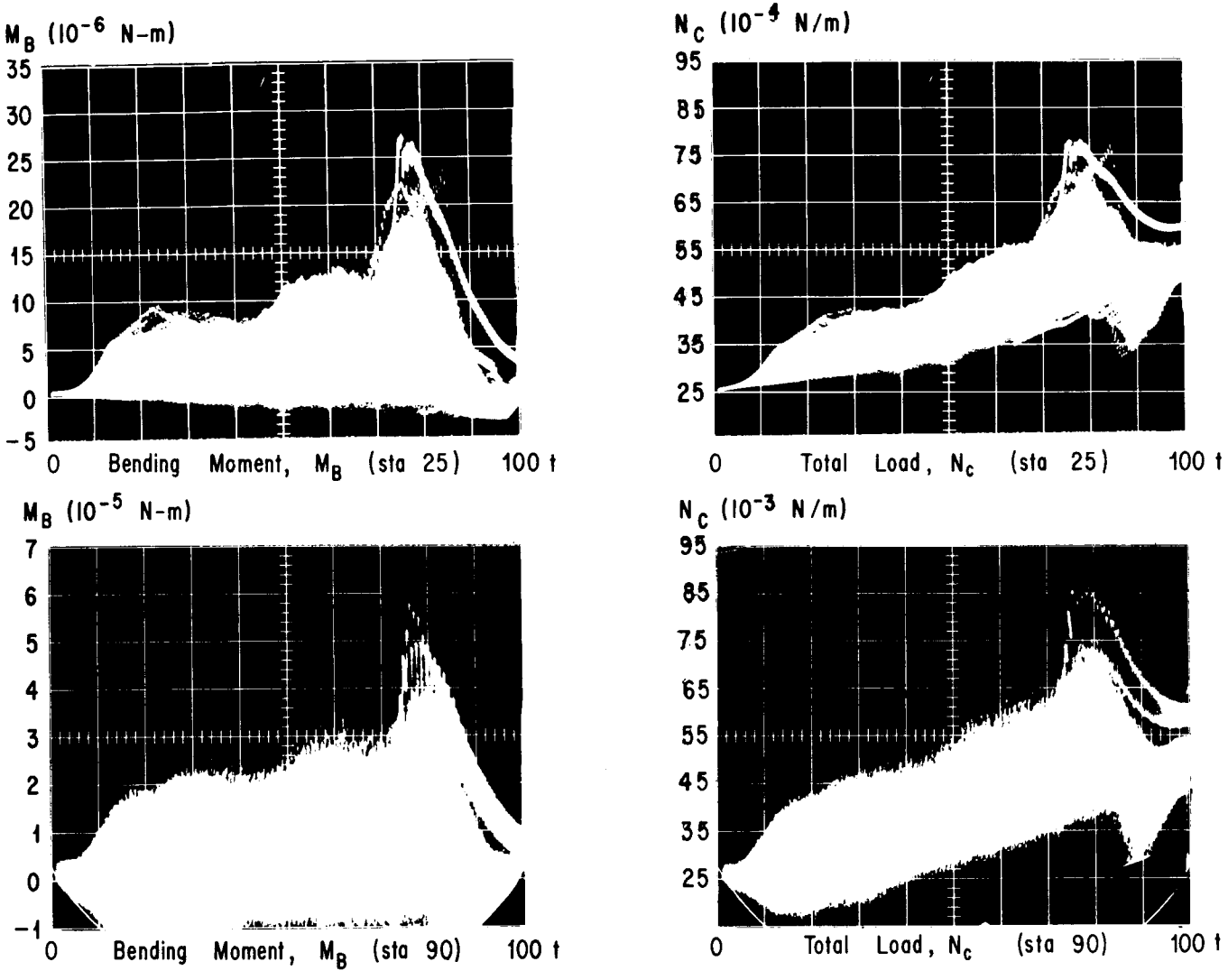

Figure 22. Synthetic Profile with Gust Compared with Wind Ensemble Unfiltered

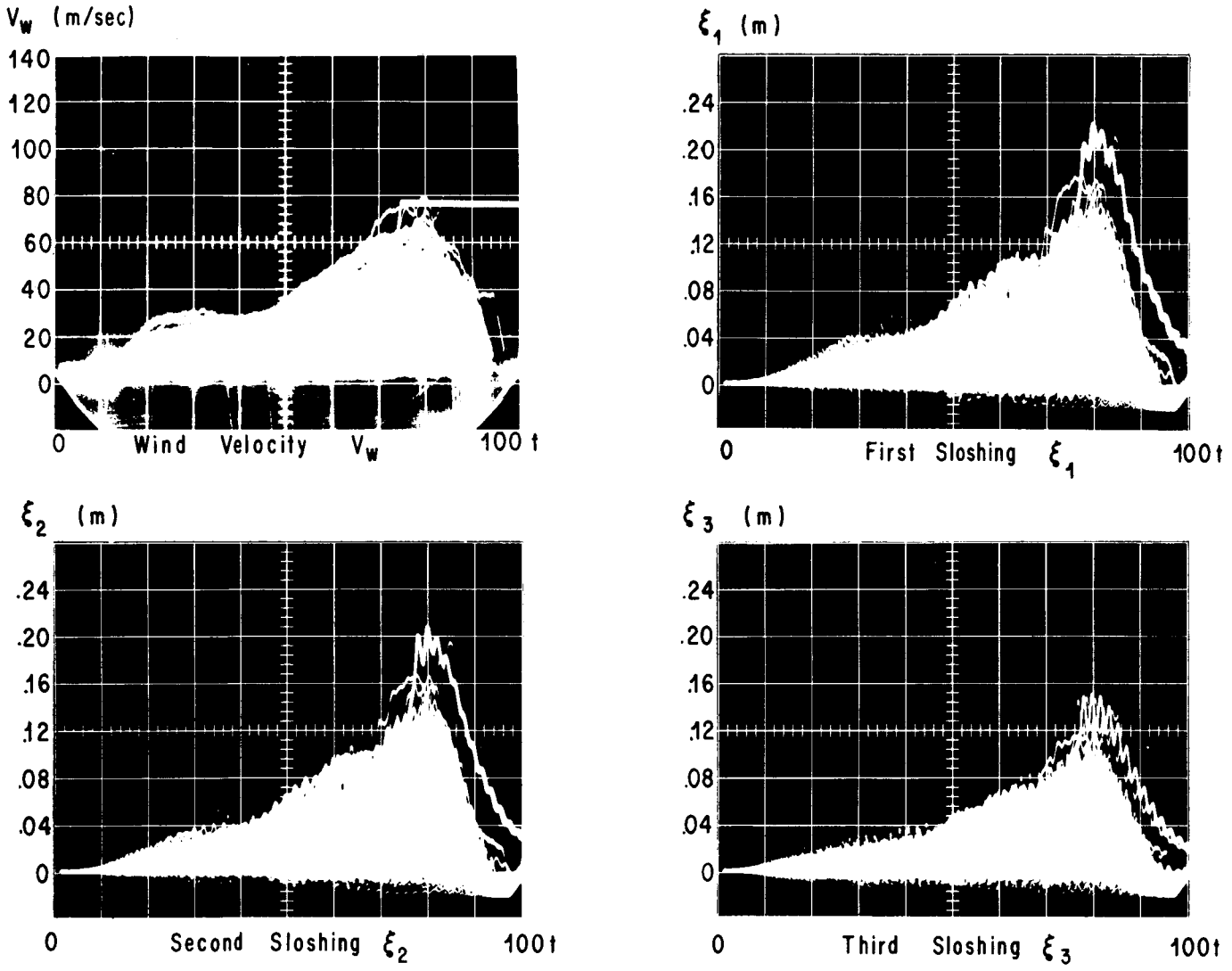

Figure 23. Synthetic Profile Without Gust Compared with Wind Ensemble Filtered

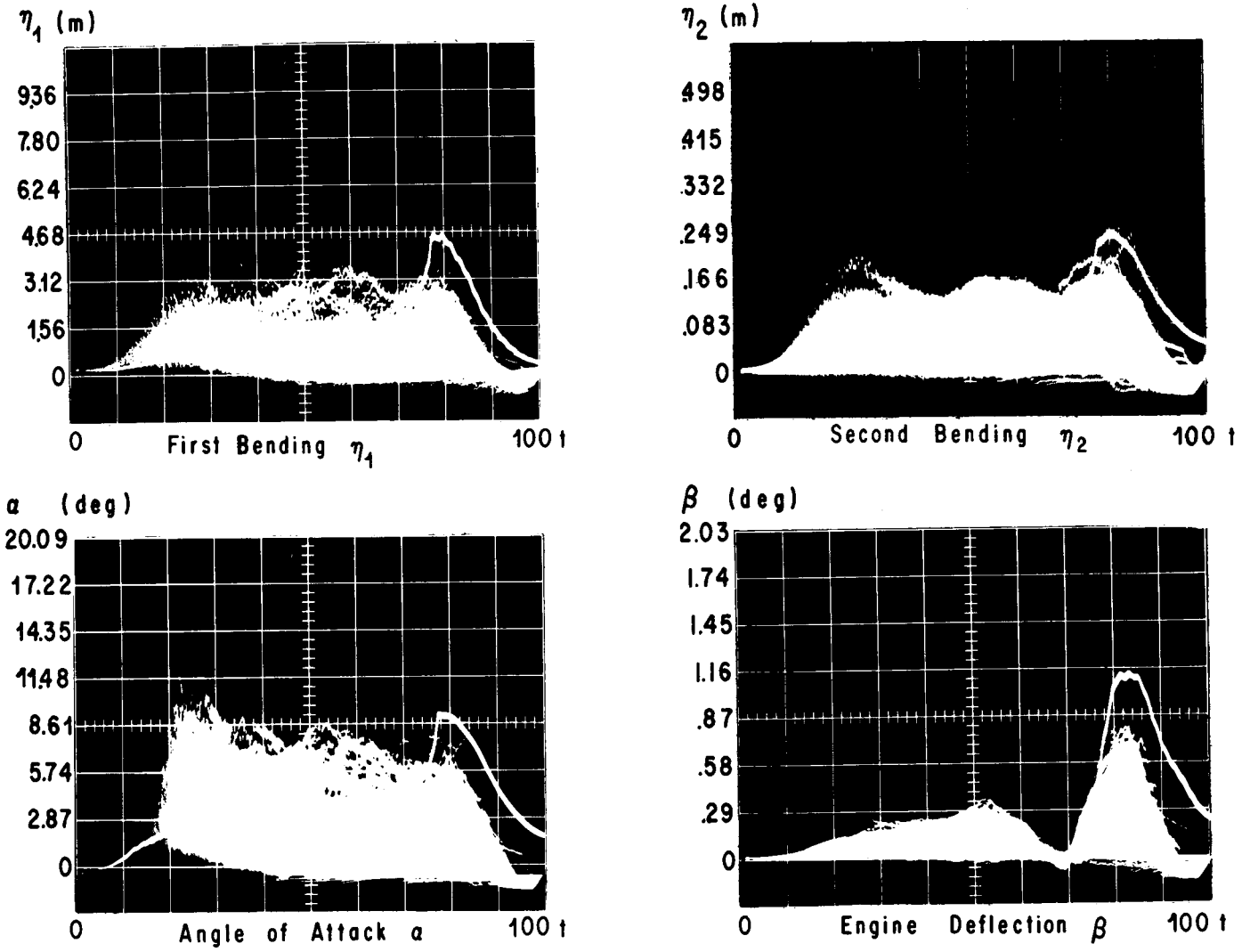

Figure 24. Synthetic Profile Without Gust Compared with Wind Ensemble Filtered

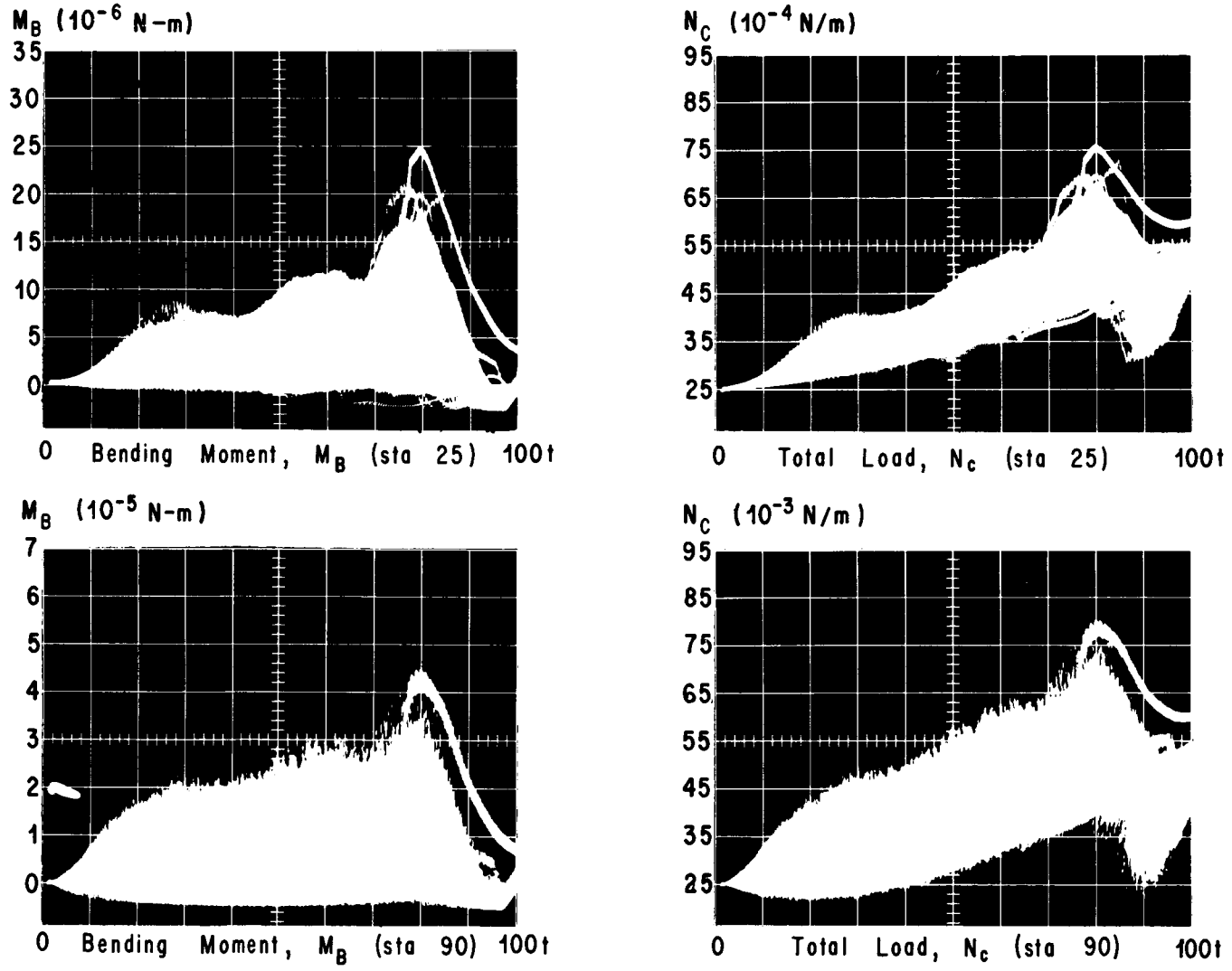

Figure 25. Synthetic Profile Without Gust Compared with Wind Ensemble Filtered

B. Effects of Wind Components on Response for Gyro Control System

The influence of the various wind components on vehicle response can be assessed in many ways. As was stated earlier, this study attempts to isolate the wind components of many individual wind profiles to study their effects on vehicle response for several types of control laws. Many ways of obtaining and representing the results are possible. The ones used are variance and mean of response output and probability output.

The mean wind speeds of the filtered and unfiltered wind ensembles are very close in magnitude throughout flight time, with the unfiltered wind ensembles always the lower value (Figure 26). The

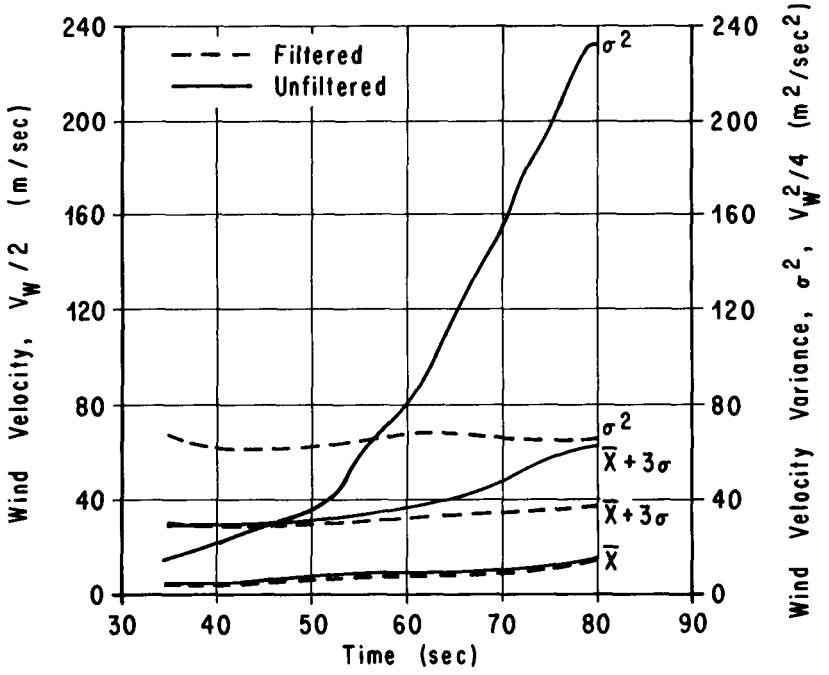

Figure 26. Mean, Variance and Mean Plus 3σ for Wind Ensemble vs Time

variance, however, is much larger in the maximum dynamic pressure region for the unfiltered ensemble, thus indicating the influence of the wind turbulence (Figure 27). There is very little difference in the vehicle engine response to the unfiltered ensemble and the filtered ensemble in both the mean and variance. This indicates a low sensitivity of the engine deflection response to turbulence, for gyro control only.

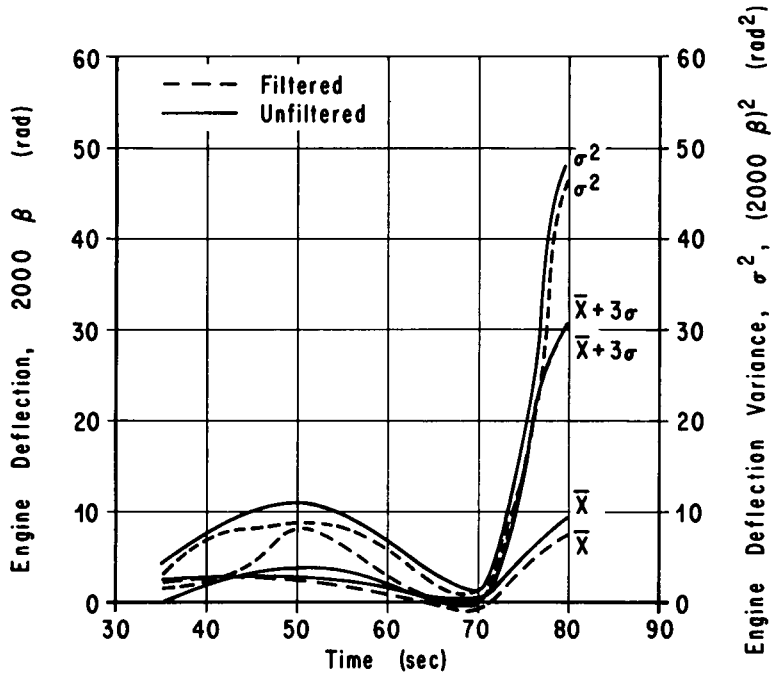

Figure 27. Mean, Variance and Mean Plus 3σ for Engine Deflection vs Time

The plots contain the variance, mean, and mean plus three times the standard deviation. Since the distribution is not Gaussian, the mean-plus-3σ value does not produce a 99 percent value, but it does guarantee that at least 87 percent of the values will fall into this level [9].

The bending moment at station 25 (Figure 28) shows a lower variance, mean, and 3σ-plus-mean for the filtered profiles in comparison to the unfiltered. However, the difference between the response is small, showing a small influence of the turbulence on response of the bending moment at this station.

At station 90, for eighty seconds flight time, the influence of turbulence becomes larger, with an increase in the mean bending moment and the mean plus 3σ value showing approximately a 30 percent increase due to the wind turbulence (Figure 29). The variance between the unfiltered and filtered winds is very close in magnitude, the main difference in response becoming the change in mean value. Although these results have shown some conclusive trends, the computation of the variance and mean on the analog computer contains inaccuracies because of the use of many multipliers. The results should therefore be interpreted in this light. Particularly, the variance should be interpreted in this manner since the small difference between two cases could easily be caused by inaccuracies in the computer.

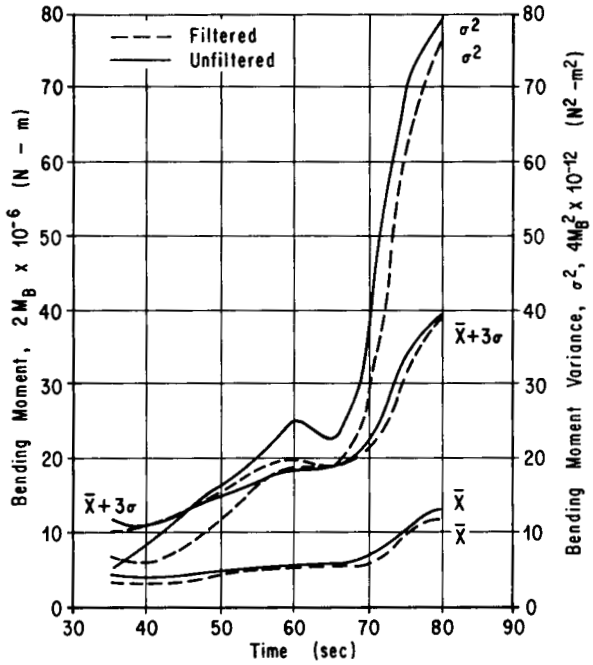

Figure 28. Mean, Variance and Mean Plus 3σ for Bending Moment (Station 25) vs Time

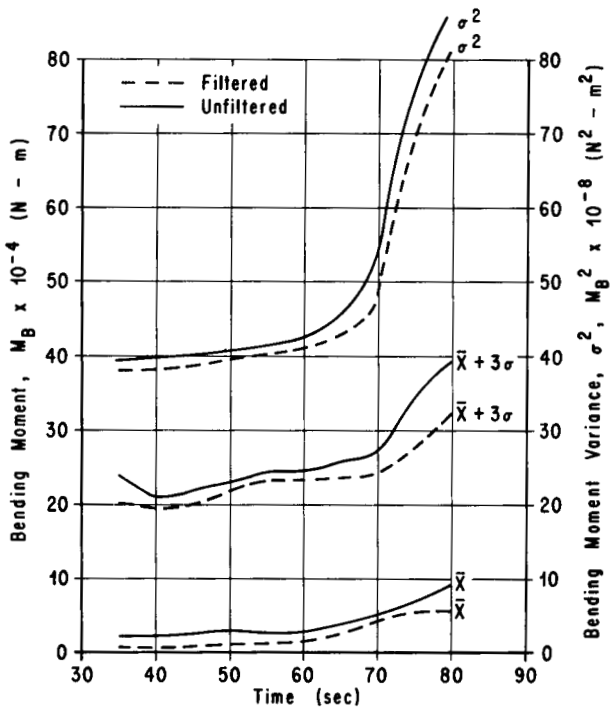

Figure 29. Mean, Variance, and Mean Plus 3σ for Bending Moment (Station 90) vs Time

Although a more accurate computation for this computer is the probability of a response, it is much too time consuming to evaluate as a function of time. Therefore, we compute the probability in terms of one exceedance per profile in the high dynamic pressure region of 50 to 80 seconds flight time. Probability can be computed in terms of an overall probability or the probability of launching during a specific period of the year, for example, the worst wind month. For this reason, results will be presented for the worst month (March) at Cape Kennedy, Florida, and for the total wind ensembles, unfiltered, filtered, and turbulence, which are measured over a two-year period. Since the MSFC synthetic wind profile has been widely used in vehicle design, results are shown on the graphs for the synthetic profile with and without gust.

Figure 30 shows that the engine deflection is influenced very little by turbulence; i.e., about a 10 percent increase. When the

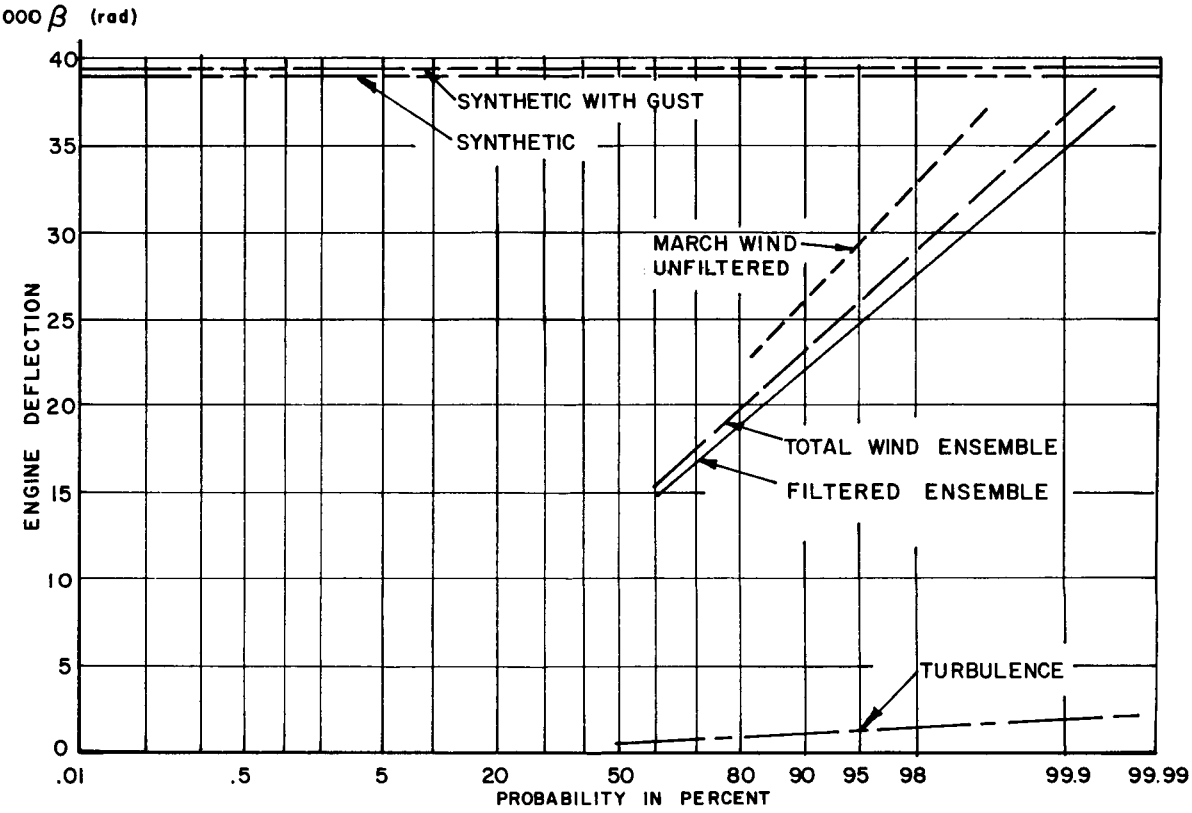

Figure 30. Engine Deflection vs Probability of Not Exceeding

ensemble is compared to the worst month case, the increase in response is doubled (~ 20 percent). The synthetic profile produces a conservative response value; however, the response of the turbulence ensemble (95 percent probability) is about equal to the difference between the response of the synthetic profile with and without gust.

The rigid body angle of attack shows approximately the same influence due to turbulence (10 percent) (Figure 31). The difference in an angle of attack due to the synthetic profile with and without

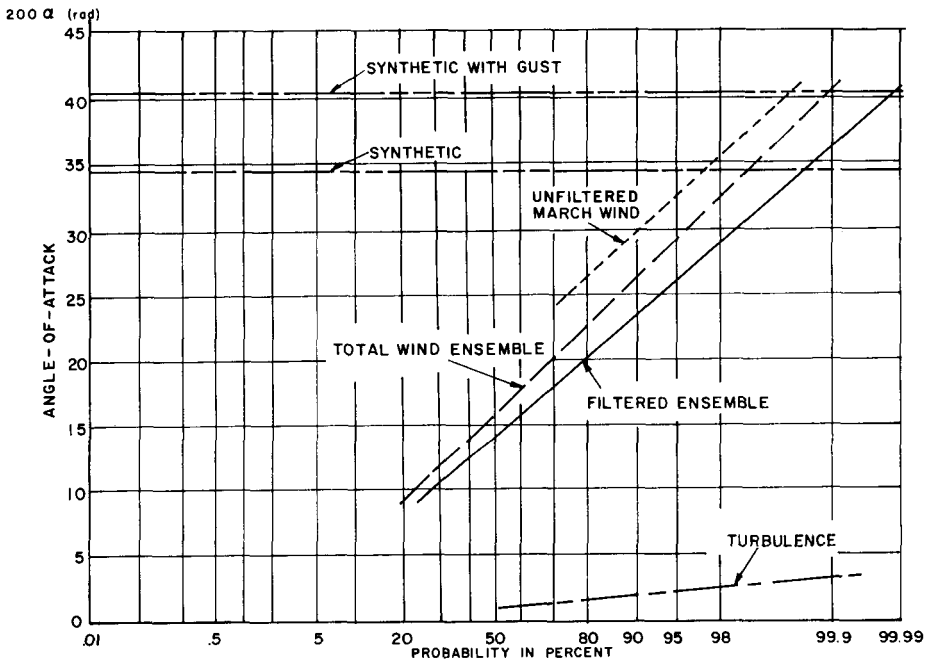

Figure 31. Angle of Attack vs Probability of Not Exceeding

gust is larger than the angle of attack obtained from the turbulence ensemble, indicating a slightly severe gust representation on the synthetic profile. A good correlation between the synthetic profile with gust and the unfiltered ensembles is obtained at the 99.9 percent probability level. The synthetic profile with gust produces a value equal to the 99 percent probability level for the March winds.

The first bending mode displacement at the vehicle nose (Figure 32) shows the same trends as the engine deflection. The second bending mode displacement (vehicle nose) (Figure 33) is similar also. However, it is slightly more sensitive to the wind turbulence.

The response of the liquid in the propellant tanks (Figures 34, 35, 36) indicates the same trends. For each of these parameters, the response due to turbulence at any one probability level can be added to the response due to the filtered ensemble to produce about the same response obtained from the unfiltered ensemble. The 99.9 percent turbulence response value approximates the difference in response obtained from the synthetic profile with and without gust.

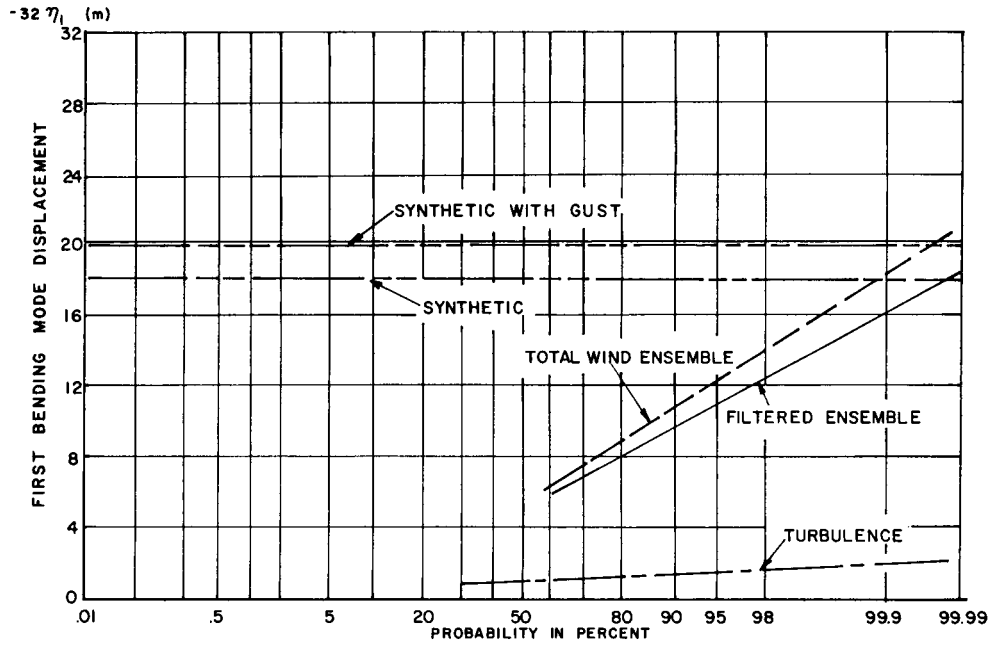

Figure 32. First Bending Mode Deflection vs Probability of Not Exceeding

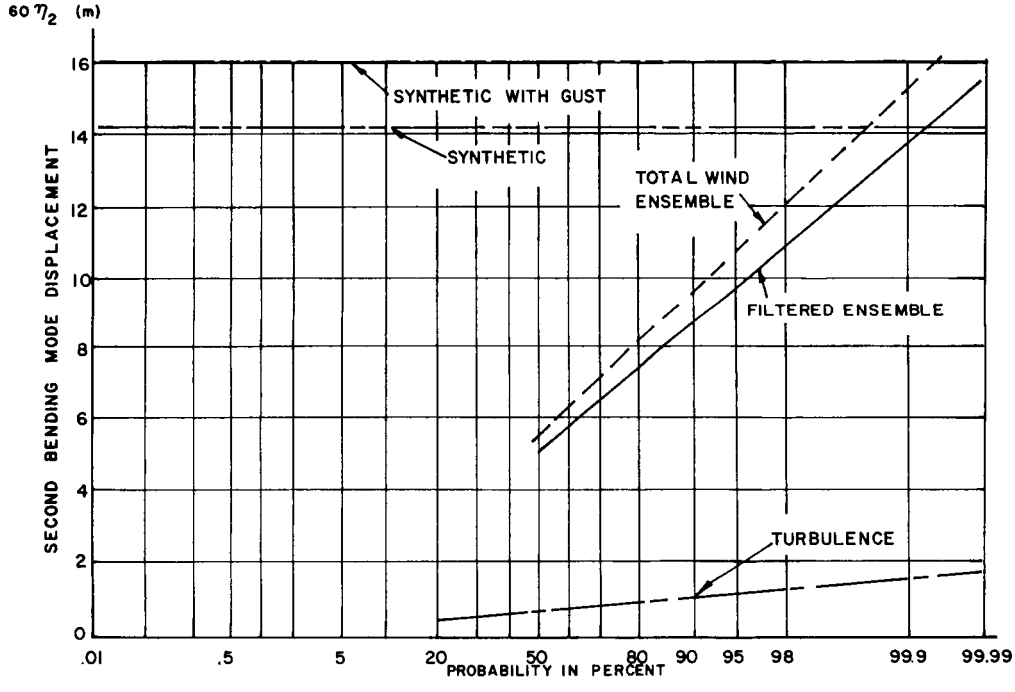

Figure 33. Second Bending Mode Deflection vs Probability of Not Exceeding

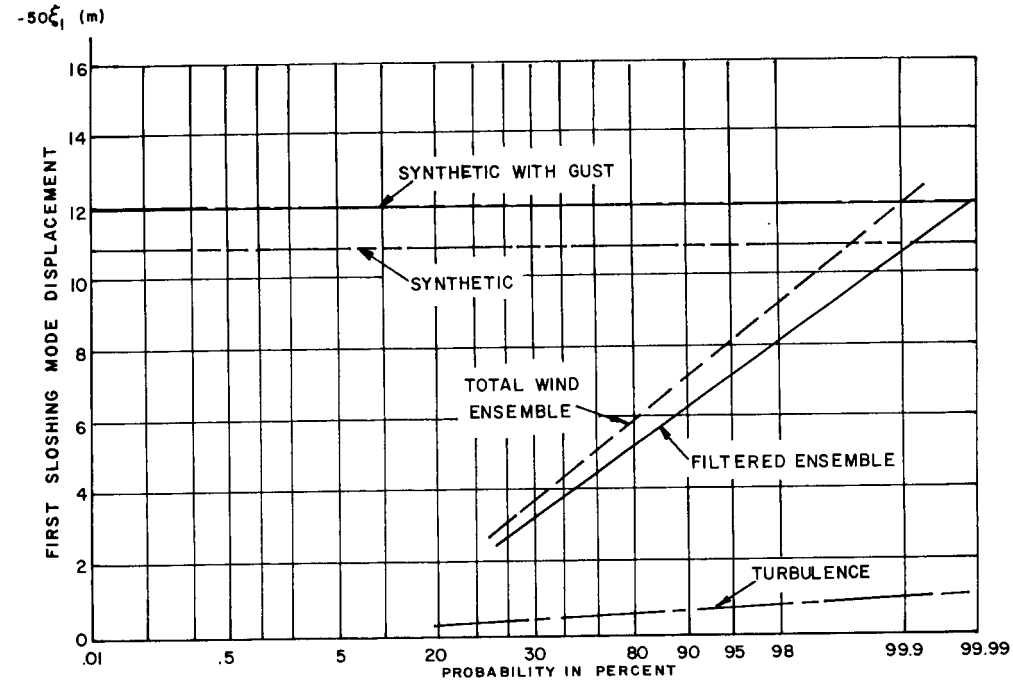

Figure 34. First Slosh Mode vs Probability of Not Exceeding

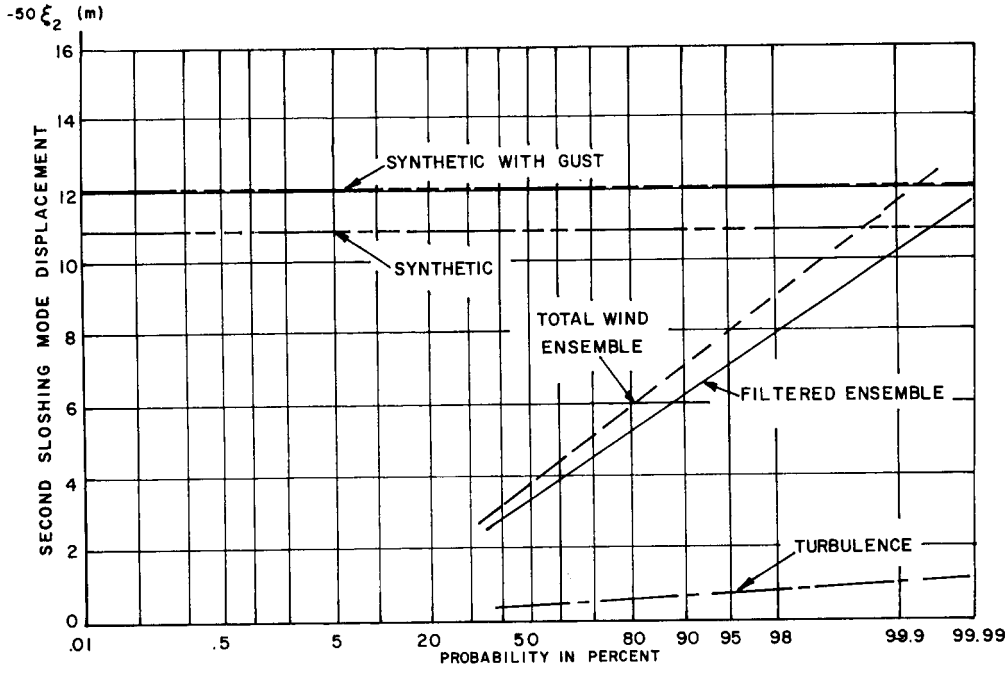

Figure 35. Second Slosh Mode vs Probability of Not Exceeding

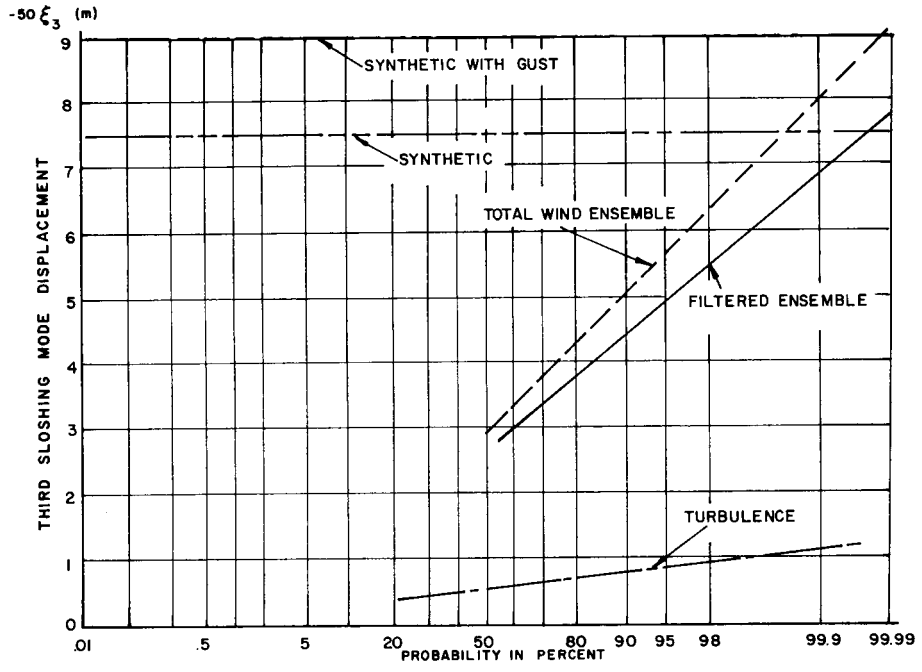

Figure 36. Third Slosh Mode Deflection vs Probability of Not Exceeding

The probability of a bending moment value not being exceeded in flying through an ensemble of winds is shown on Figure 37 for vehicle station 25. The influence of turbulence on this bending moment is small, correlating again the influence of turbulence with the influence of bending dynamics on bending moment values. When one probability level of the vehicle response to the turbulence is added to the same probability level of the vehicle response to the filtered ensemble, the resulting value closely approximates the response value obtained for the total ensemble.

The synthetic profile with gust produces a response value that has approximately a 0.1 percent probability of being exceeded in terms of the total ensemble, and approximately a 1.0 percent probability in terms of March winds. Similarly, the synthetic profile without gust produces a response value with a 0.1 percent probability of being exceeded in terms of the filtered ensemble.

As was expected, the influence of turbulence at station 90 (30 percent) is much higher than at station 25 (see Figure 38). As already pointed out, this corresponds to a region with a large influence of bending dynamics on the bending moment. The spectral density of the turbulence shows a large concentration of energy in the one to two Hertz region (Figure 9) indicating the source of excitation of bending dynamics.

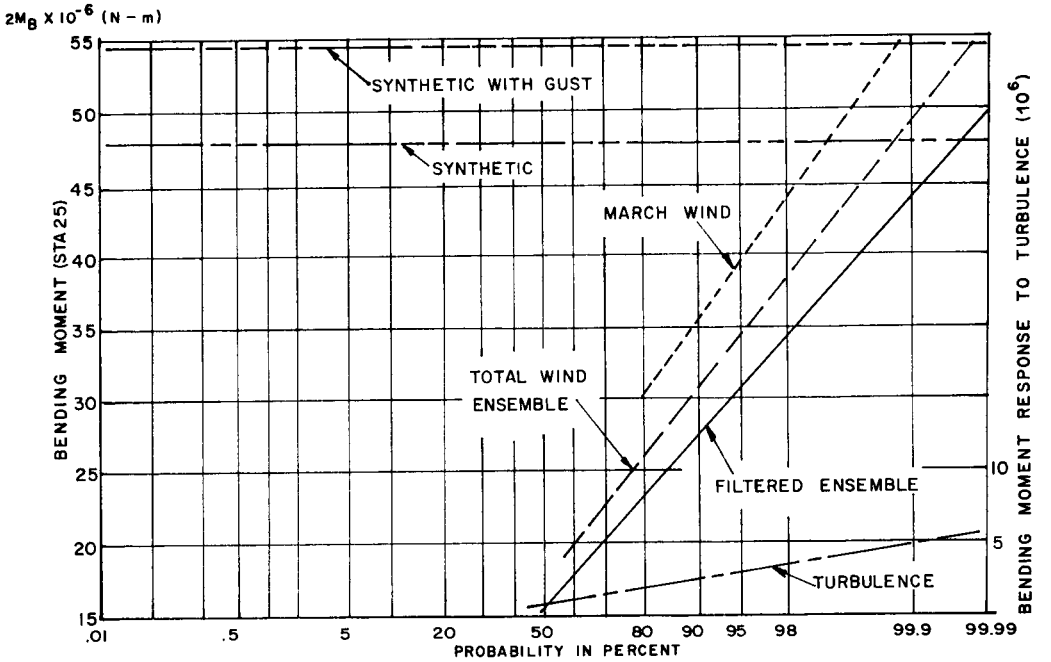

Figure 37. Bending Moment at Station 25 vs Probability of Not Exceeding

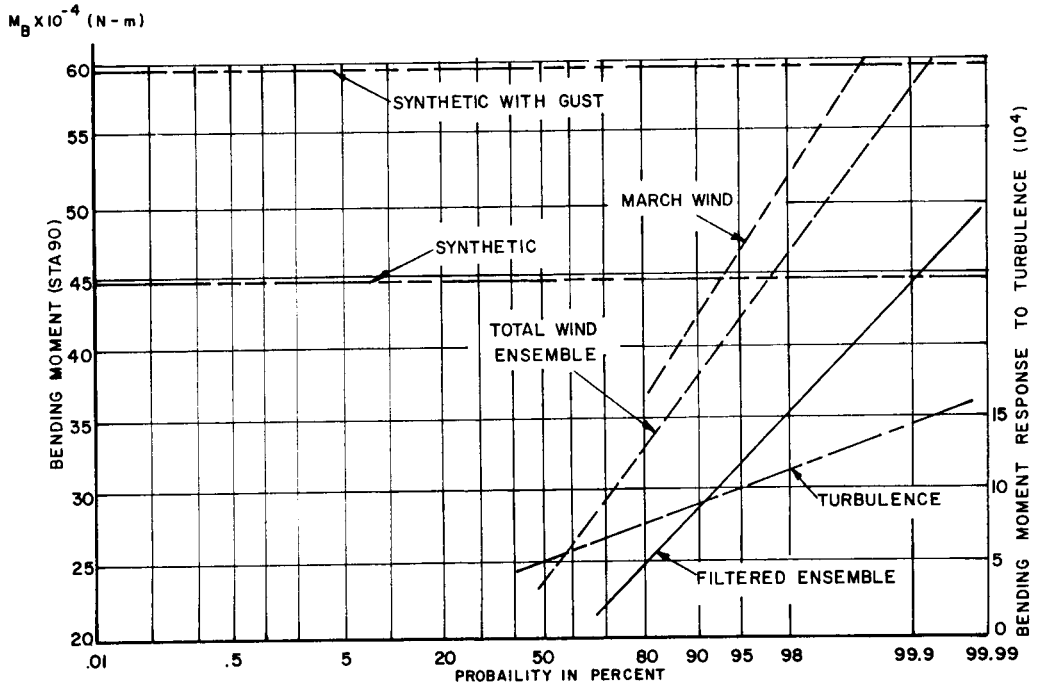

Figure 38. Bending Moment at Station 90 vs Probability of Not Exceeding

The total unit compressive load follows the same trend as the bending moment, except that the longitudinal loading dilutes the bending dynamics effect (Figures 39, 40). At station 25, turbulence contributes only about four percent to the total load. The contribution of turbulence to the total load at station 90 is approximately 10 percent.

A vehicle's bending moment or load can be influenced significantly by wind turbulence. The amount of influence is determined by the frequency characteristics of the vehicle and of the turbulence. It was shown that when these frequency conditions were met, the influence of turbulence could be related to the influence of elastic body dynamics on the total bending moment.

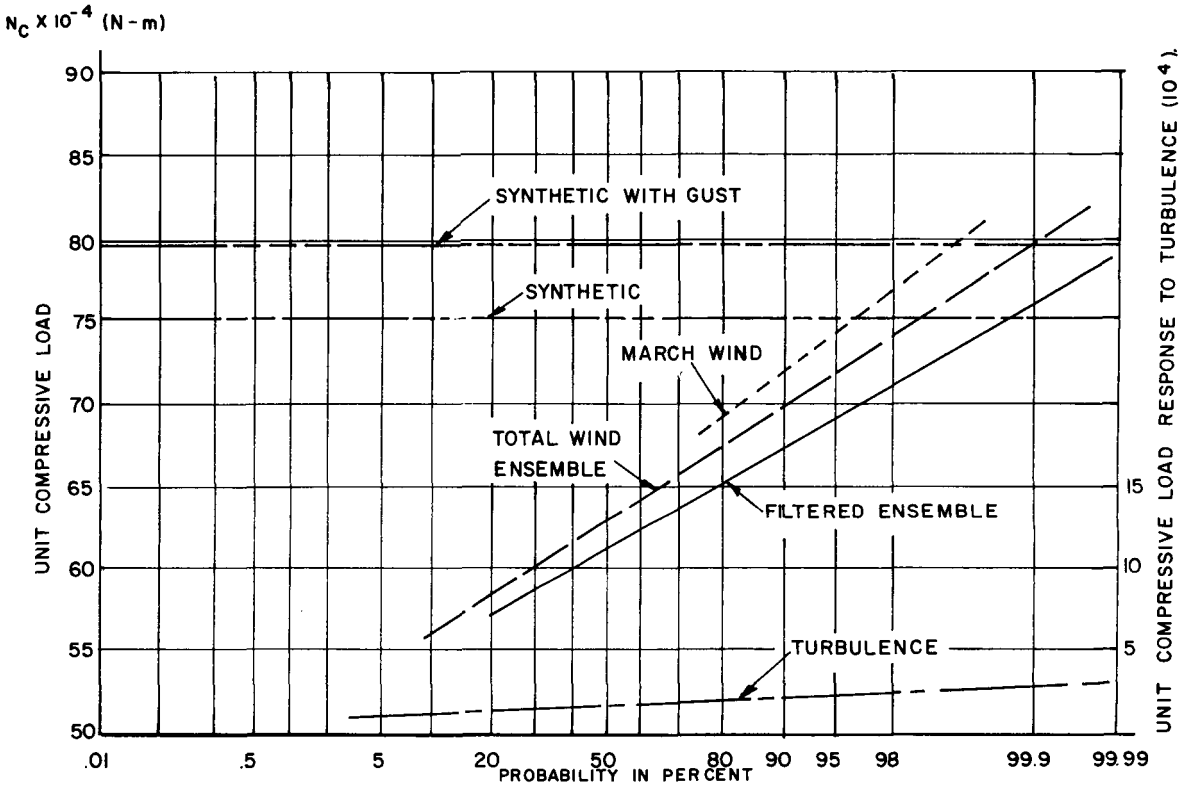

Figure 39. Total Load at Station 25 vs Probability of Not Exceeding

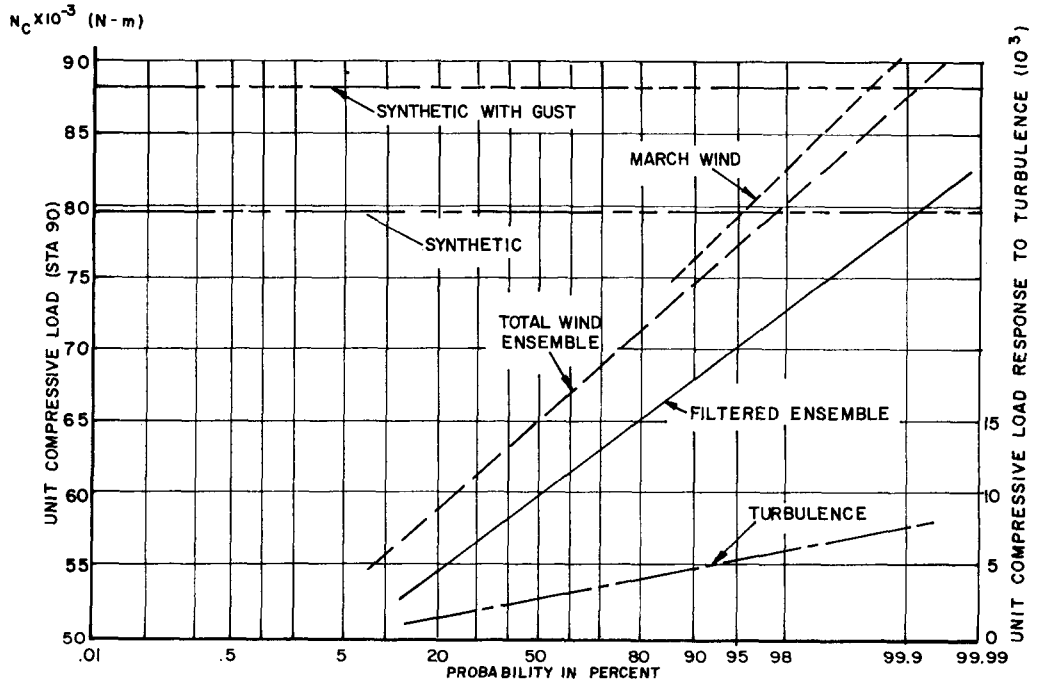

Figure 40. Total Load at Station 90 vs Probability of Not Exceeding

C. Severe Profiles

Additional insight into the turbulence effect is gained if profiles causing excessive bending moment values are isolated. Severe profiles were isolated using the bending moment at station 90. Two distinct types of profiles were found: (1) high wind magnitude and moderate wind shears, and (2) moderate wind magnitude and large wind shears. Both types of profiles were severe using the loading at station 90 as an indicator, but only the large wind magnitude profile produced severe loads at station 25.

A typical profile shows the bending moment at station 25 resulting from the high wind magnitude with only a negligible increase caused by the turbulence (Figures 41, 42). Station 90, for this same wind, shows a higher sensitivity to the turbulence compared to the mean wind magnitude. However, the influence is still moderate with the large wind speed creating a substantial part of the load.

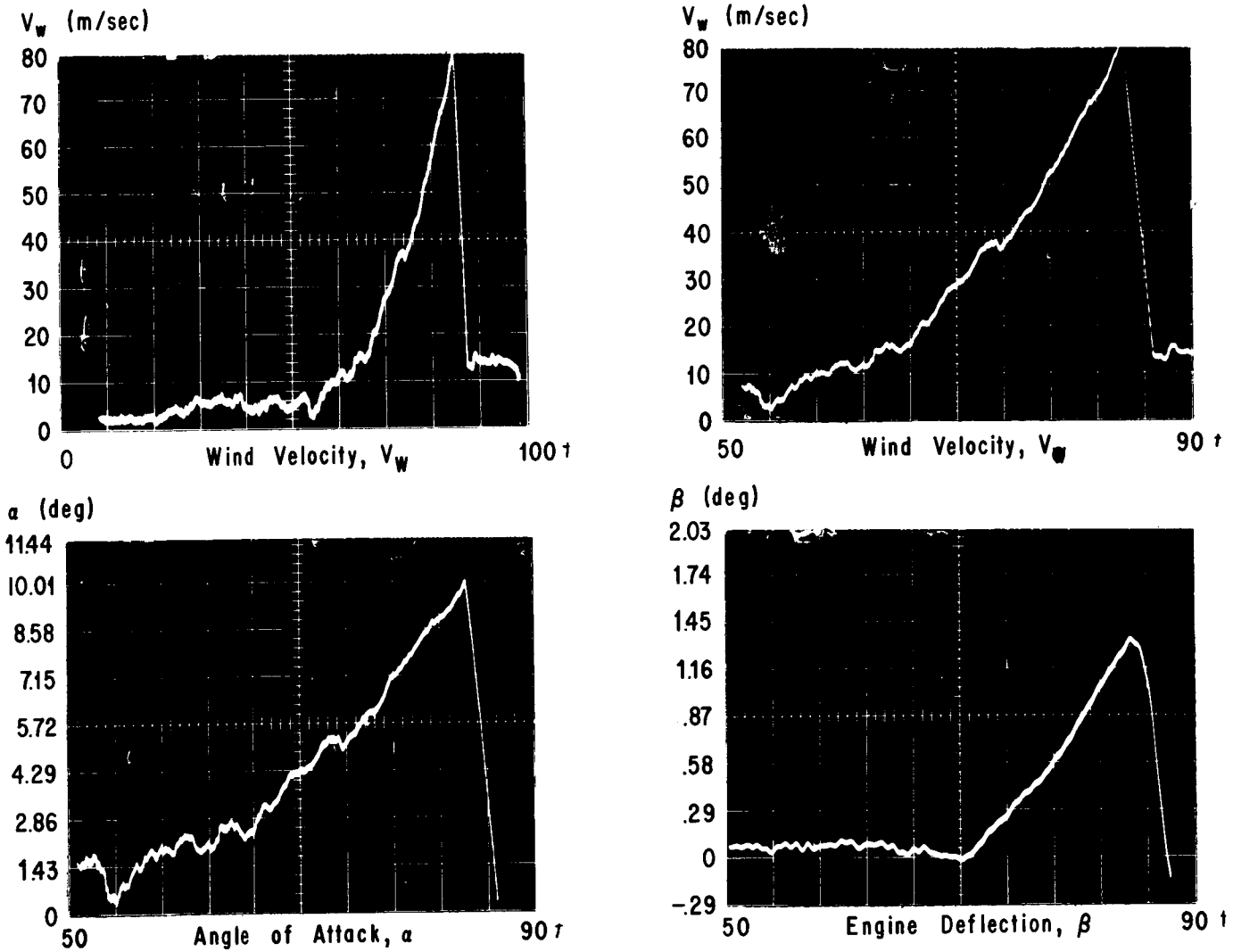

Figure 41. Vehicle Response for Wind (9/15/65 at 1:00 P.M.)

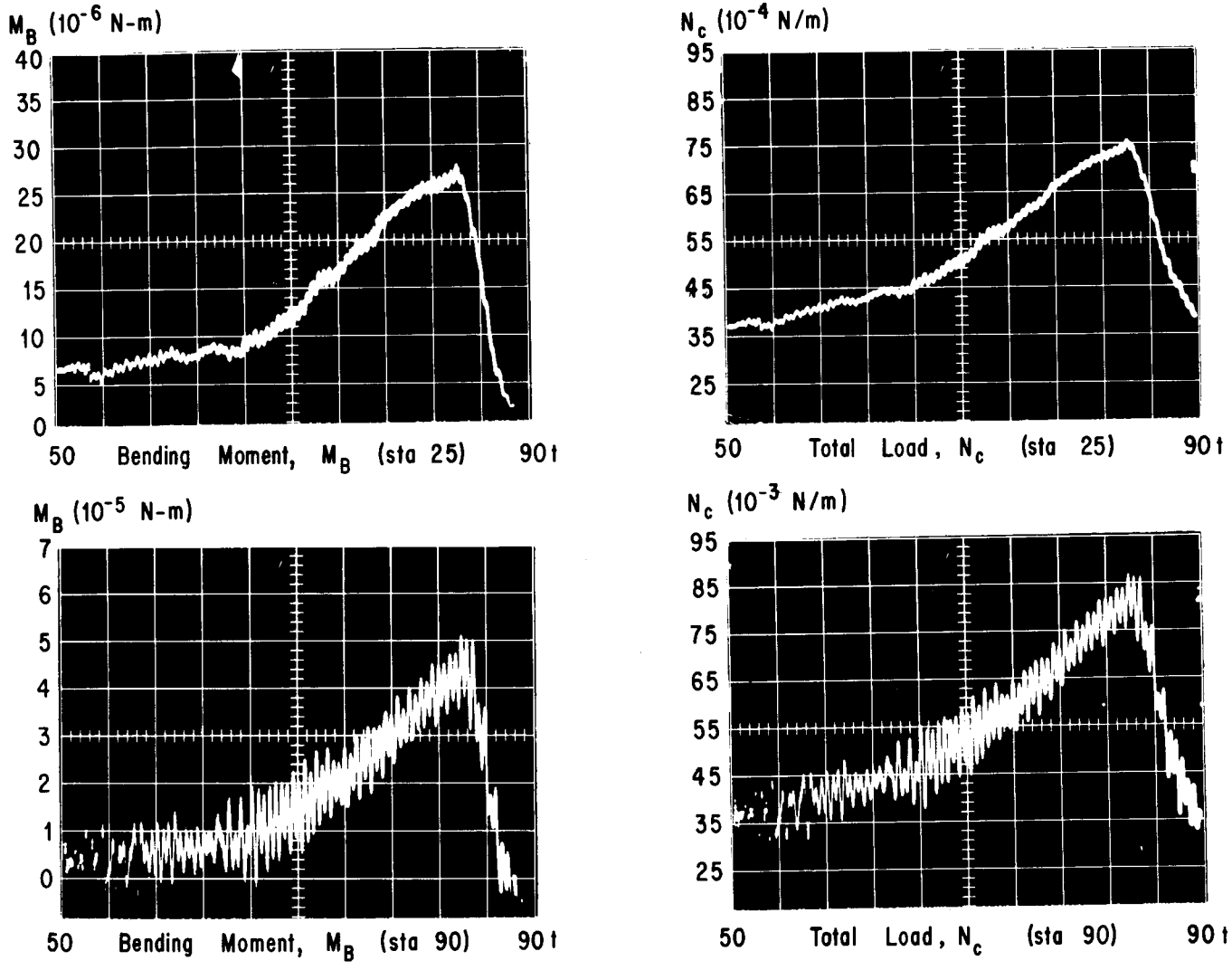

Figure 42. Vehicle Response for Wind (9/15/65 at 1:00 P.M.)

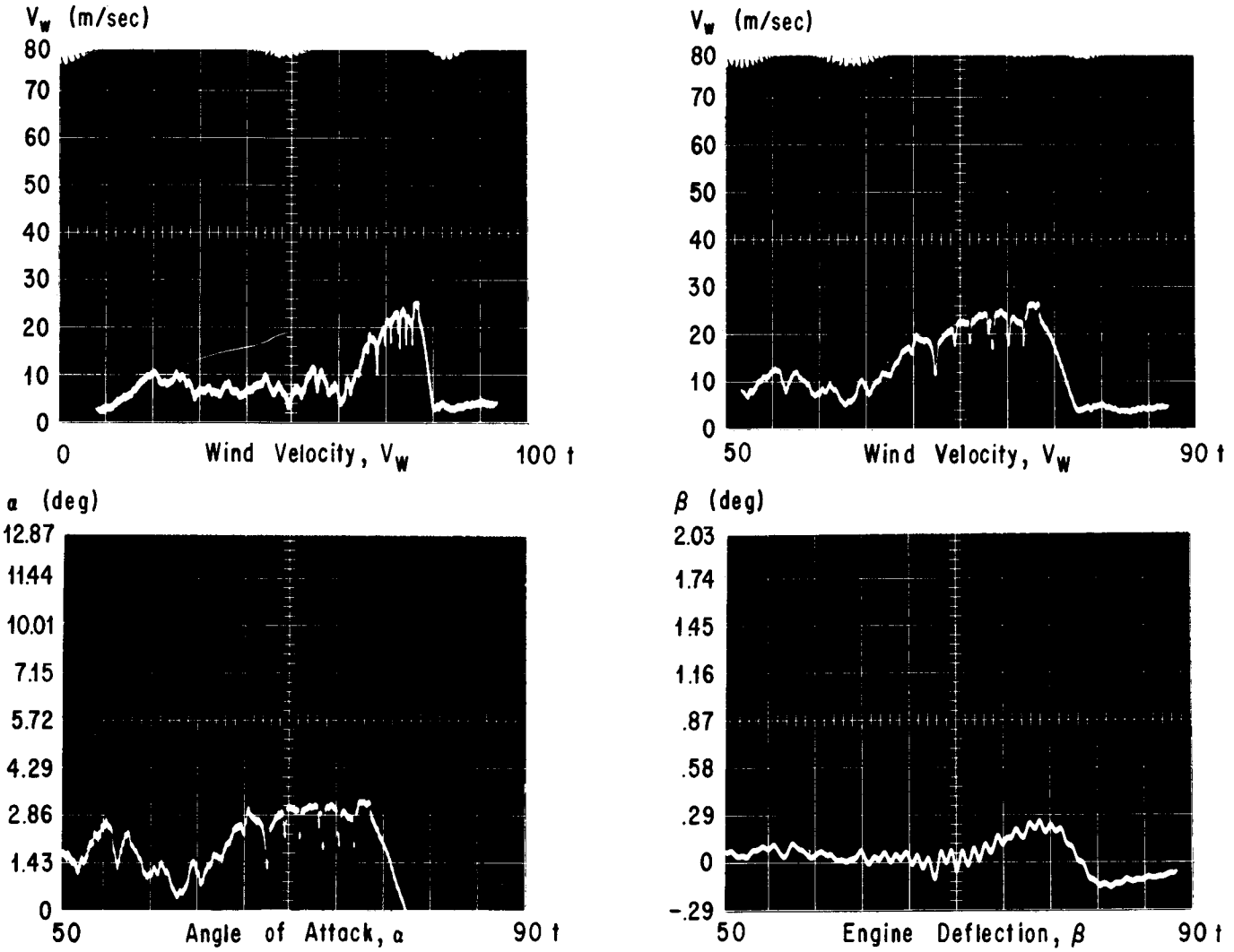

Figure 43. Vehicle Response for Wind (1/23/65 at 1:00 A.M.)

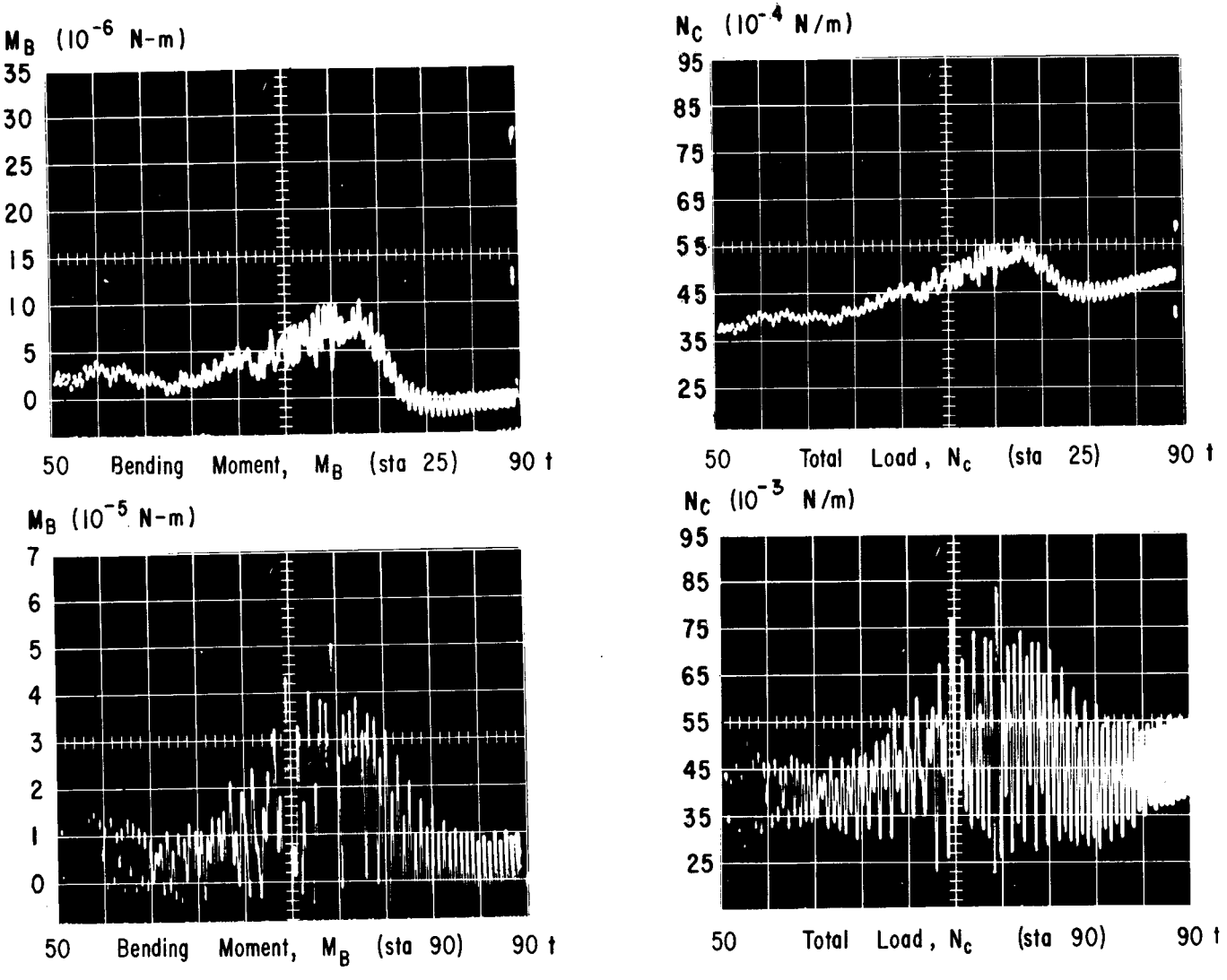

Figure 44. Vehicle Response for Wind (1/23/65 at 1:00 A.M.)

The low wind magnitude, high wind turbulence profile, found to be severe at station 90 (Figures 43, 44), shows large excitation of the bending dynamics. The small mean wind value of this profile resulted in only moderate bending moment response at station 25. This particular profile produced the largest bending moment value obtained from the whole ensemble at station 90 (5.2×10^5 Nm). The previous wind (large wind magnitude) produced a bending moment value of 4.8×10^5 Nm at this station. Of the twenty most severe wind profiles for station 90, six were of this low wind speed, large turbulence variety (Figures 43, 1A, 3A, 23A, 27A). It is obvious that this type of wind will influence operational procedures. That is, a decision to launch cannot be made on wind measurement alone; it must include prelaunch monitoring. This prelaunch monitoring simulates the vehicle flight through winds measured during various periods before the predicted launch and determines launch decisions as to structural loads versus structural capability using statistics of wind persistence (Figure 45).

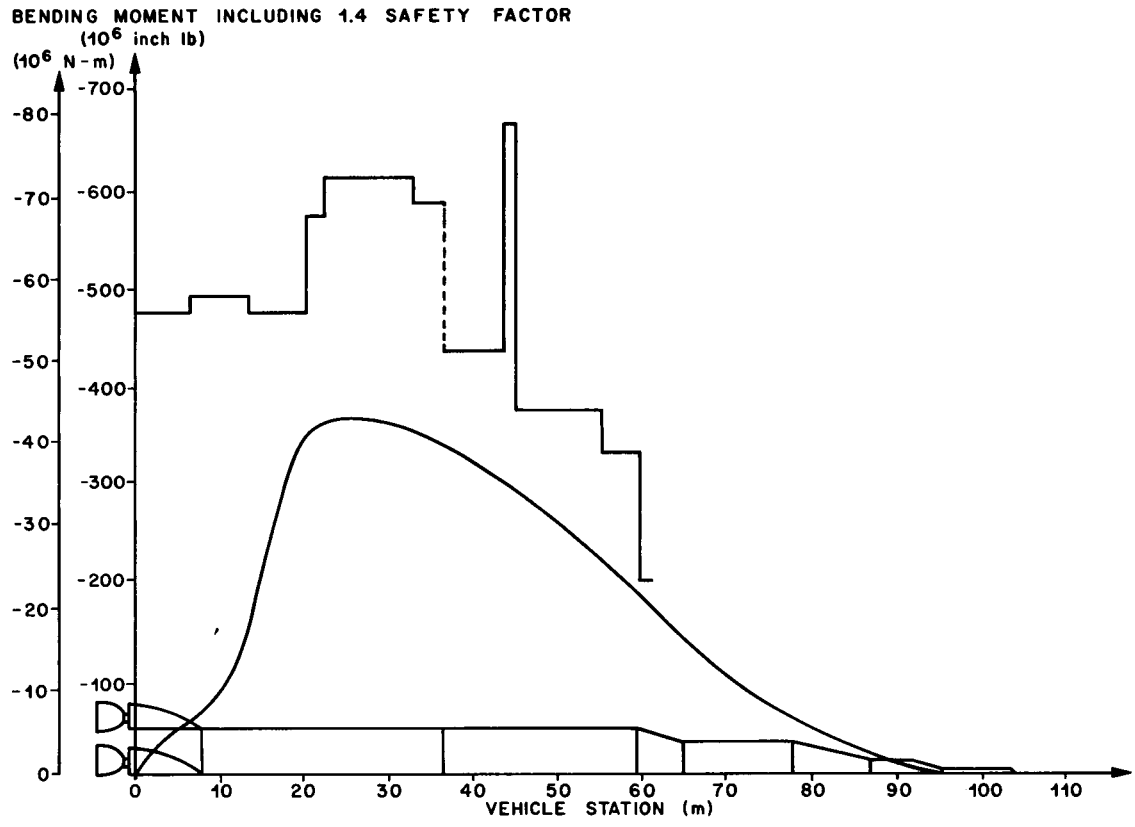

Figure 45. Saturn V Failing Moment vs Station, 70 Seconds

These results show the necessity of total vehicle simulation in prelaunch wind monitoring and show the fallacy of using wind magnitude or engine deflection and angle of attack as a criterion for making launch decisions. The additional worst profiles ranked at station 90 and the vehicle responses in the order of severity are given in the appendix. Several profiles of low wind magnitude, high wind shear occur in this upper 20 percent grouping.

The influence of these two types of wind profiles on the engine deflection and angle of attack is very pronounced. The large wind profile produces large angle of attack and engine deflections (Figures 41, 43). The low wind magnitude profile, however, produces small engine deflections and angle of attack as shown in Figures 41 and 43.

D. Small Duration Wind Disturbance Effects on Control System Optimization

The influence of wind shears on control system design is more complicated to assess than structural loads. Many factors are involved; for example, trade-off of vehicle response versus stability margins. Again, the effect of turbulence on the results corresponds to the region of high bending dynamic influence. Control gains, using an accelerometer optimized for bending moment or total load at station 25, show negligible influence of turbulence, indicating that a reasonable reduction in bending moment can be obtained by increasing the accelerometer gain, g_2. This is illustrated using the filtered and unfiltered profiles, with both showing approximately the same percentage reduction. The difference in total value is due to the higher peak winds of the unfiltered profiles (Figures 46, 47).

At station 90, the influence of turbulence is pronounced. Very little reduction in bending moment or total load is possible using the unfiltered profiles; however, the filtered profiles show a good reduction in bending moment as g_2 increases (Figures 48, 49).

The effect is summarized by plotting the 99 percent bending moment value for the three wind ensembles versus the ratio of accelerometer gain to position gyro gain (Figure 50). Also included are the results obtained using the spectrum of the turbulence. This figure shows that increasing the accelerometer gain increases the bending moment for the turbulence profile while decreasing the moment for the unfiltered and filtered ensemble, where the reduction is less for the unfiltered ensemble. Turbulence or small shears must be included if control system gains are to be optimized for forward stations. Stations where bending dynamics effects are small show very little change in the optimal gains between the filtered and unfiltered winds. The effect of small scale shears on control system design is therefore dictated by the critical vehicle station for which the gains are to be optimized.

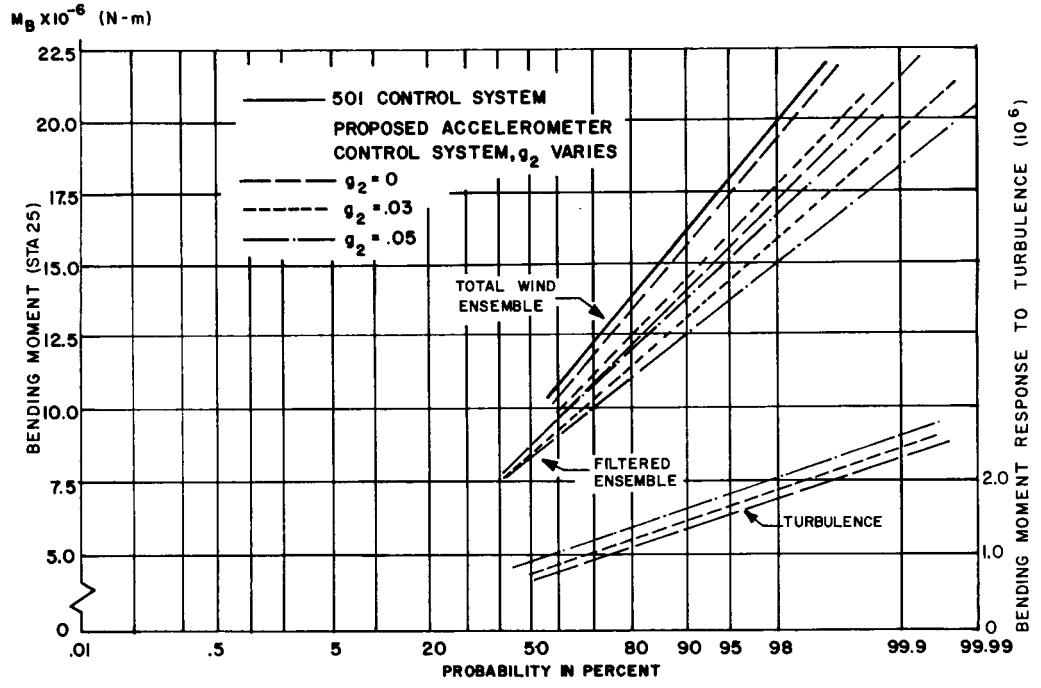

Figure 46. Bending Moment at Station 25 vs Probability of Not Exceeding for Total Wind Ensemble and Filtered Ensemble

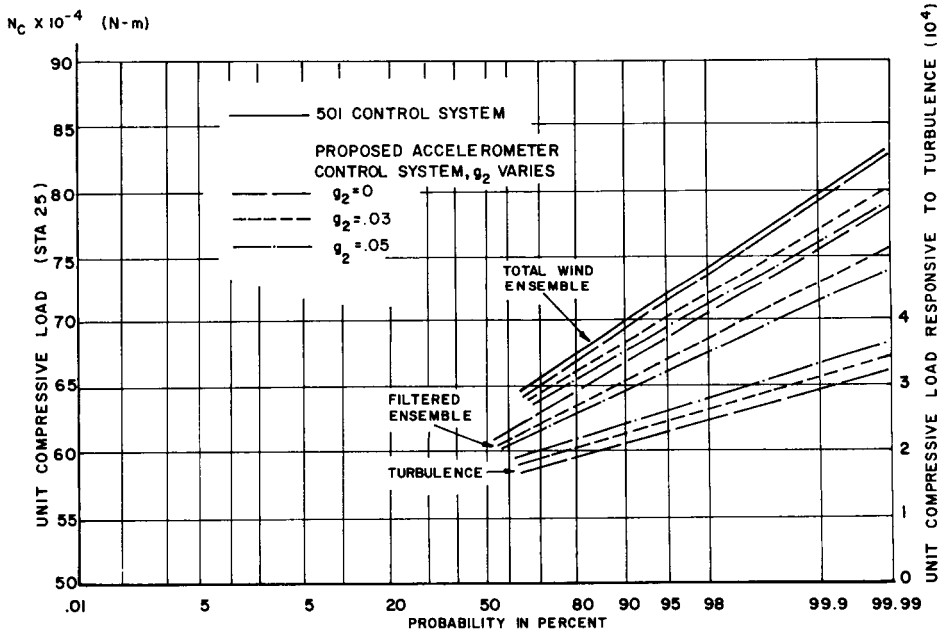

Figure 47. Total Load at Station 25 vs Probability of Not Exceeding for Total Wind Ensemble and Filtered Ensemble

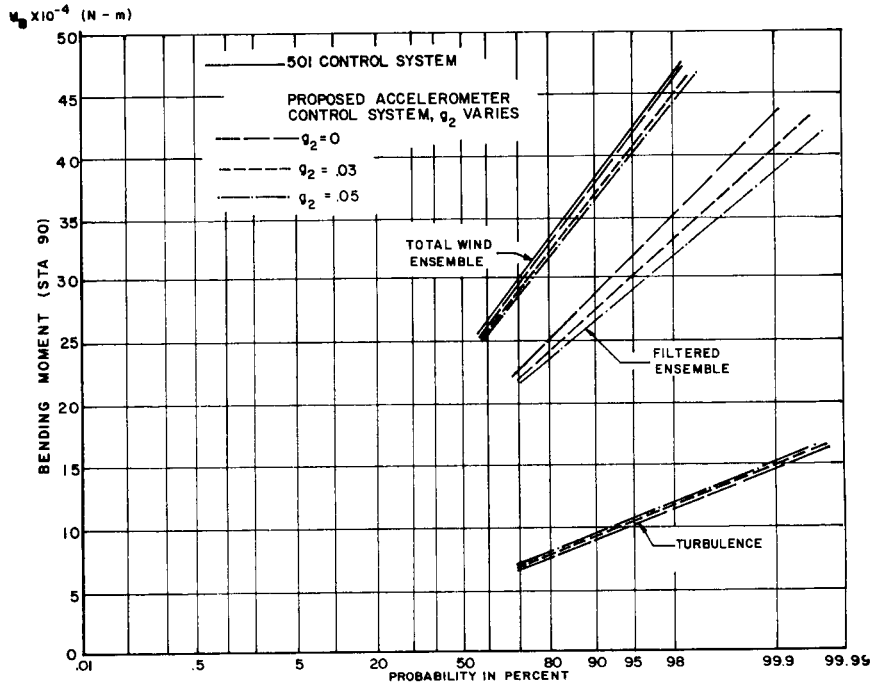

Figure 48. Bending Moment at Station 90 vs Probability of Not Exceeding For Total Wind Ensemble and Filtered Ensemble

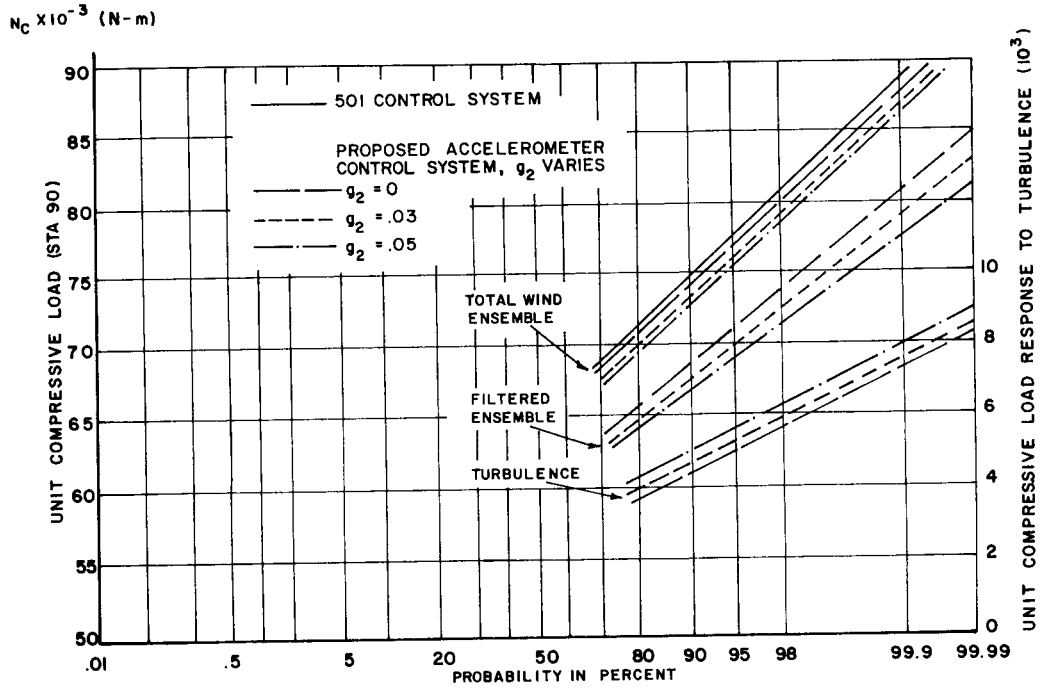

Figure 49. Total Load at Station 90 vs Probability of Not Exceeding for Total Wind Ensemble and Filtered Ensemble

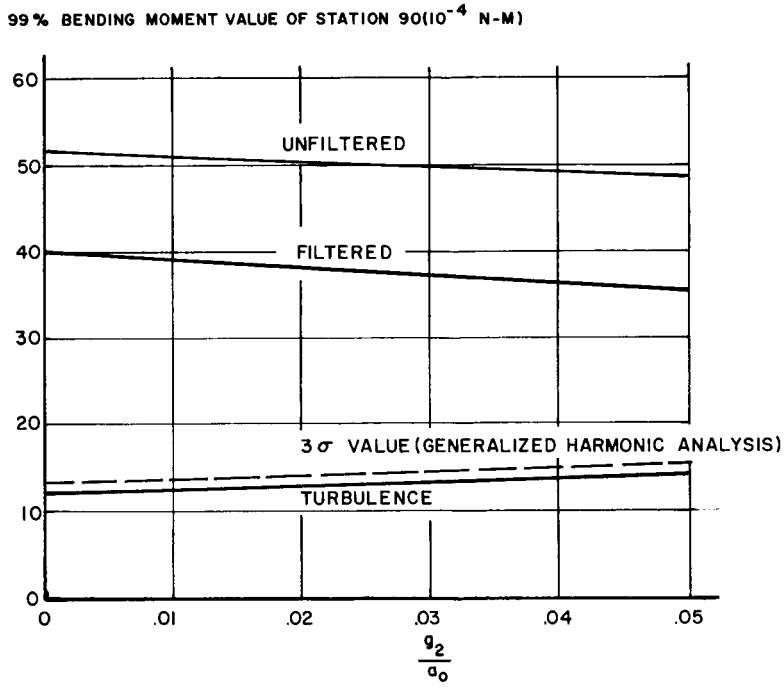

Figure 50. Comparison of Analog Results Using Detail Wind Profiles with Generalized Harmonic Analysis Using Spectrum for Turbulence

In general, this can be determined only after the structure has been designed. At this stage of design, the vehicle response is evaluated and compared to the structural design values to determine the weak areas. If the weak areas occur in the forward third of the vehicle, turbulence should be included in the final optimization of the control system.

The influence of the turbulence in optimizing the control system gains to response of engine deflection or angle of attack is shown in Figures 51 and 52. Increasing the accelerometer gain reduces the engine deflection significantly for the filtered profiles (20 percent) while for the unfiltered profiles engine deflection is reduced only 8 percent. In the turbulence ensemble, increasing g_2 increases the engine deflection about 10 percent.

There is very little influence on the angle of attack. In all cases increasing g_2 reduces the angle of attack a maximum of 10 percent.

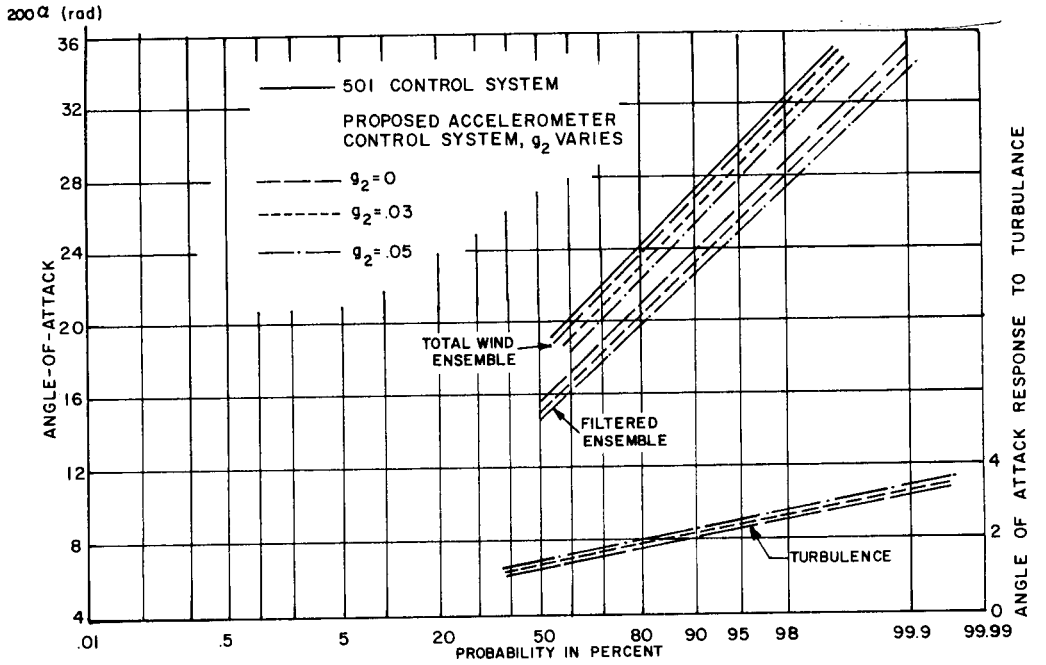

Figure 51. Engine Deflection vs Probability of Not Exceeding for Total Wind Ensemble and Filtered Ensemble

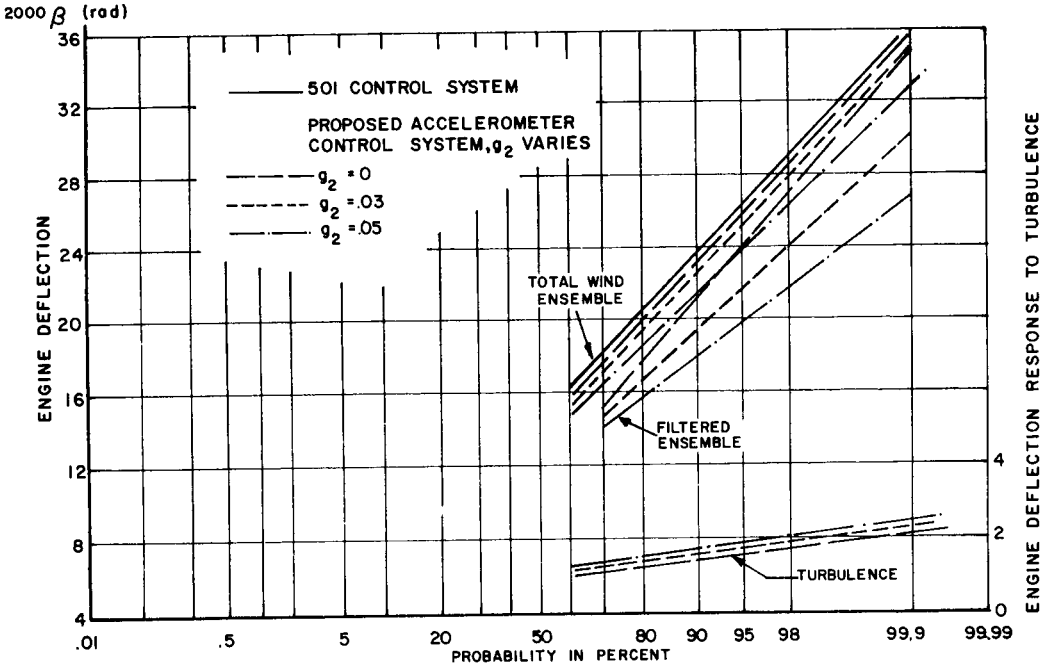

Figure 52. Angle of Attack vs Probability of Not Exceeding for Total Wind Ensemble and Filtered Ensemble

The trends are summarized on Figure 53 which shows the results obtained using a spectrum of the wind turbulence. Included in these results are the influence of the position gyro gain a_0 and the ratio of

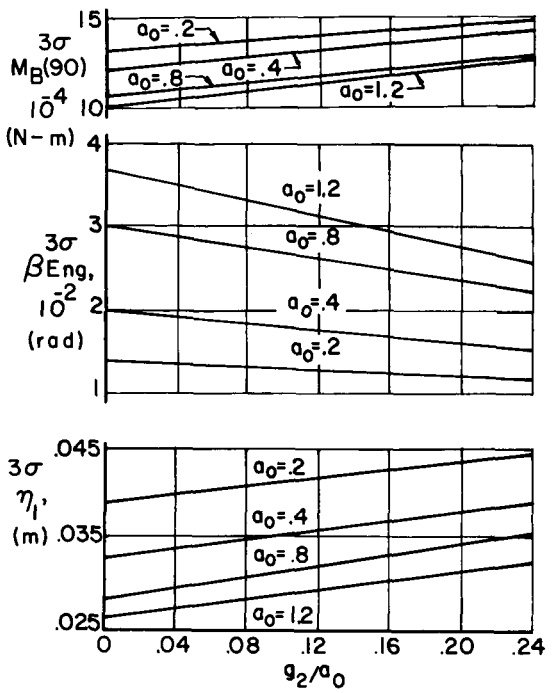

Figure 53. Effect of Control System Gains on Engine Deflection Using Spectrum of Wind Turbulence

accelerometer gain g_2 to the position gyro gain a_0. At station 90, the bending moment, engine deflection, and first bending mode deflection increase with increasing accelerometer gain g_2. Increasing the position gyro gain a_0 increases the engine deflection, but decreases the bending moment (station 90) and the first bending mode displacement.

These results show that the turbulence influences the optimization of the control system gains. Introducing angle of attack feedback in the form of α meter or accelerometer can reduce the engine response, angle of attack, bending moment and total load for steady state winds, and slowly changing shears. This same system increases the responses for turbulence alone.

These same trends can be illustrated in another manner by computing the mean and variance as a function of flight time using accelerometer gain g_2 as a parameter (Figures 54 through 59). Increasing g_2 reduces the mean response for bending moments at stations 25 and 90. In general, there is a slight increase in the variance, although this trend is not conclusive because of probable errors in computing variances on an analog computer.

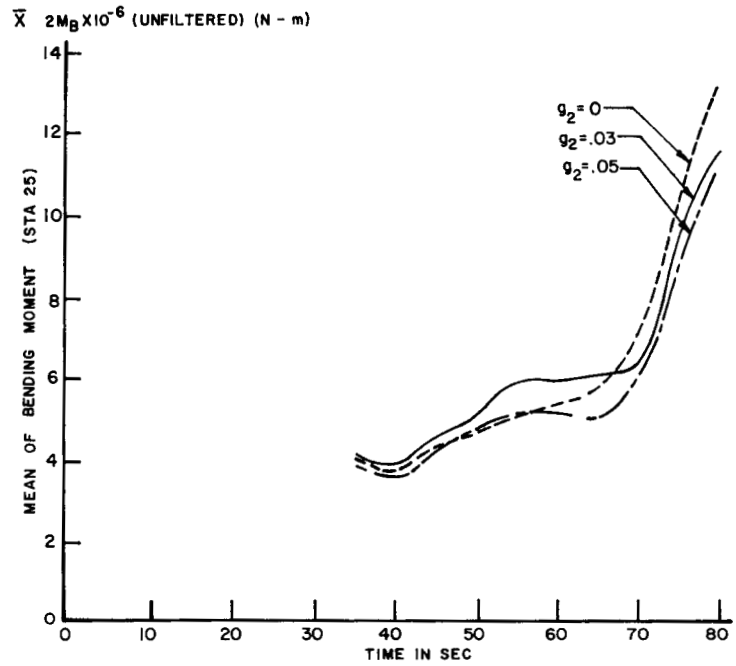

Figure 54. Mean of Bending Moment Station 25, g_2 Varies

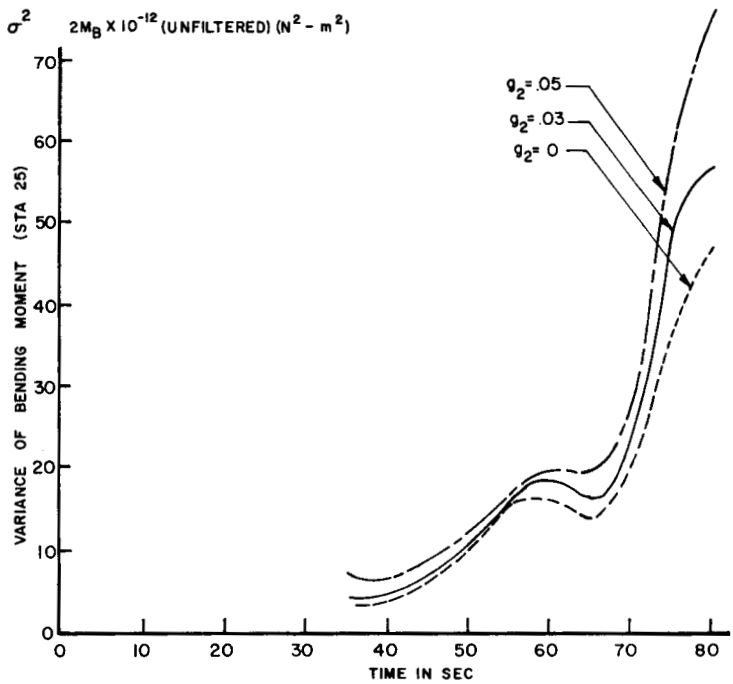

Figure 55. Variance of Bending Moment Station 25, g_2 Varies

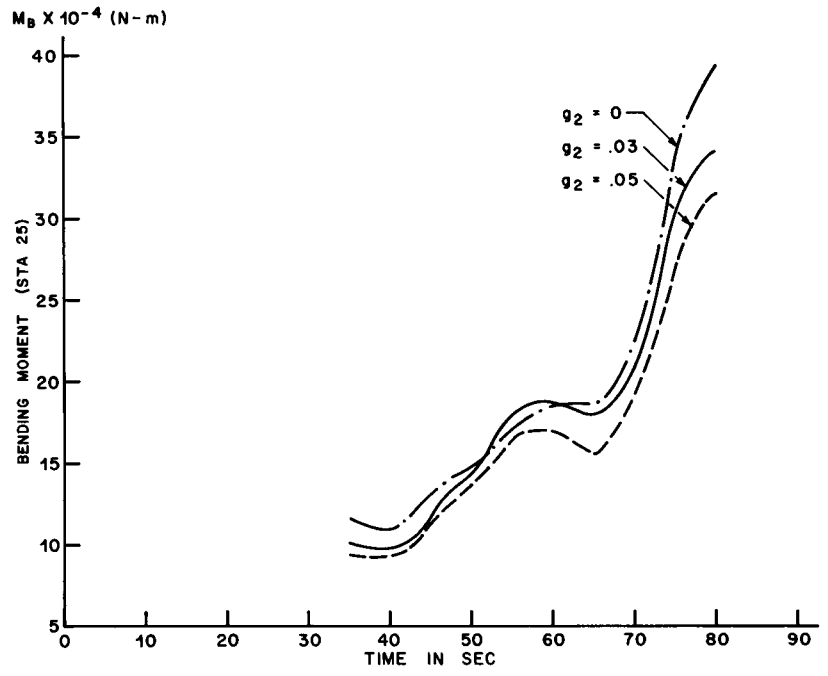

Figure 56. Mean Plus Three Times the Standard Deviation for Bending Moment (Station 25), g_2 Varies

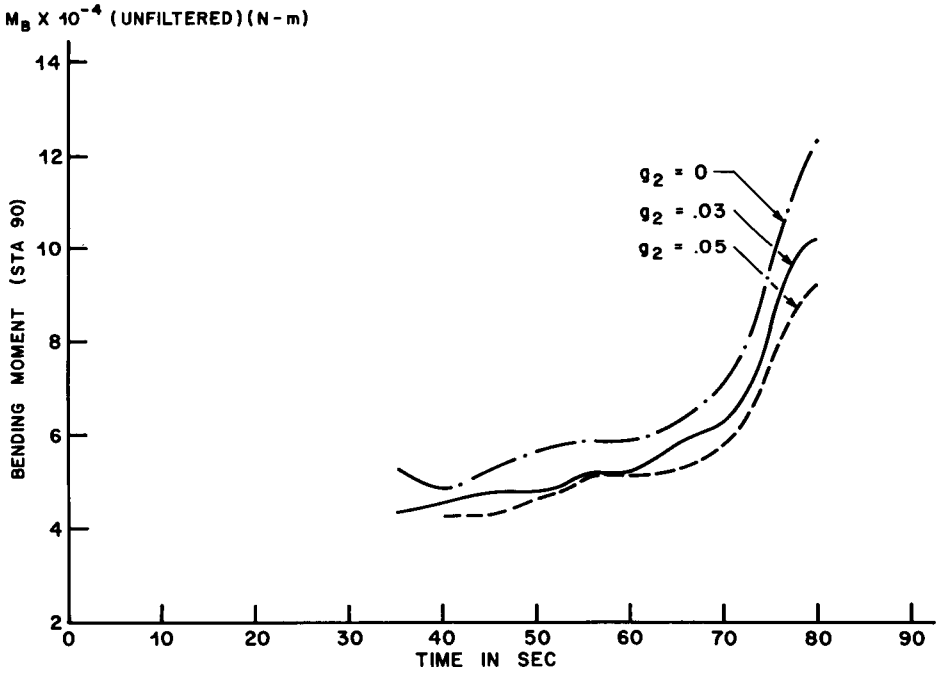

Figure 57. Mean of Bending Moment (Station 90), g_2 Varies

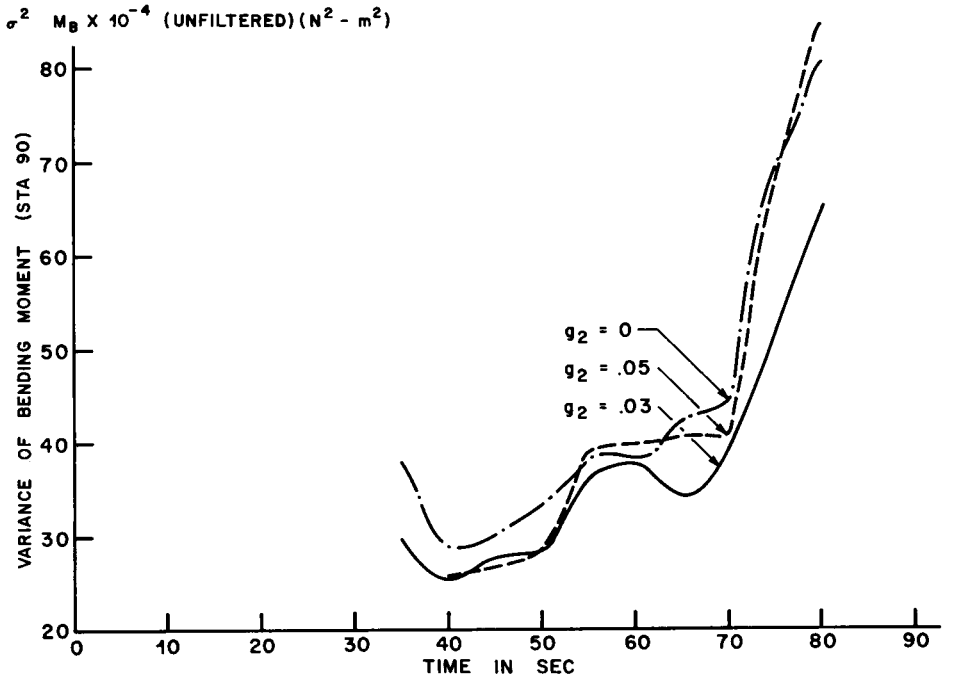

Figure 58. Variance of Bending Moment (Station 90), g_2 Varies

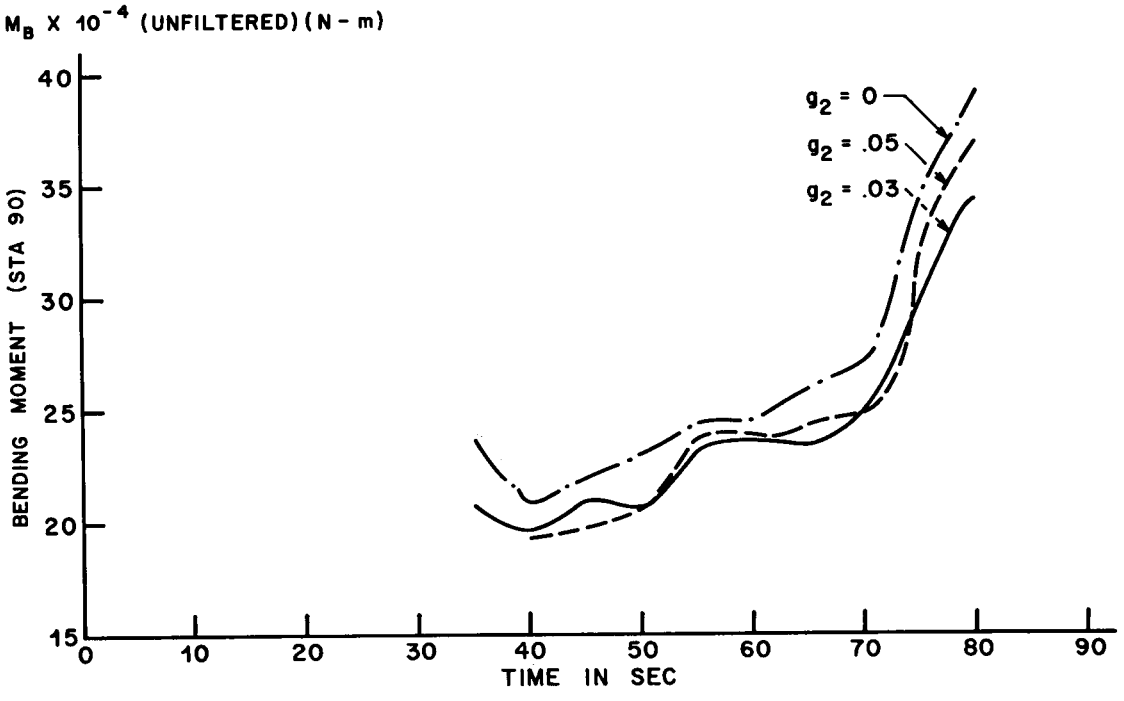

Figure 59. Mean Plus Three Times the Standard Deviation for Bending Moment (Station 90), g_2 Varies

E. Comparison of Methods

The merits of the various approaches for handling wind inputs have been illustrated by showing values obtained from (1) the synthetic profile with and without gust, (2) unfiltered, filtered and turbulence ensembles, and (3) the generalized harmonic analysis. The following tables compare the 99.8 percent values obtained from the ensembles with the synthetic profiles and the spectral analysis for an attitude control system.

Variable	Synthetic with Gust	Synthetic without Gust	Unfiltered	Filtered	Turbulence	Generalized Harmonics Analysis
α	11.74°	9.8°	11.5°	10.3°	0.86°	0.92°
β	1.17°	1.07°	1.05°	1.00°	0.055°	0.035°
$M_B^*(25)$	27	24	25.5	27	2.5	2.8
$M_B^*(90)$	0.59	0.45	0.57	0.44	0.13	0.14

*Bending moment (M_B) given in Nm x 10^6.

Acc. Gain g_2	Synthetic with Gust	Synthetic without Gust	Unfiltered	Filtered	Turbulence	Generalized Harmonics Analysis
0	0.59	0.45	0.57	0.44	0.13	0.14
0.03	0.50	0.42	0.55	0.43	0.13	0.14
0.05	0.47	0.39	0.54	0.41	0.14	0.15

*Bending moment at station 90 given in Nm x 10^6.

The values obtained from generalized harmonic analysis are slightly conservative when compared to the turbulence ensemble with the exception of the engine deflection, β. The synthetic profile with gust produced an excessive bending moment at station 90 when compared to the unfiltered ensemble. Otherwise, a good comparison is obtained between the synthetic profile (without gust) and filtered ensemble, and between

synthetic profile (with gust) and unfiltered ensemble. These results indicate that, for vehicles such as Saturn V, a good structural design could be obtained using almost any combination of approaches which accounted for the gust or turbulence.

The influence on the optimization of control systems for the various methods of handling wind inputs is determined by comparing the bending moment at station 90 for various accelerometer gains (g_2).

Comparison of the synthetic profile with the unfiltered wind ensemble at station 25 shows that the synthetic profile is a good representation of wind input for gyro control. For drift minimum control ($g_2 = 0.03$), the synthetic profile is a good representation of the wind input for the determination of the bending moment at both stations; however, for gyro control, it is too severe at station 90 where there is more sensitivity to turbulence than to wind magnitude. Also, for high load reduction accelerometer gains, the synthetic profile is too optimistic at stations that are sensitive to turbulence. The results indicate that the synthetic profile can be a very useful tool once it has been verified for a particular type of vehicle.

F. Impact of Results on Launch Vehicle Design and Flight Operations

This study of the Saturn V launch vehicle response to various aspects of detailed wind components has shown the necessity for a reorientation in the design and operational philosophy for launch vehicles. In presenting the results, it has been tacitly assumed that the reader understood the response of the vehicle to the quasi-steady or mean wind speed, as illustrated for a special wind case for the rigid vehicle. The major emphasis has been placed on the change in this basic response due to elastic vehicle dynamics and wind turbulence. This section discusses these impacts on structural design, control system optimization, and flight operations.

The only realistic approach to structural design appears to be a complete system analysis of the vehicle dynamics and control with a good representation of the wind field (magnitude, shear, and gust). This is due to the established influence of bending dynamics and turbulence on the bending moment and unit compressive load. Bending moment responses due to turbulence, in some cases are as much as 30 percent higher than indicated for the nonturbulent winds.

The MSFC design profile is a synthetic representation of the magnitude, shear, and gust of the wind. A simplified preliminary analysis can be made using a rigid body approach with the synthetic profile without gust, plus results from the elastic body system, using generalized harmonic analysis. The results obtained from the total elastic system would be added to the peak values from the rigid body

response to obtain the design value. This method would save computer time since 3σ spreads in vehicles parameters must be considered in obtaining the peak values [8]. Although this approach does not properly account for the phasing of all vehicle responses in calculating the load, the results should be more than adequate for preliminary work.

The final verification of the structural design should be made in terms of the individual profiles. The number and cross section of available profiles must be determined by the design philosophy. For example, if a worst wind magnitude month was chosen, then only the March winds would be used.

As was true for structural design in control system optimization, only a complete system analysis with complete wind statistics is acceptable. To date, the best and most accurate approach uses many detailed wind profiles for input. Here again, the choice of which profiles to use depends upon the design philosophy. The most economical approach appears to be the use of the synthetic profile with gust for a preliminary determination of the optimum gains, using the individual profiles for final adjustment and verification.

The most significant impact on philosophy appears to be in the area of flight operations. The danger of wind-biasing trajectories, based on wind magnitude, is evident. The large influence of turbulence on the load in the spacecraft could be disastrous if a wind direction reversal (opposite to bias direction) occurred simultaneously with a highly turbulent wind profile. Wind-biased trajectories must be used, therefore, in terms of the probability of the persistence of wind direction for launch date.

Setting of emergency detection system limits for astronaut safety requires the most refined vehicle model and wind data available. Since abort or near-abort conditions occur, in general, for some component failure mode, the total trajectory, vehicle dynamics, and control system must be simulated simultaneously. Because so many vehicle responses enter into the structural failure, the unit compressive and tension load for the weakest station must be used as a criterion for setting abort limits. Use of any other criteria would be misleading because of the rapidly changing relationships between response parameters during malfunctions. Generation of the unit loads simultaneously with the total simulation produces the correct phasing between these rapidly changing response conditions, thus producing the actual load experienced, and a more accurate red-lining of instruments. Since timing is critical for safety, knowledge of the influence of the total wind field is a necessity, especially since the influence of the wind on bending dynamics response is high.

Prelaunch wind monitoring is becoming an accepted procedure for making launch decisions. The use of rigid body representation for vehicle dynamics is not adequate; total elastic body must be used. Since the details of the wind turbulence has its greatest impact on this operation, they must be accurately incorporated. Accuracy of simulation and wind input does not, however, assure good launch decisions. These can only be adequately determined by comparing the induced unit load (compressive and tension) for weak stations versus the vehicle capability. The fallacy of using any criteria other than unit loads was clearly shown in the response to the most severe profiles.

CONCLUSIONS

The use of total vehicle dynamic model in conjunction with a complete statistical representation of the wind field (magnitude, shear, gust) is necessary for structural design, control system optimization, and flight operations. The influence of wind turbulence was shown to be a function of the vehicle elastic body characteristics, having influence on the load where elastic body effects were high.

APPENDIX

APPENDIX

Aerodynamic Coefficients

$$B_{ij} = \frac{1}{4D_o} \int_{-L/2}^{L/2} C'_{Z\alpha}(x)\, Y_i(x)\, Y_j(x)\, dx + \frac{1}{4}\, C_{Z\alpha f}\, Y_i(x_f)\, Y_j(x_f)$$

$$C_{ij} = \frac{1}{4D_o} \int_{-L/2}^{L/2} C'_{Z\alpha}(x)\, Y_i(x)\, Y'_j(x)\, dx + \frac{1}{4}\, C_{Z\alpha f}\, Y_i(x_f)\, Y_j(x_f)$$

$$D_{i_{or j}} = \frac{1}{4D_o} \int_{-L/2}^{L/2} C'_{Z\alpha}(x)\, Y_j(x)\, dx + \frac{1}{4}\, C_{Z\alpha f}\, Y_j(x_f)$$

$$\bar{D}_{i_{or j}} = \frac{1}{4D_o} \int_{-L/2}^{L/2} C'_{Z\alpha}(x)\, Y_j(x)\, \bar{X}(x)\, dx + \frac{1}{4}\, C_{Z\alpha f}\, Y_j(x_f)$$

$$E_i = \frac{1}{4D_o} \int_{-L/2}^{L/2} C'_{Z\alpha}(x)\, Y'_j(x)\, dx + \frac{1}{4}\, C_{Z\alpha f}\, Y'_j(x_f)$$

$$\bar{E}_i = \frac{1}{4D_o} \int_{-L/2}^{L/2} C'_{Z\alpha}(x)\, Y'_j(x)\, \bar{X}(x)\, dx + \frac{1}{4}\, C_{Z\alpha f}\, Y'_j(x_f)\, \bar{X}(x_f)$$

$$F_k = \frac{1}{4D_o} \int_{-L/2}^{L/2} C'_{Z\alpha}(x)\, \bar{x}^k \, dx + \frac{1}{4} C_{Z\alpha f}\, \bar{x}_f^k \qquad k = 0, 1, 2$$

$$C_1 = \frac{-2Q\, F_1}{I} \qquad C_2 = \frac{-F_s\, \bar{x}_E}{I}$$

$$K_1 = \bar{g} \qquad K_2 = \frac{2Q\, F_o}{m} \qquad K_3 = F_s/m$$

Bending Moment Coefficients

$$M'_\alpha = \frac{q_s}{D_o} \int_{x_k}^{x_v} C'_{Z\alpha}(x - x_k)\, dx - K_2 \int_{x_k}^{x_v} m'(x)\, (x - x_k)\, dx$$

$$- C_1 \int_{x_k}^{x_v} m'(x)\, (x - x_k)\, (x - x_{cg})\, dx.$$

$$M'_\beta = -K_2 \int_{x_k}^{x_v} m'(x)\, (x - x_k)\, dx + C_2 \int_{x_k}^{x_v} m'(x)(x - x_k)(x - x_{cg})\, dx$$

$$M'_{\xi_i} = \frac{m_{si}}{m} \int_{x_k}^{x_v} m'(x)\, (x - x_k)\, dx + \frac{m_{si}}{I} (x_{si} - x_{cg}) \int_{x_k}^{x_v} m'(x)(x - x_k)(x - x_{cg})\, dx$$

$$- m_{si}\, (x_{si} - x_k)$$

$$M'_{\ddot{\eta}_i} = - \int_{x_k}^{x_v} m'(x)\ (x - x_k)\ Y_i(x)\ dx$$

Miscellaneous Definitions

$$\varphi_i = \varphi + \sum_{j=1}^{n} \eta_j\ Y'_j(x_\varphi)$$

$$\dot{\varphi}_i = \dot{\varphi} + \sum_{j=1}^{n} \dot{\eta}_j\ Y'_j(x_g)$$

$$\alpha_i = \varphi - \frac{\dot{y}}{V} + \sum_{j=1}^{n} \eta_j\ Y'_j(x_\alpha) - \sum \frac{\dot{\eta}_j\ Y_j}{V}(x_\alpha) - \frac{\bar{X}_\alpha \dot{\varphi}}{V} + \frac{V_w}{V}$$

Control Frequency

$$\omega_c = \sqrt{(a_o + b_o)\ C_1 + C_2}$$

Control Frequency Damping

$$2\zeta_c \omega_c = a_1 C_2$$

Rigid Angle of Attack

$$\alpha = \varphi - \frac{\dot{y}}{V} + \frac{V_w}{V}$$

Equations of Motion

Translation

$$\left(m + m_E\right)\ddot{y} + \left[-S_E\, Y_j'(x_E) + M_E\, Y_j(x_E)\right]\ddot{\eta}_j + M_{fs}\,\ddot{\xi}_s - S_E\ddot{\beta}_E + \frac{2Q}{V}\,F_1\dot{\phi}$$

$$- \left[(m + m_E)g\right]\varphi + \frac{2Q}{V}\,D_j\,\dot{\eta}_j - \left[2QE_j + (m + m_E)\,\bar{g}\,Y_j'(x_E)\right]\eta_j$$

$$- F_s\beta_E = \frac{2Q}{V}\,F_o\alpha.$$

Rotation

$$(I - I_{corr})\ddot{\phi} + \left[(\theta_E - S_E\bar{x}_E)\,Y_j'(x_E) - S_E Y_j(x_E) + m_E\bar{x}_E\,Y_j(x_E)\right]\ddot{\eta}_j$$

$$- m_{fs}\,\bar{x}_{fs}\,\ddot{\xi}_s + (\theta_E - S_E\bar{x}_E)\,\ddot{\beta}_E + \frac{2QF_2}{V}\,\dot{\phi} + \frac{2Q}{V}\,\bar{D}_j\dot{\eta}_j$$

$$- \Big\{m_E\bar{g}\,Y_j(x_E) - S_E\bar{g}\,Y_j'(x_E) + 2Q\bar{E}_j + m_E\,\bar{g}\,Y_j(x_E)$$

$$- (m + m_E)\bar{g}\,\bar{x}_E\,Y_j'(x_E)\Big\}\eta_j - m_{fs}\,\bar{g}\,\xi_s + (S_E\bar{g} - F_s\bar{x}_E)\,\beta_E$$

$$= + \frac{2Q}{V}\,F_1\alpha.$$

Swivel Engine

$$\frac{S_E\ddot{y}}{\theta_E} + \left(1 - \frac{S_E\bar{x}_E}{\theta_E}\right)\ddot{\varphi} - \left[Y'_j(x_E) + \frac{S_E\, Y_j(x_E)}{\theta_E}\right]\ddot{\eta}_j + \ddot{\beta}_E + \frac{S_E\bar{g}}{\theta_E}\,\varphi + \frac{S_E\bar{g}}{\theta_E}\; Y'_j(x_E)\;\eta_j$$

$$+ 2\zeta_E\omega_E\dot{\beta}_E + \left(\omega_E^2 + \frac{S_E\bar{g}}{\theta_E}\right)\beta_E - 2\zeta_E\omega_E\dot{\beta}_c - \omega_E^2\beta_c = 0.$$

Control Equation

$$m_2\ddot{\beta}_c + m_1\dot{\beta}_c + \beta_c = a_o\left[\varphi + \sum_{j=1}^{n} Y'_j(x_\varphi)\;\eta_j\right] + a_1\left[\dot{\varphi} + \sum_{j=1}^{n} Y'_j(x_g)\;\dot{\eta}_j\right]$$

$$+ b_o\left[\varphi - \frac{\dot{y}}{V} + \sum_{j=1}^{n} Y'_j(x_\alpha)\;\eta_j - \sum_{j=1}^{n}\frac{\dot{\eta}_j}{V}\,Y_j(x_\alpha) - \frac{\bar{x}_\alpha\dot{\varphi}}{V} + \frac{V_w}{V}\right].$$

Rate Gyro

$$\frac{\ddot{\theta}_i}{\omega_g^2} + \frac{2\zeta_g}{\omega_g}\,\dot{\theta}_i + \theta_i = \dot{\varphi}_g = \dot{\varphi} + \sum_{j=1}^{n}\dot{\eta}_j\; Y'_j(x_g).$$

α-Meter

$$\ddot{\alpha}_i + 2(\zeta_A + \zeta_m)\;\omega_\alpha\,\dot{\alpha}_i + \omega_\alpha^2\,\alpha_i = \ddot{\varphi} + \left(2\zeta_A\omega_\alpha - \frac{\bar{x}_\alpha}{V}\;\omega_\alpha^2\right)\dot{\varphi}$$

$$+ \sum_{j=1}^{n}(\ddot{\eta}_j + 2\zeta_A\;\omega_\alpha\,\dot{\eta}_j + \omega_\alpha^2\,\eta_j)\;Y'_j(x_\alpha) - \frac{\omega_\alpha^2}{V}\sum_{j=1}^{n}\dot{\eta}_j\;Y_j(x_\alpha) - \frac{\omega_\alpha^2}{V}\,\dot{y}.$$

Bending

$$\left[m_E\, Y_i(x_E) - S_E Y_j'(x_E)\right]\ddot{y} + \left[\; m_E(\bar{x}_E - \ell_E)\, Y_i(x_E) + Y_j'(x_E)(\theta_E - S_E\bar{x}_E)\right]\ddot{\varphi}$$

$$+ M_{Bi}\ddot{\eta}_i + \left\{m_E\, Y_i(x_E)\left[\ell_E\, Y_j'(x_E) + Y_j(x_E)\right] + Y_i'(x_E)\left[\theta_E\, Y_j'(x_E)\right.\right.$$

$$\left.\left. - S_E Y_j(x_E)\right]\right\}\ddot{\eta}_j + m_{fs}\, Y_i(x_s)\,\ddot{\xi}_s + \left[- S_E Y_i(x_E) + \theta_E Y_i'(x_E)\right]\ddot{\beta}_E$$

$$+ 2\,\frac{Q\bar{D}_i}{V}\,\dot{\varphi} - \left[m_E\bar{g}\, Y_i(x_E) - S_E\bar{g}\, Y_i'(x_E)\right]\varphi$$

$$+ 2\omega_{Bi}\, M_{Bi}\,\zeta_{Bi}\,\dot{\eta}_i + \left[\frac{2Q}{V}\, B_{ij}\right]\dot{\eta}_j + \omega_{Bi}^2\, M_{Bi}\,\eta_i + \left[-m_E\bar{g}\, Y_i(x_E)\, Y_j'(x_E)\right.$$

$$\left. - m_E\bar{g}\, Y_i'(x_E)\, Y_j(x_E) + S_E\bar{g}\, Y_j'(x_E)\, Y_i'(x_E) - 2QC_{ij}\right]\eta_j$$

$$- \left[+\bar{g}\, m_{fs}\, Y_i'(x_{fs})\right]\xi_s + \left[S_E\bar{g}\, Y_i'(x_E) - F_s\, Y_i(x_E)\right]\beta_E = 2\,\frac{Q}{V}\, D_i\alpha.$$

Fuel Sloshing

$$\ddot{y} + \bar{x}_{fs}\ddot{\varphi} + Y_j(x_{fs})\,\ddot{\eta}_j + \ddot{\xi}_s - \bar{g}\varphi - \left[\;\bar{g}\, Y_j'(x_{fs})\right]\eta_j + \left[+\, 2\omega_{fs}\,\zeta_{fs}\right]\dot{\xi}_s$$

$$+ \omega_{fs}^2\,\xi_s = 0.$$

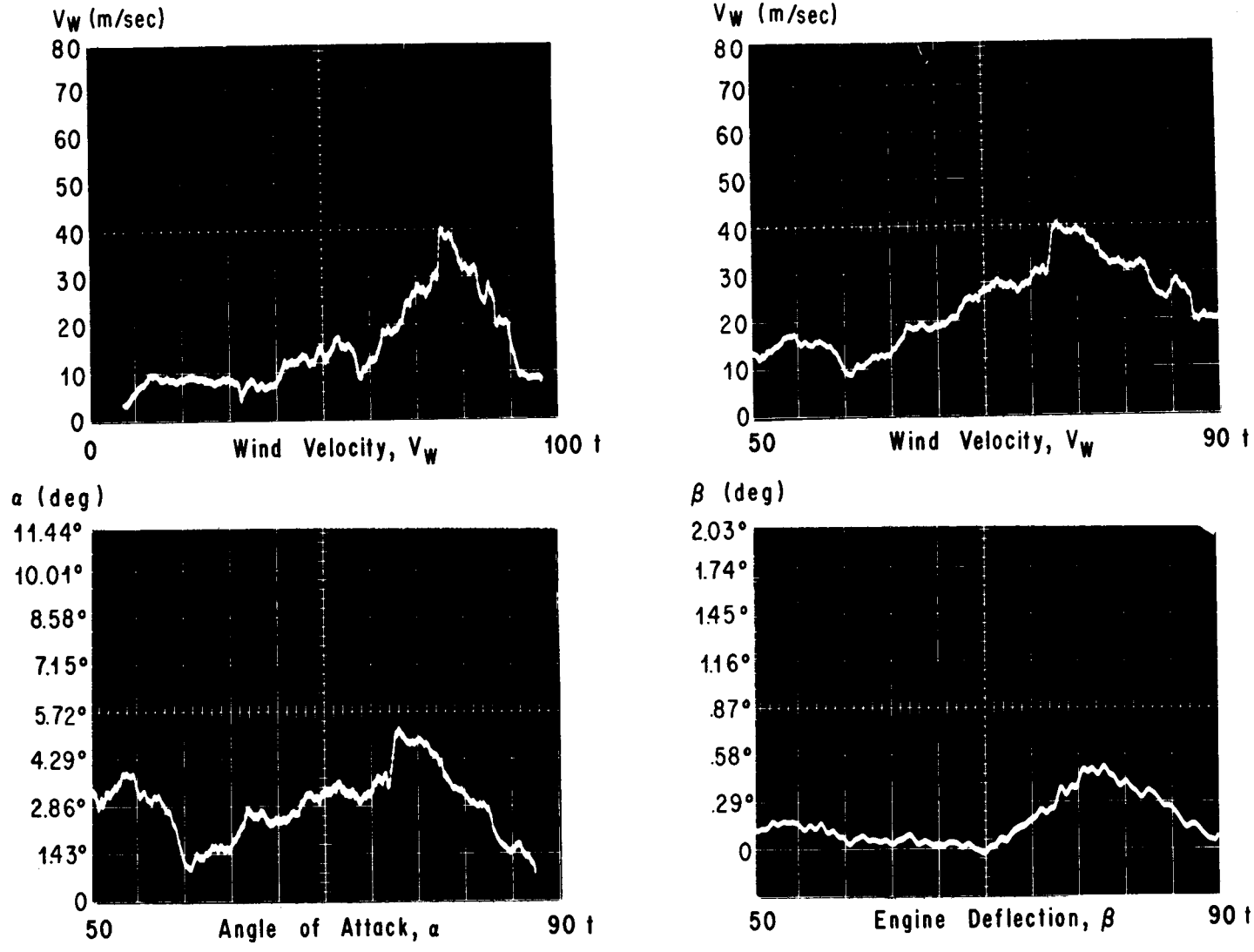

FIG. 1A. VEHICLE RESPONSE FOR WIND (2/15/65 AT 9:13 P.M.)

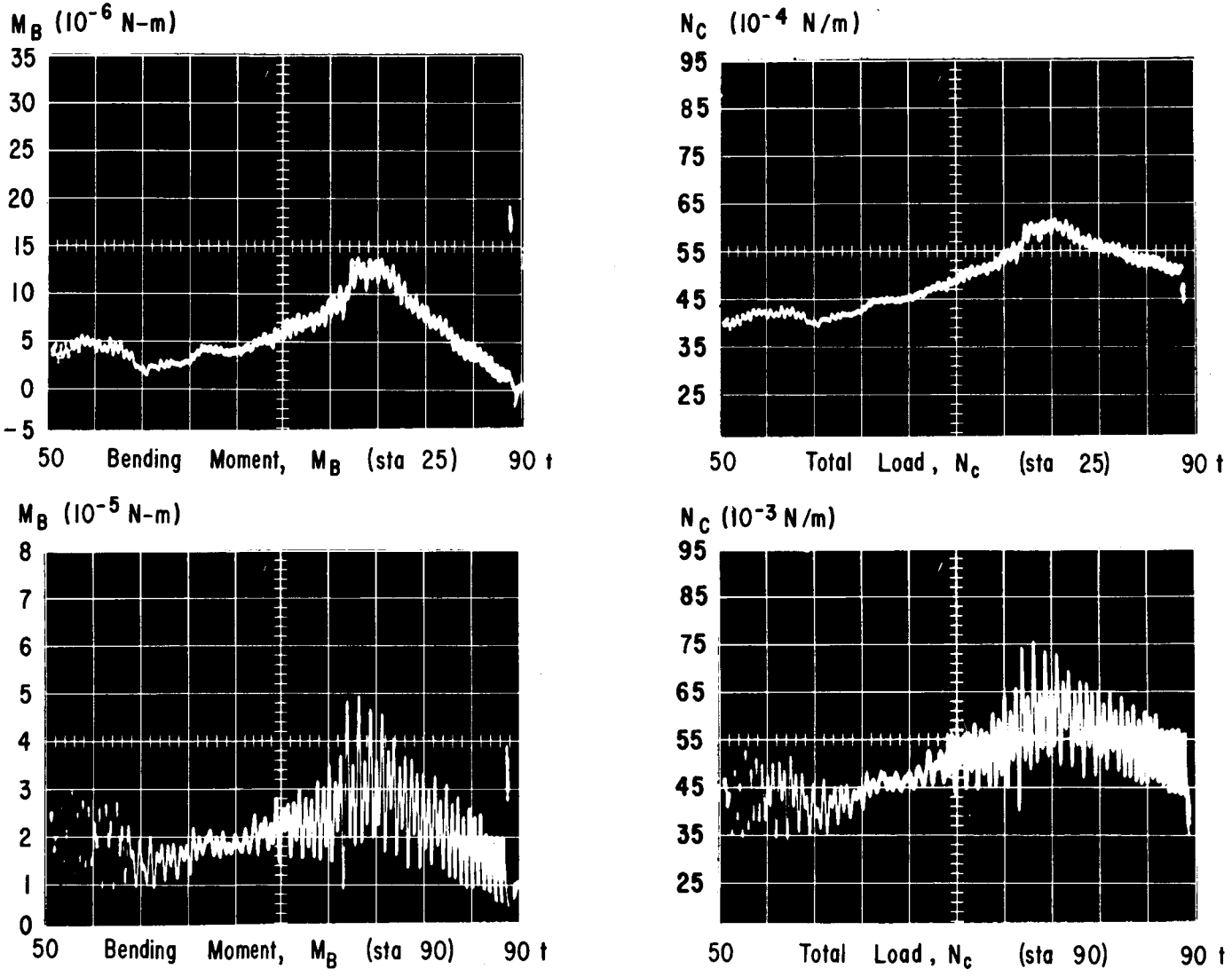

FIG. 2A. VEHICLE RESPONSE FOR WIND (2/15/65 AT 9:13 P.M.)

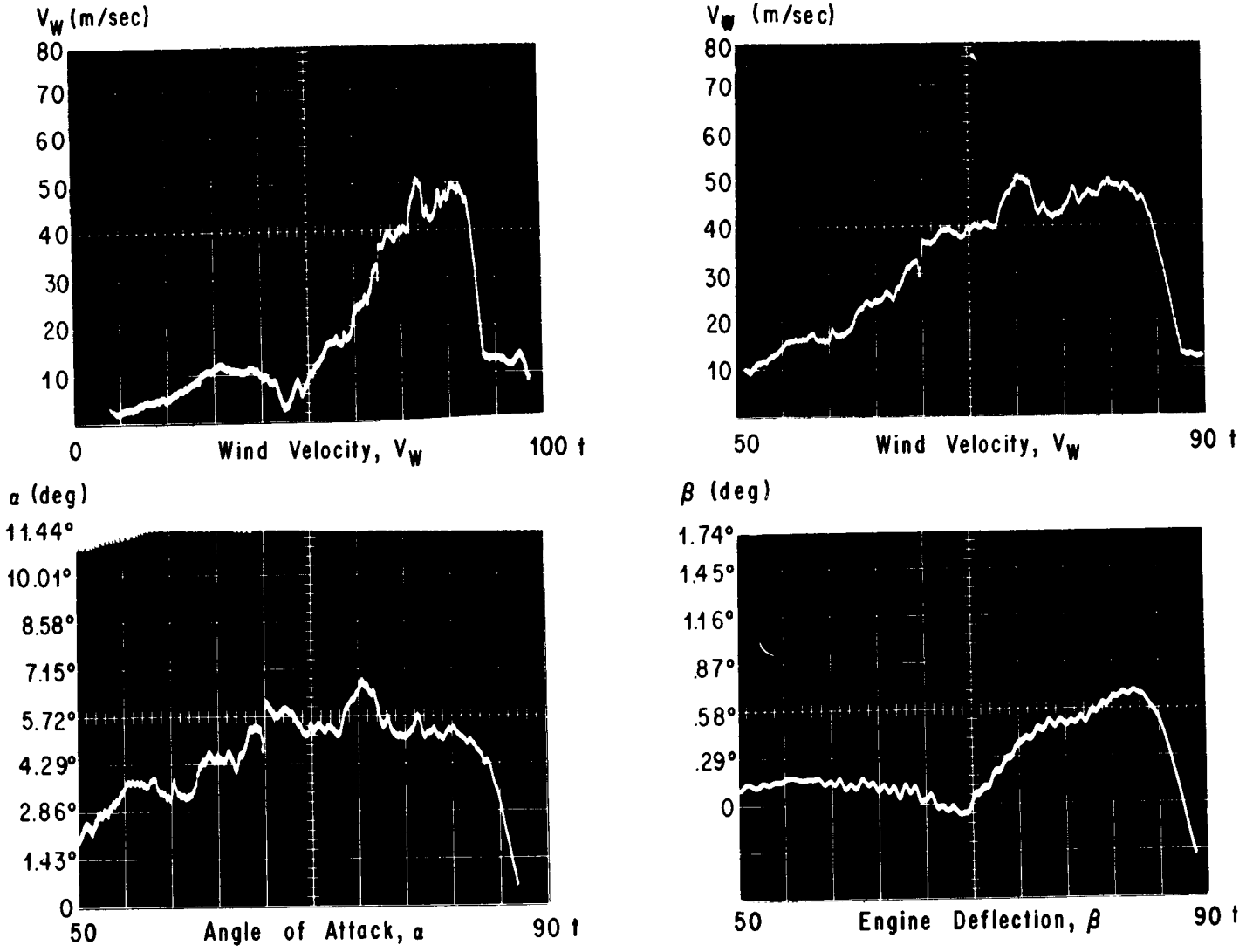

FIG. 3A. VEHICLE RESPONSE FOR WIND (1/4/65 AT 1:00 A.M.)

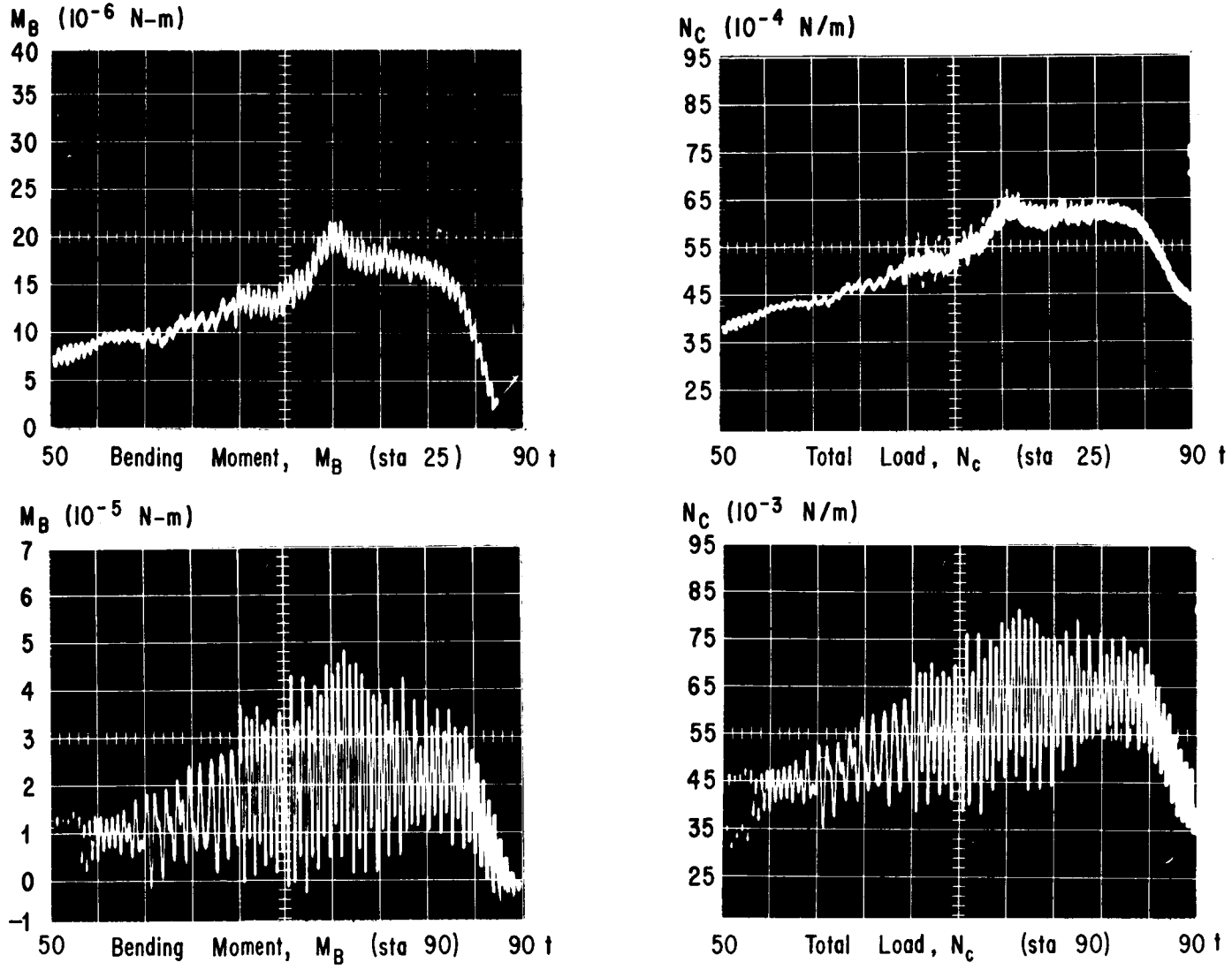

FIG. 4A. VEHICLE RESPONSE FOR WIND (1/4/65 AT 1:00 A.M.)

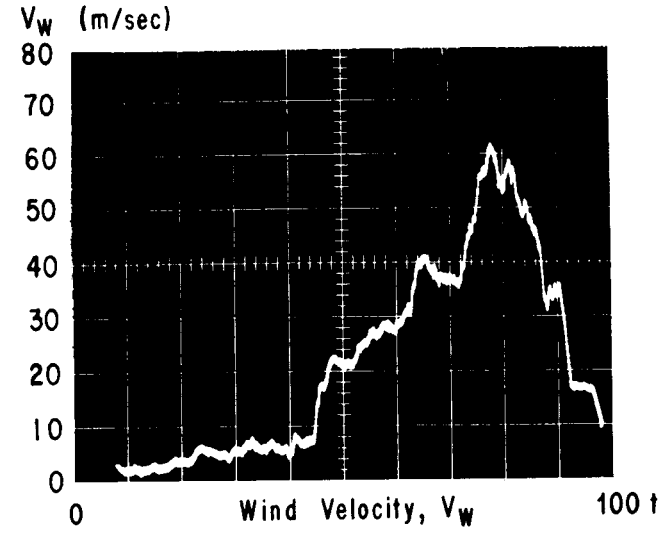

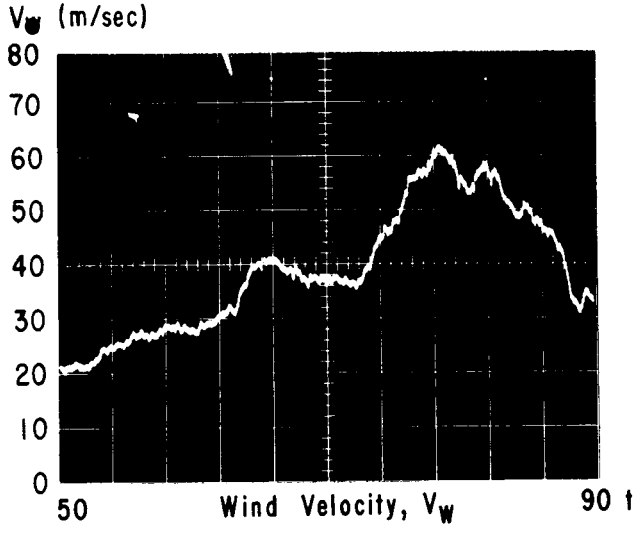

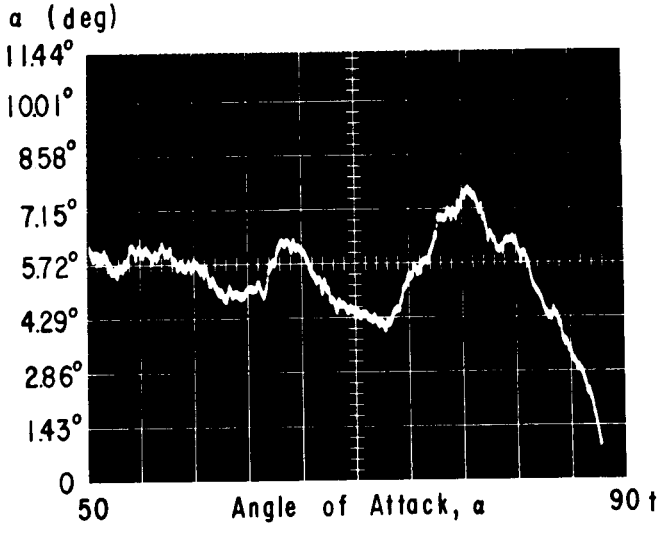

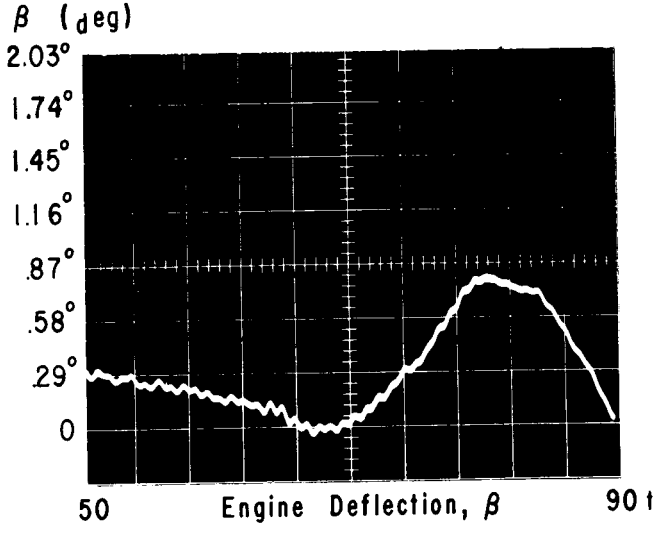

FIG. 5A. VEHICLE RESPONSE FOR WIND (2/4/65 AT 5:18 P.M.)

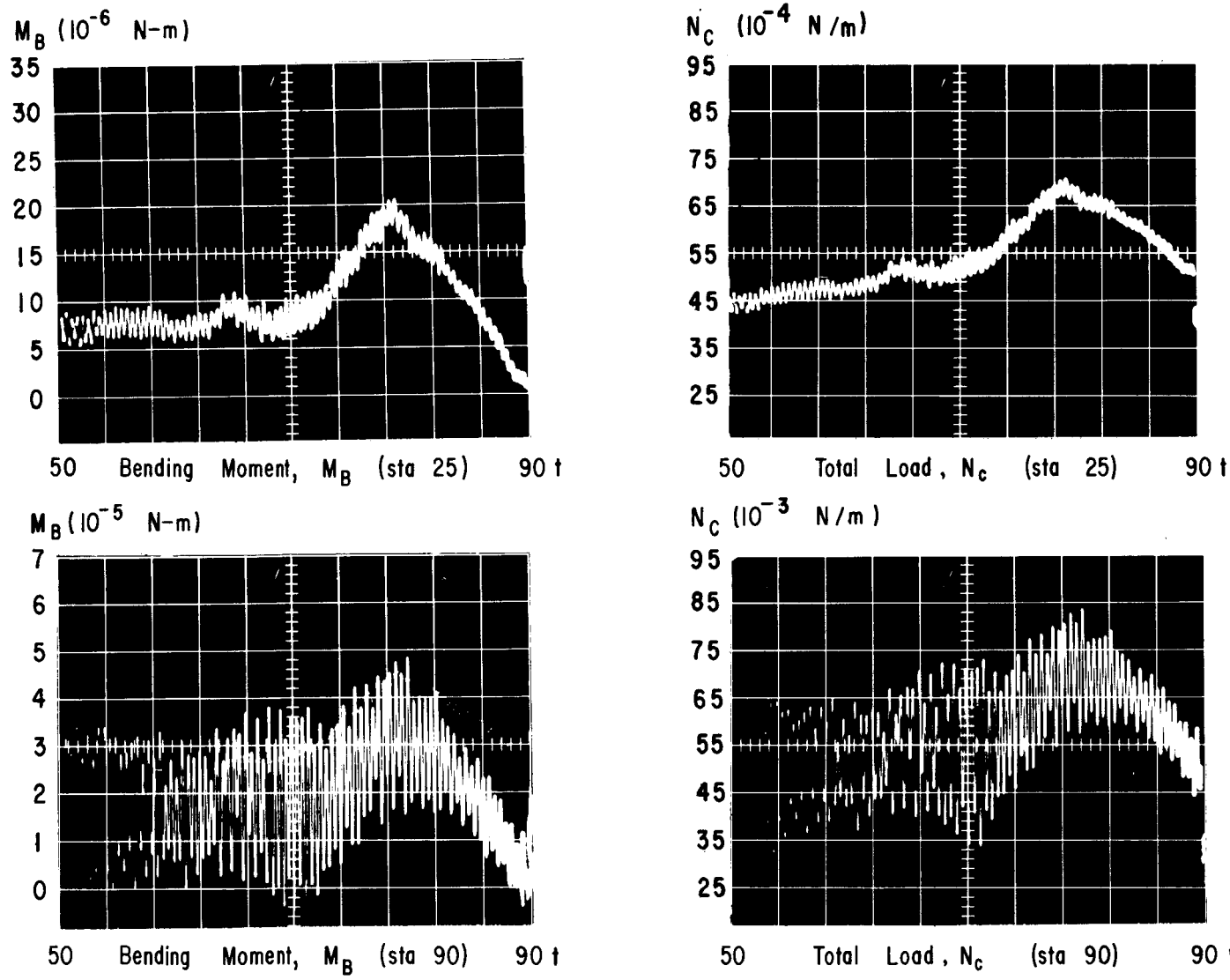

FIG. 6A. VEHICLE RESPONSE FOR WIND (2/4/65 AT 5:18 P.M.)

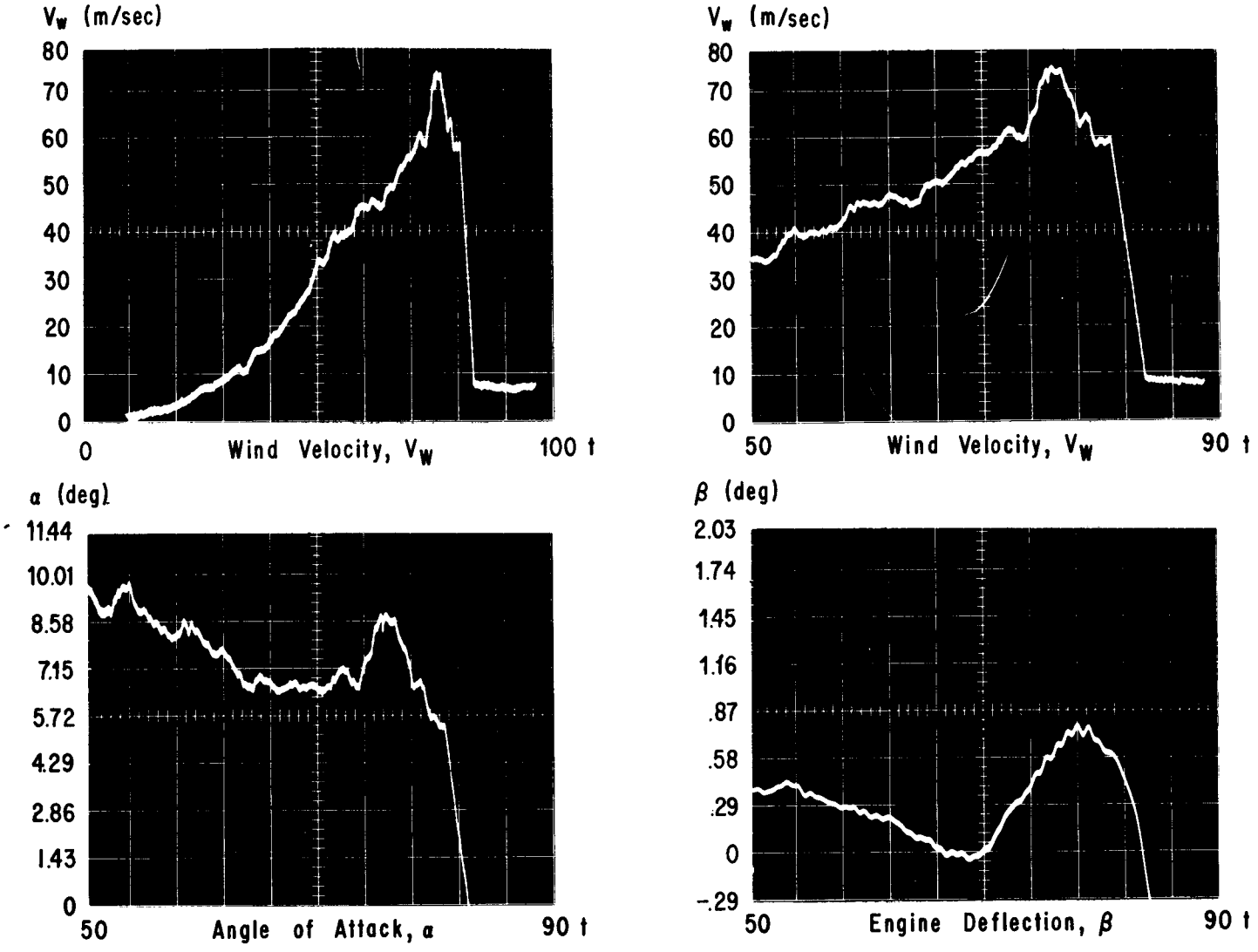

FIG. 7A. VEHICLE RESPONSE FOR WIND (3/8/65 AT 2:15 P.M.)

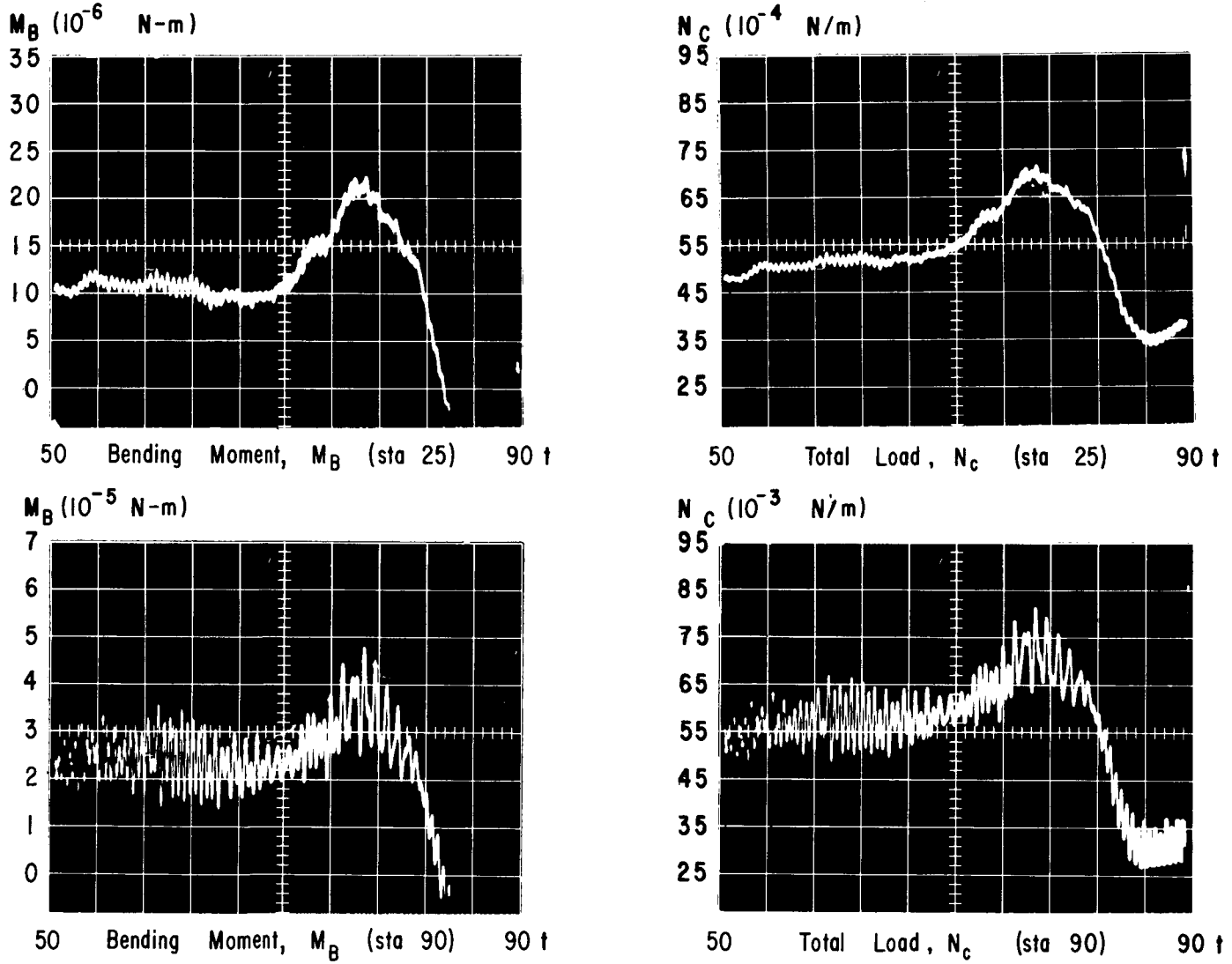

FIG. 8A. VEHICLE RESPONSE FOR WIND (3/8/65 AT 2:15 P.M.)

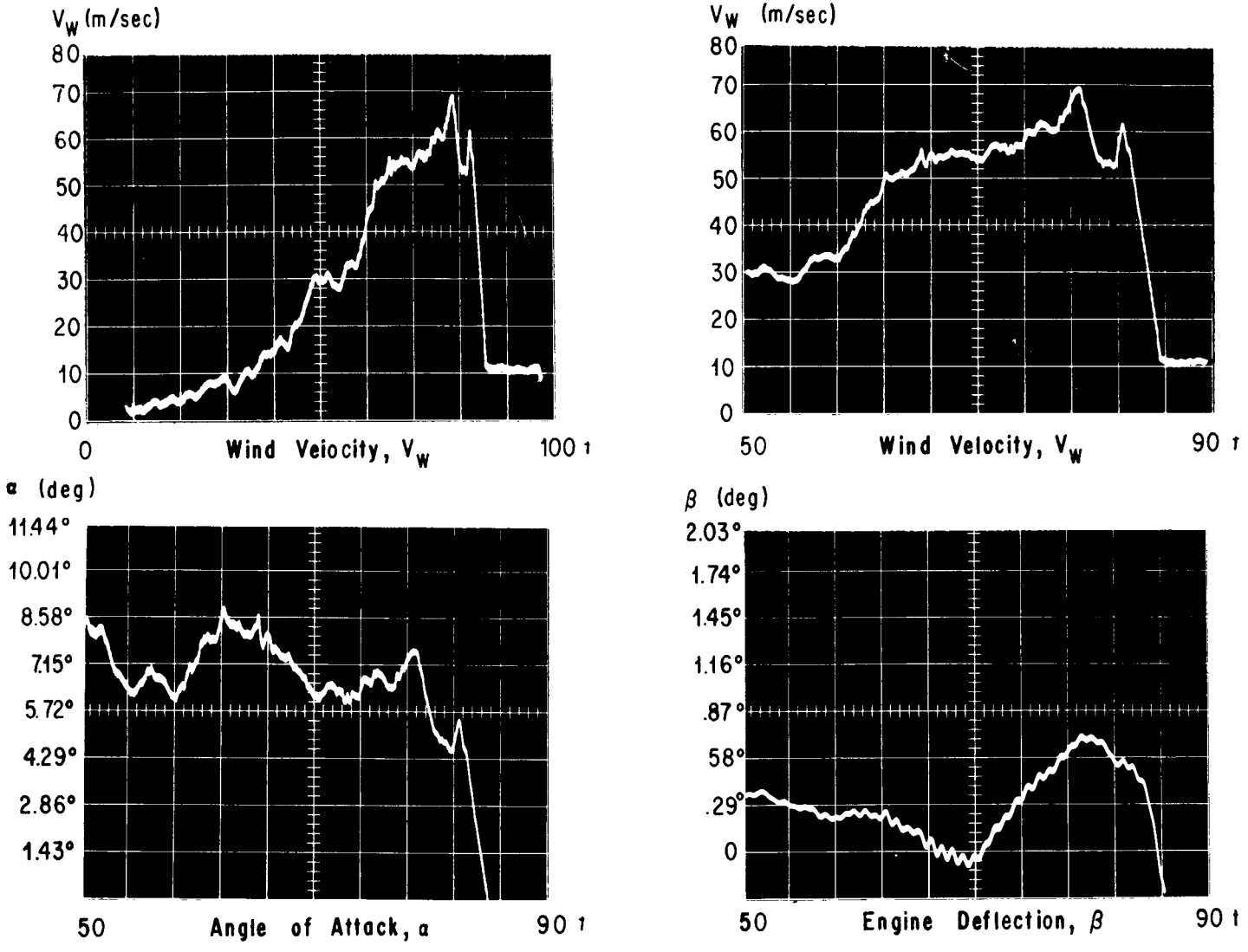

FIG. 9A. VEHICLE RESPONSE FOR WIND (3/10/65 AT 12:01 P.M.)

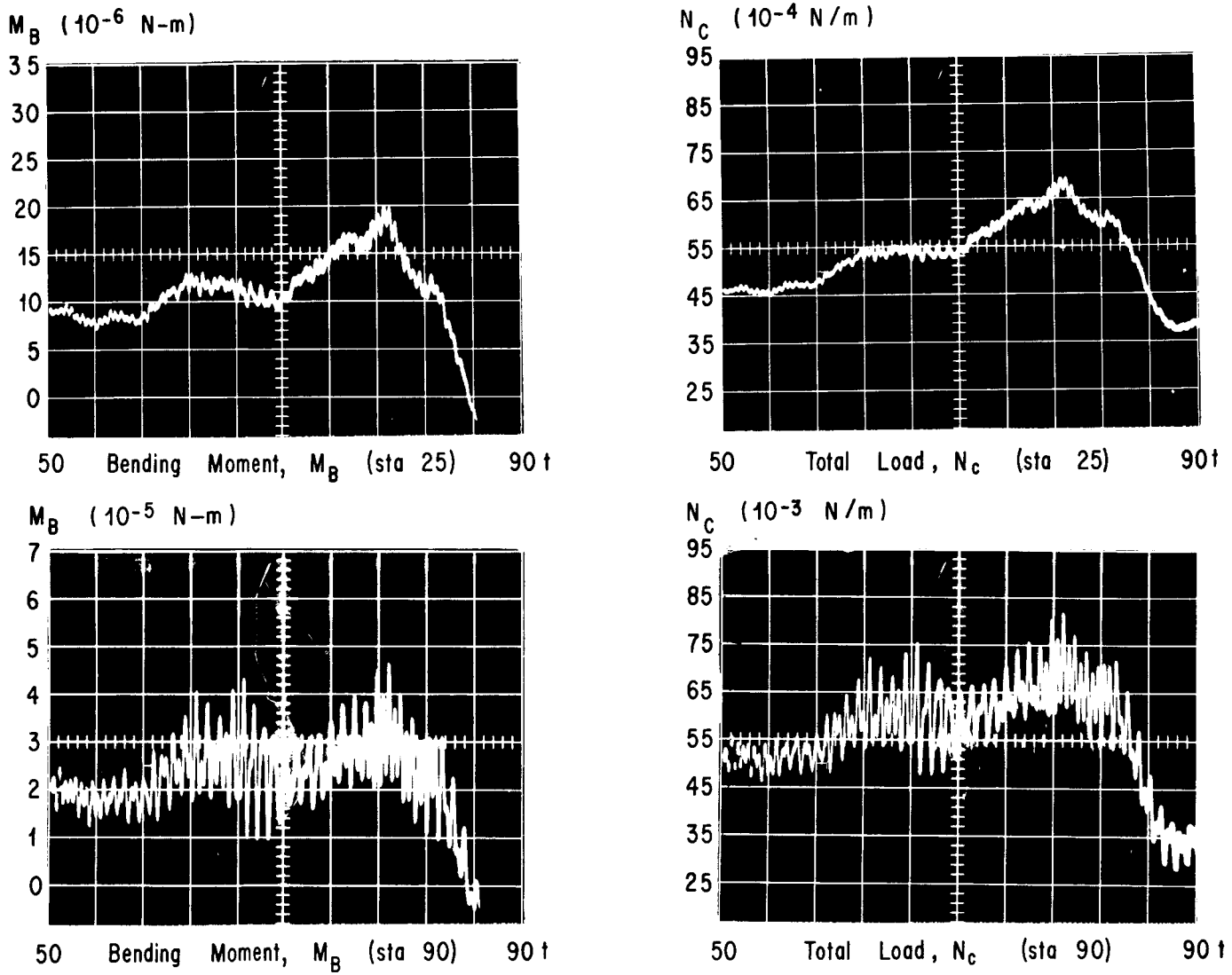

FIG. 10A. VEHICLE RESPONSE FOR WIND (3/10/65 AT 12:01 P.M.)

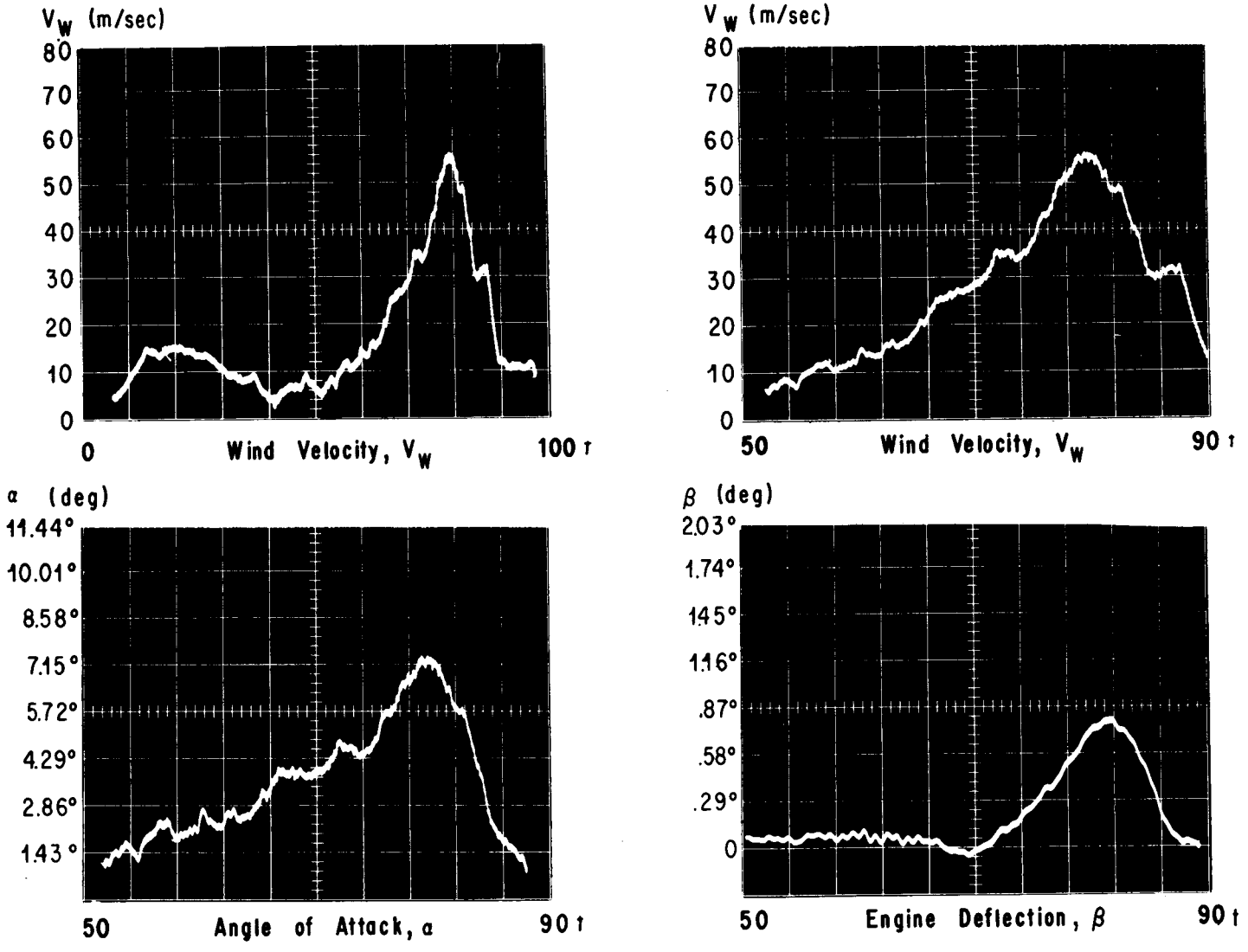

FIG. 11A. VEHICLE RESPONSE FOR WIND (2/5/65 AT 1:08 P.M.)

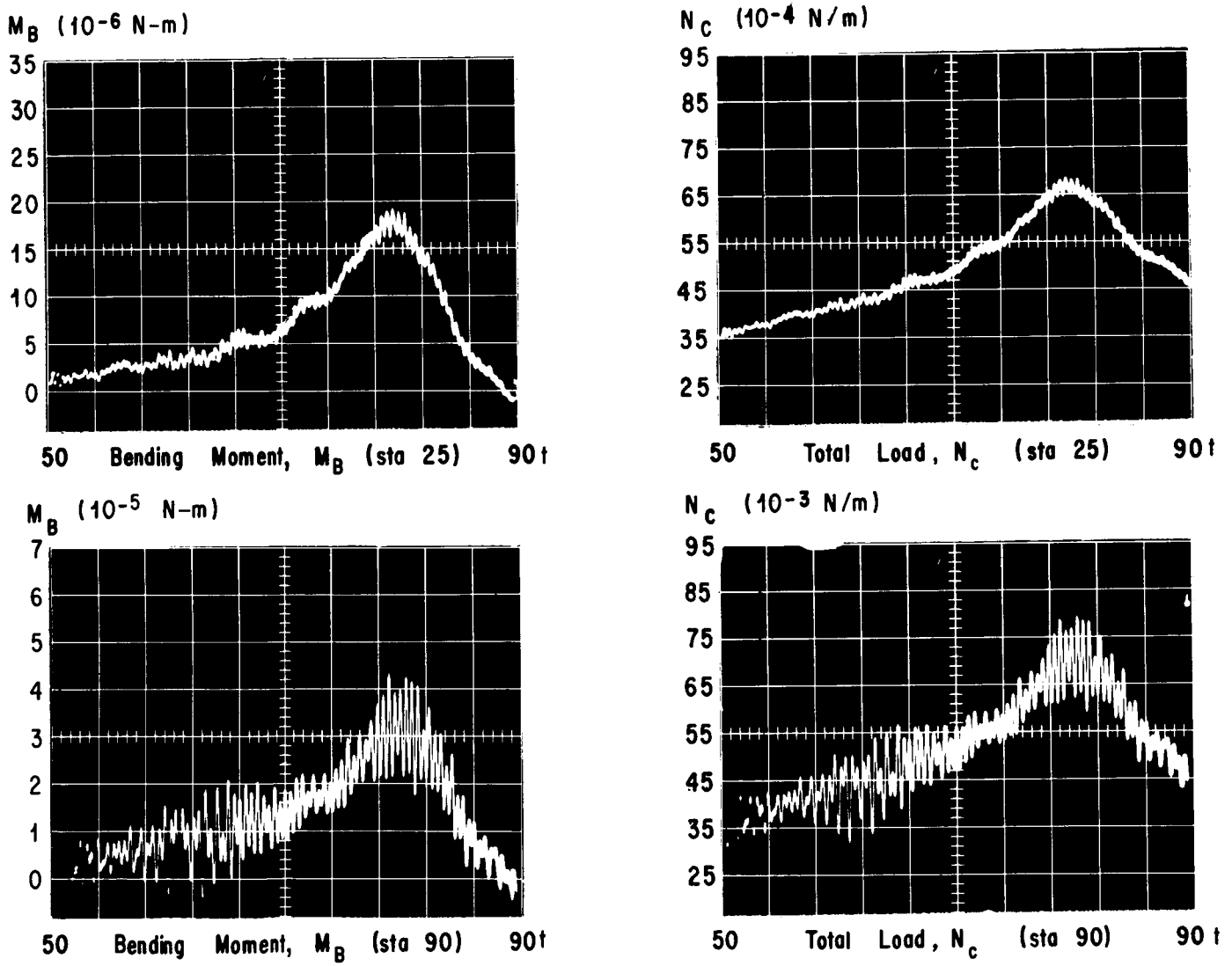

FIG. 12A. VEHICLE RESPONSE FOR WIND (2/5/65 AT 1:08 P.M.)

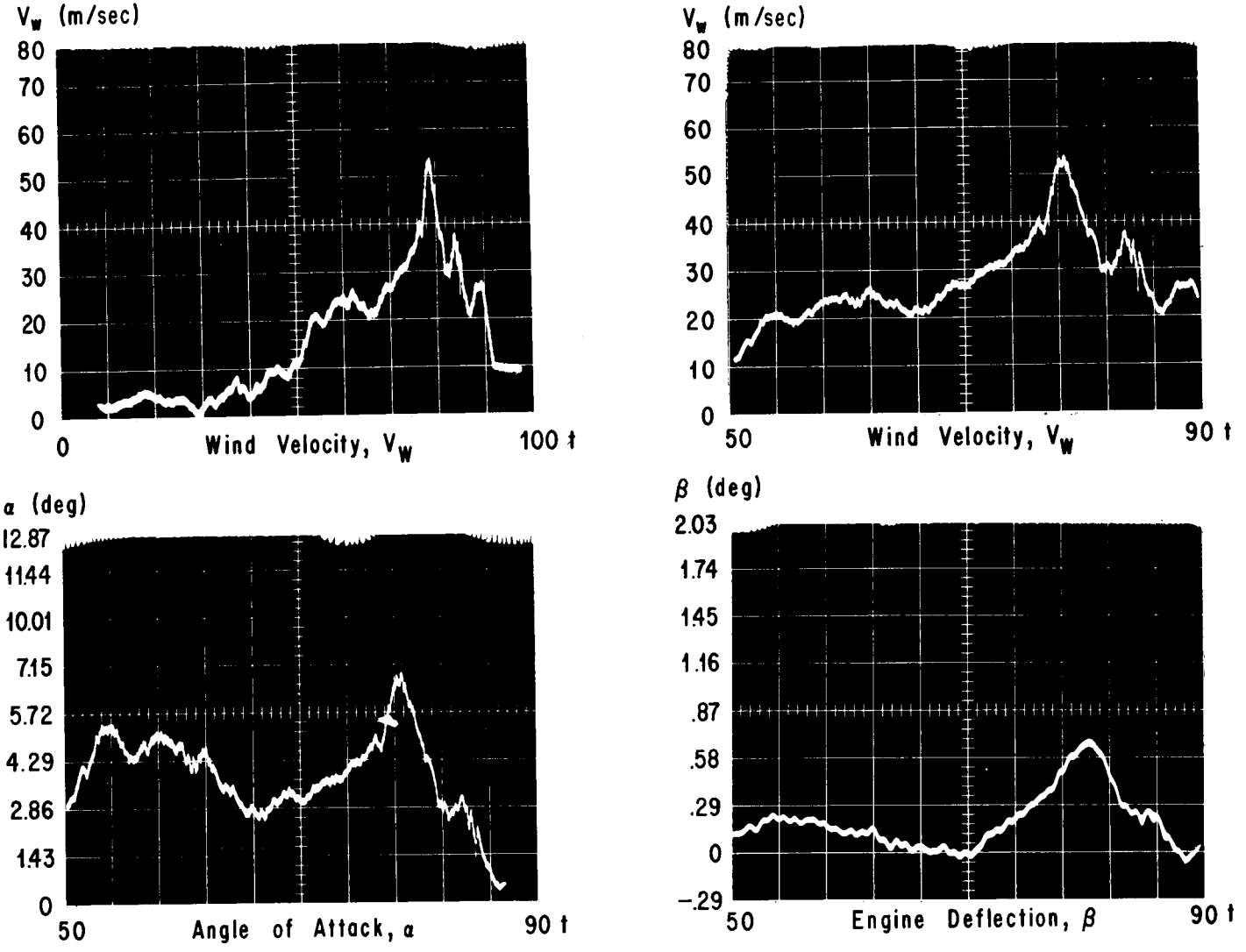

FIG. 13A. VEHICLE RESPONSE FOR WIND (1/20/65 AT 5:01 P.M.)

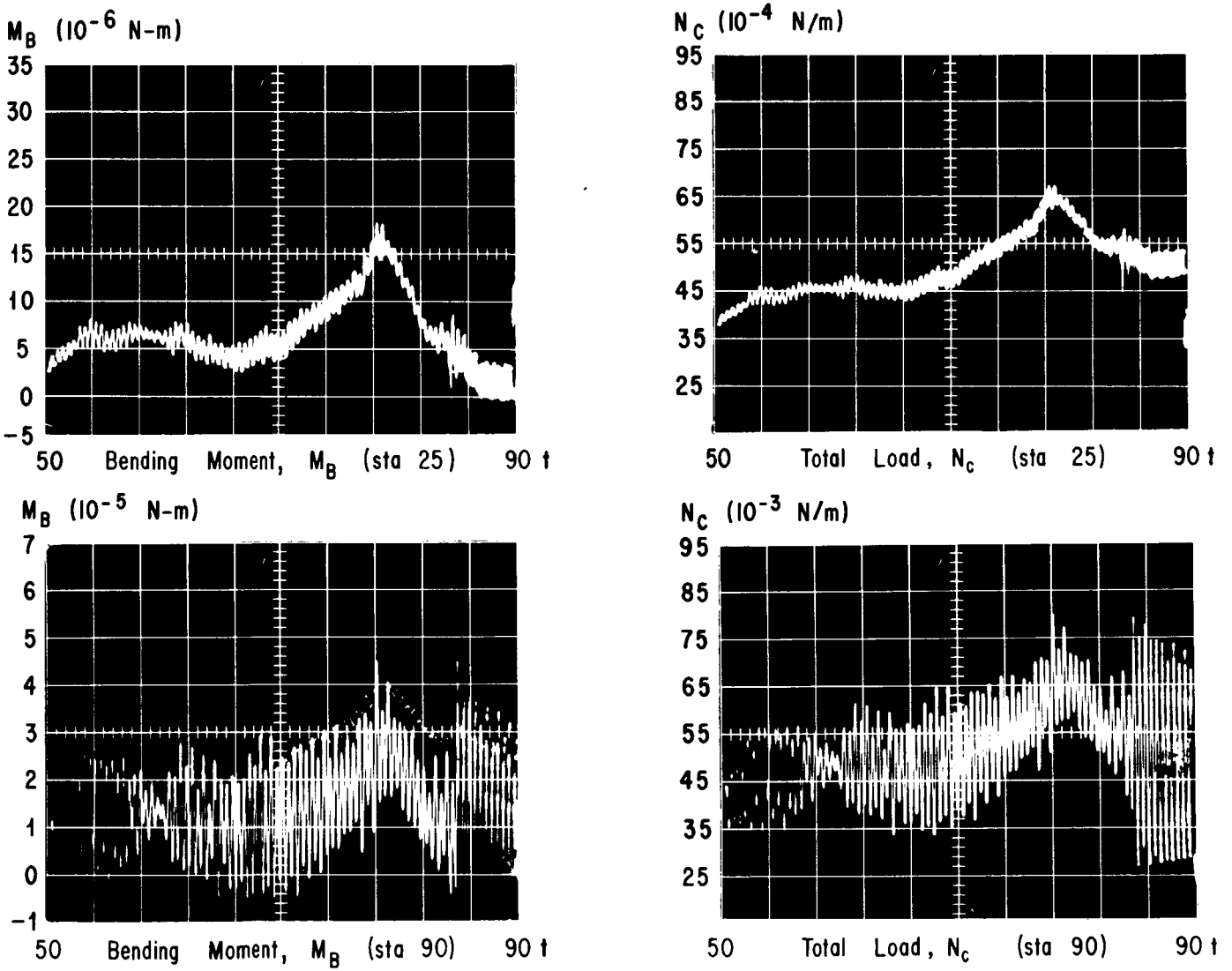

FIG. 14A. VEHICLE RESPONSE FOR WIND (1/20/65 AT 5:01 P.M.)

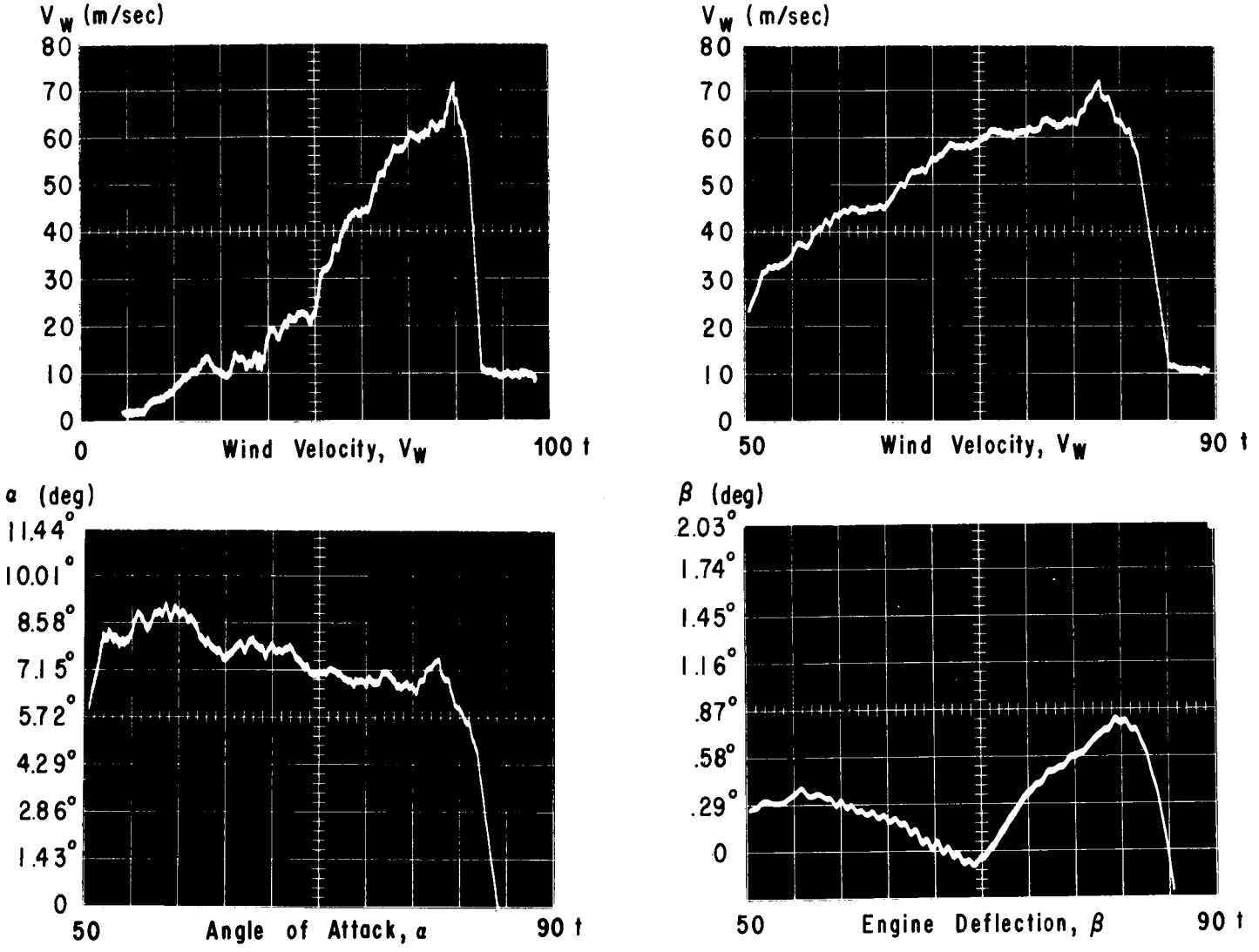

FIG. 15A. VEHICLE RESPONSE FOR WIND (3/9/65 AT 10:00 A.M.)

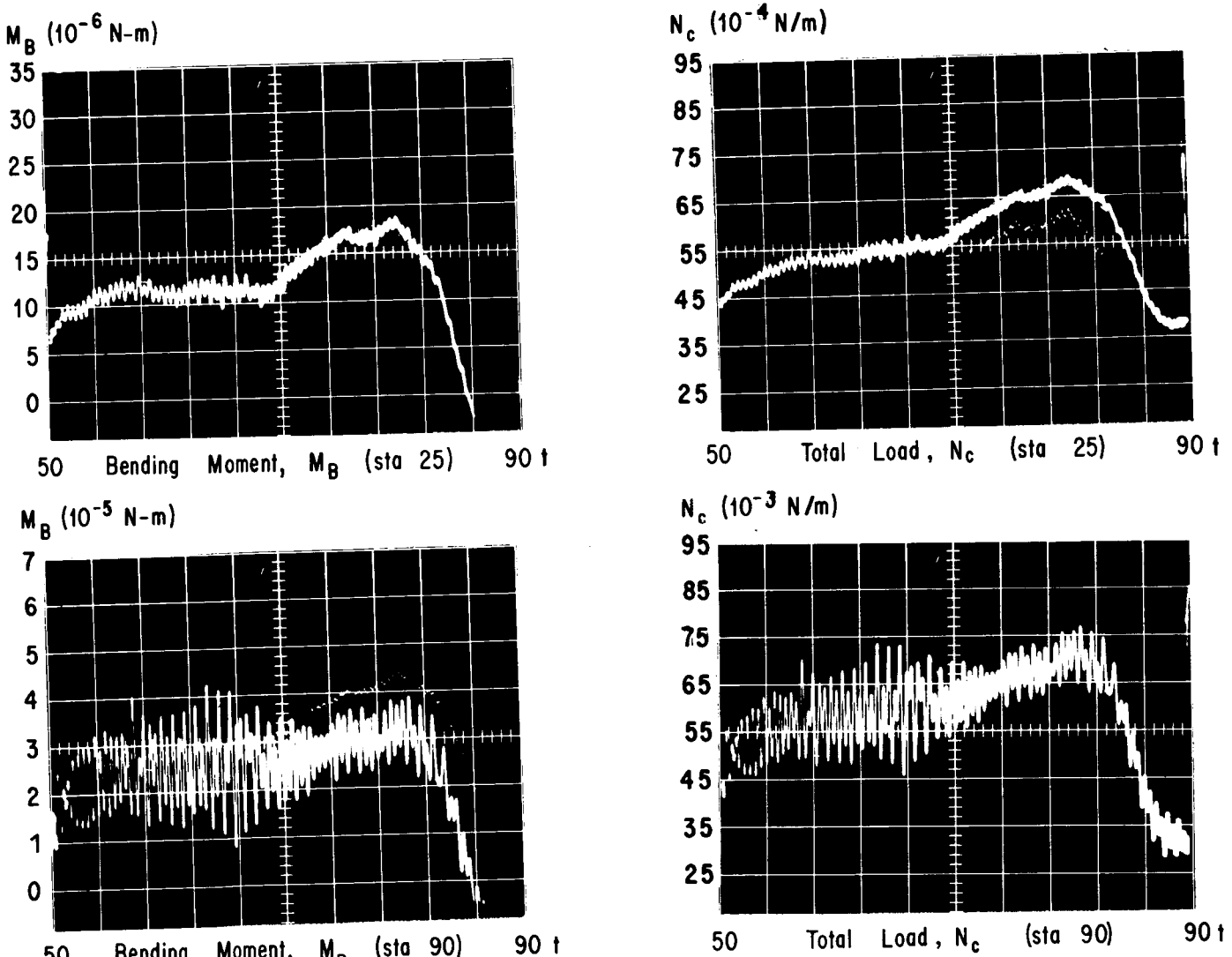

FIG. 16A. VEHICLE RESPONSE FOR WIND (3/9/65 AT 10:00 A.M.)

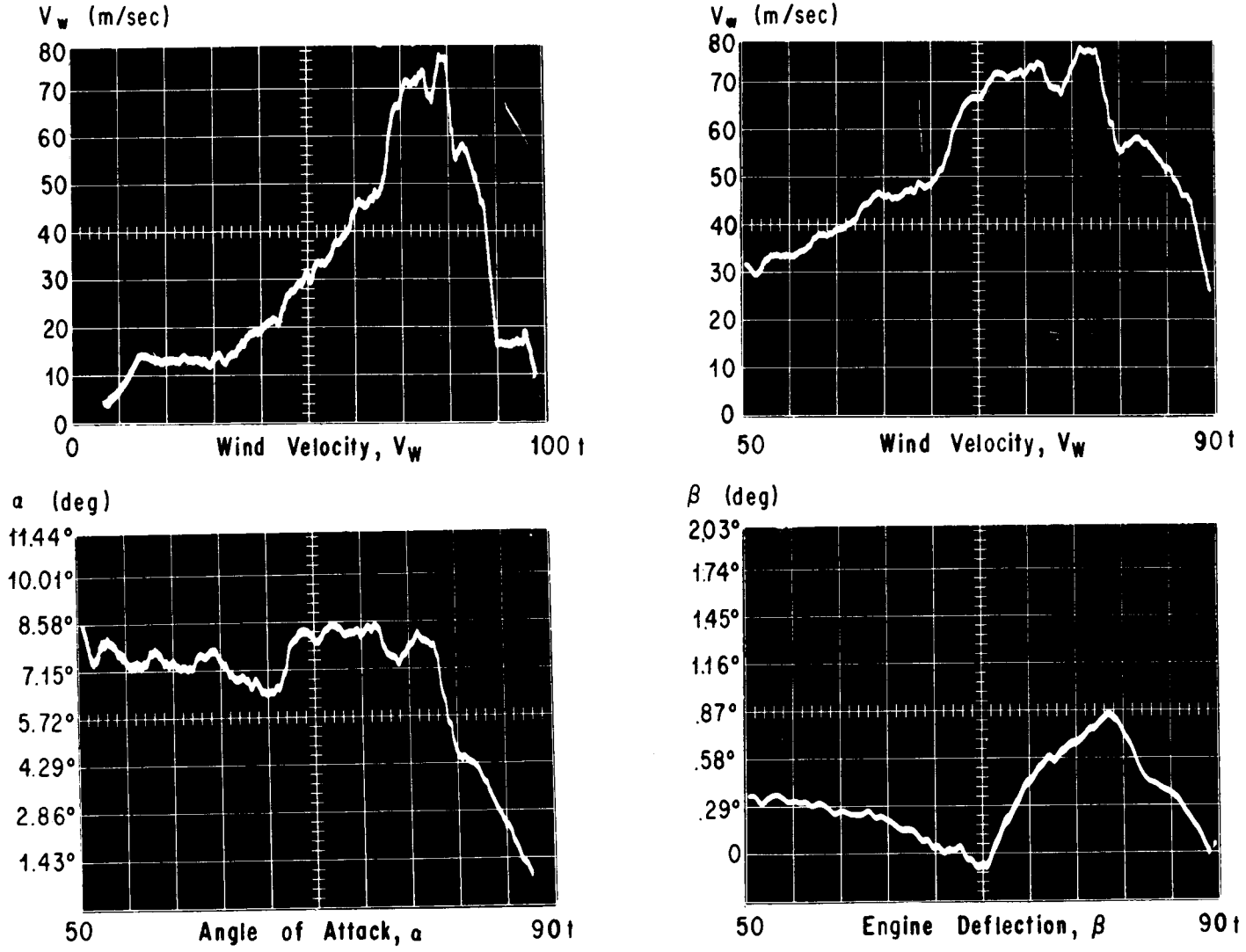

FIG. 17A. VEHICLE RESPONSE FOR WIND (3/9/65 AT 1:00 A.M.)

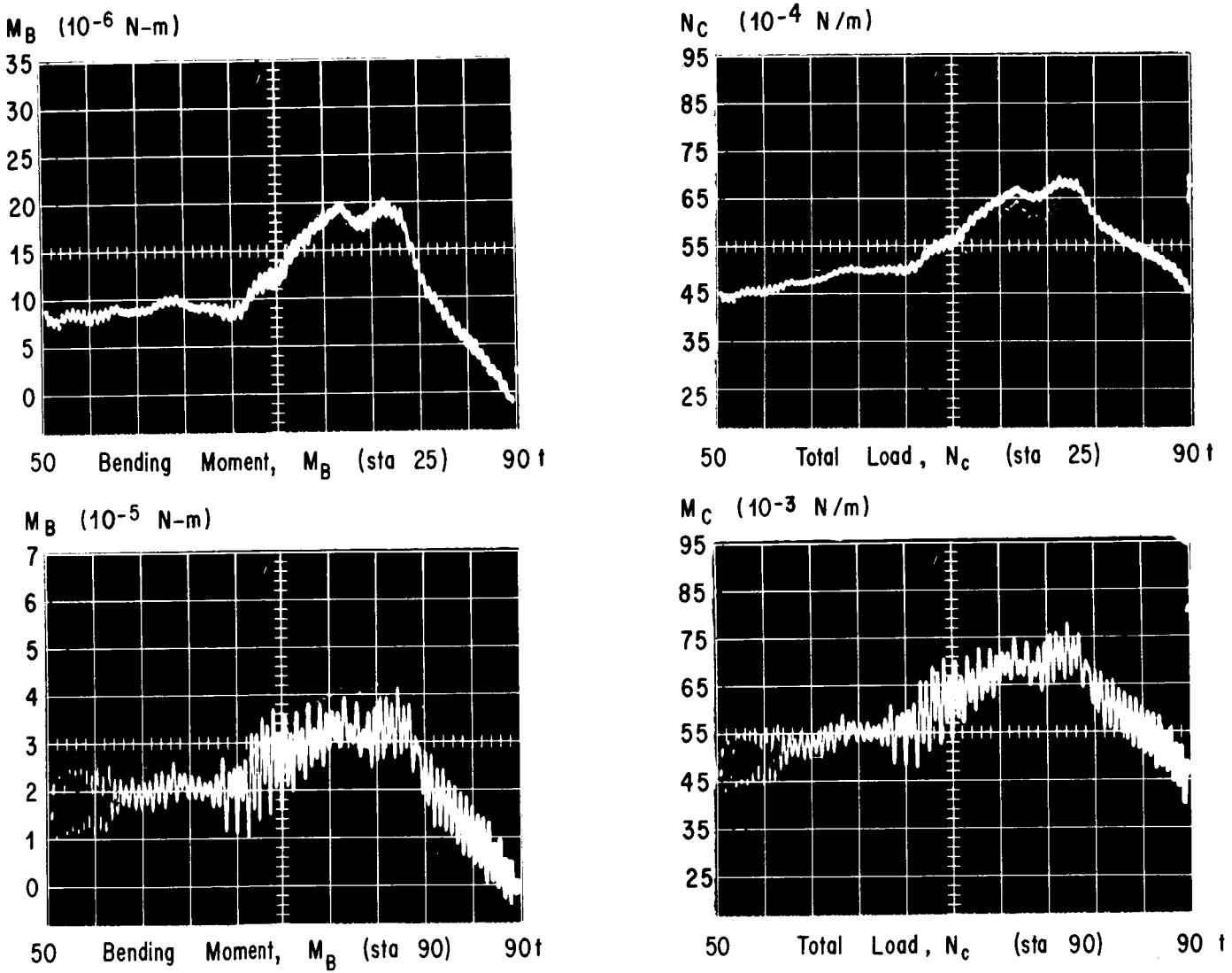

FIG. 18A. VEHICLE RESPONSE FOR WIND (3/9/65 AT 1:00 A.M.)

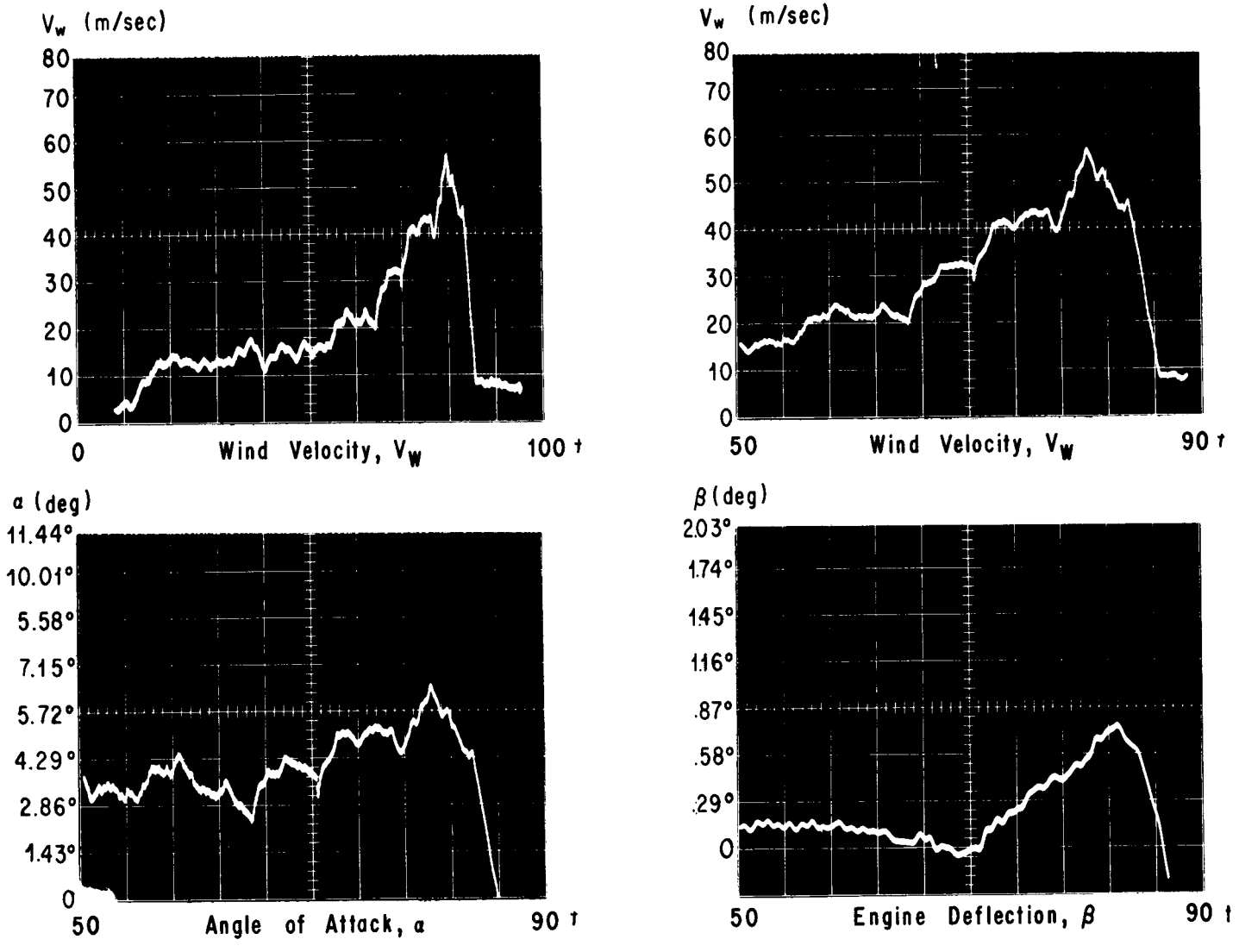

FIG. 19A. VEHICLE RESPONSE FOR WIND (2/2/65 AT 1:00 A.M.)

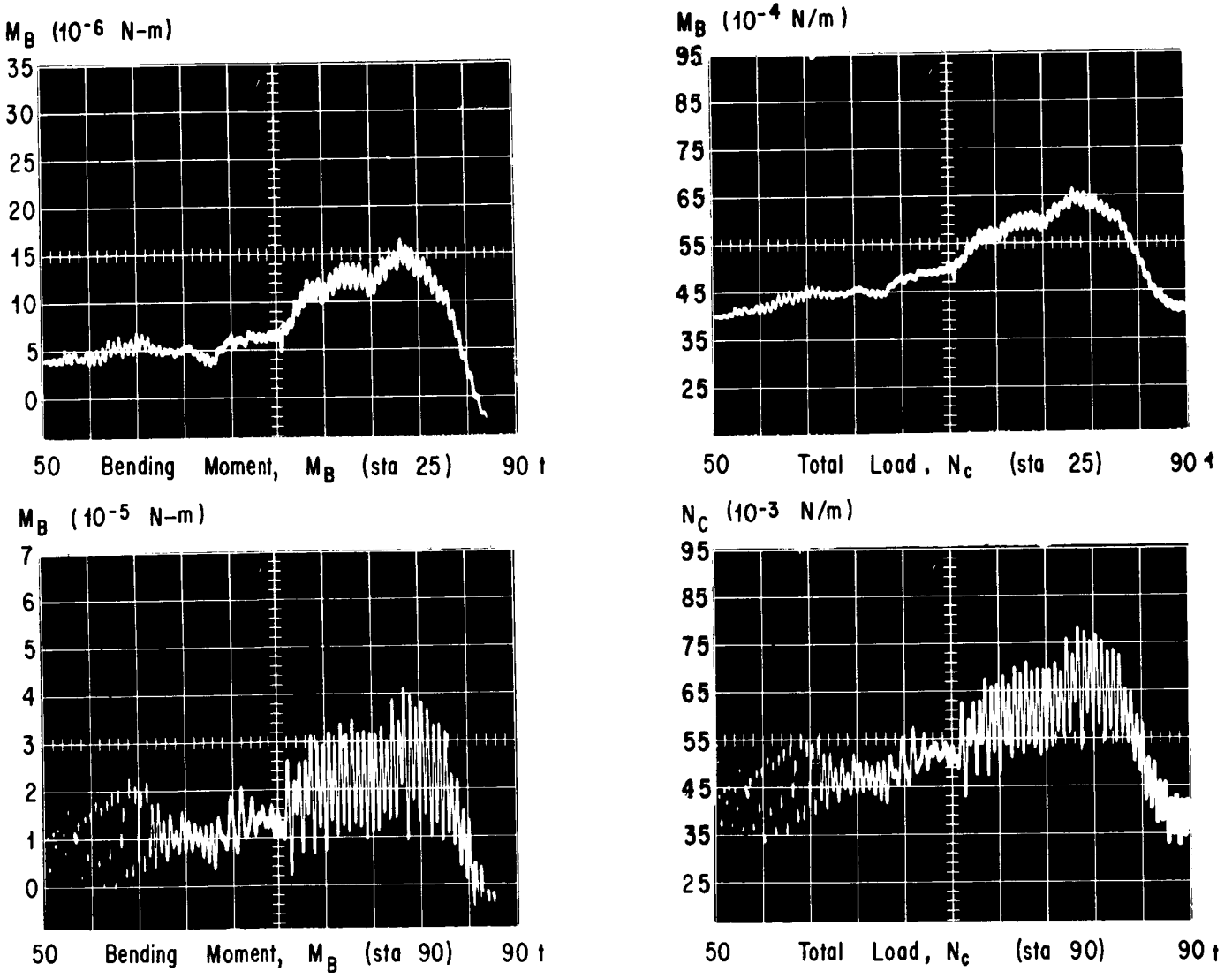

FIG. 20A. VEHICLE RESPONSE FOR WIND (2/2/65 AT 1:00 A.M.)

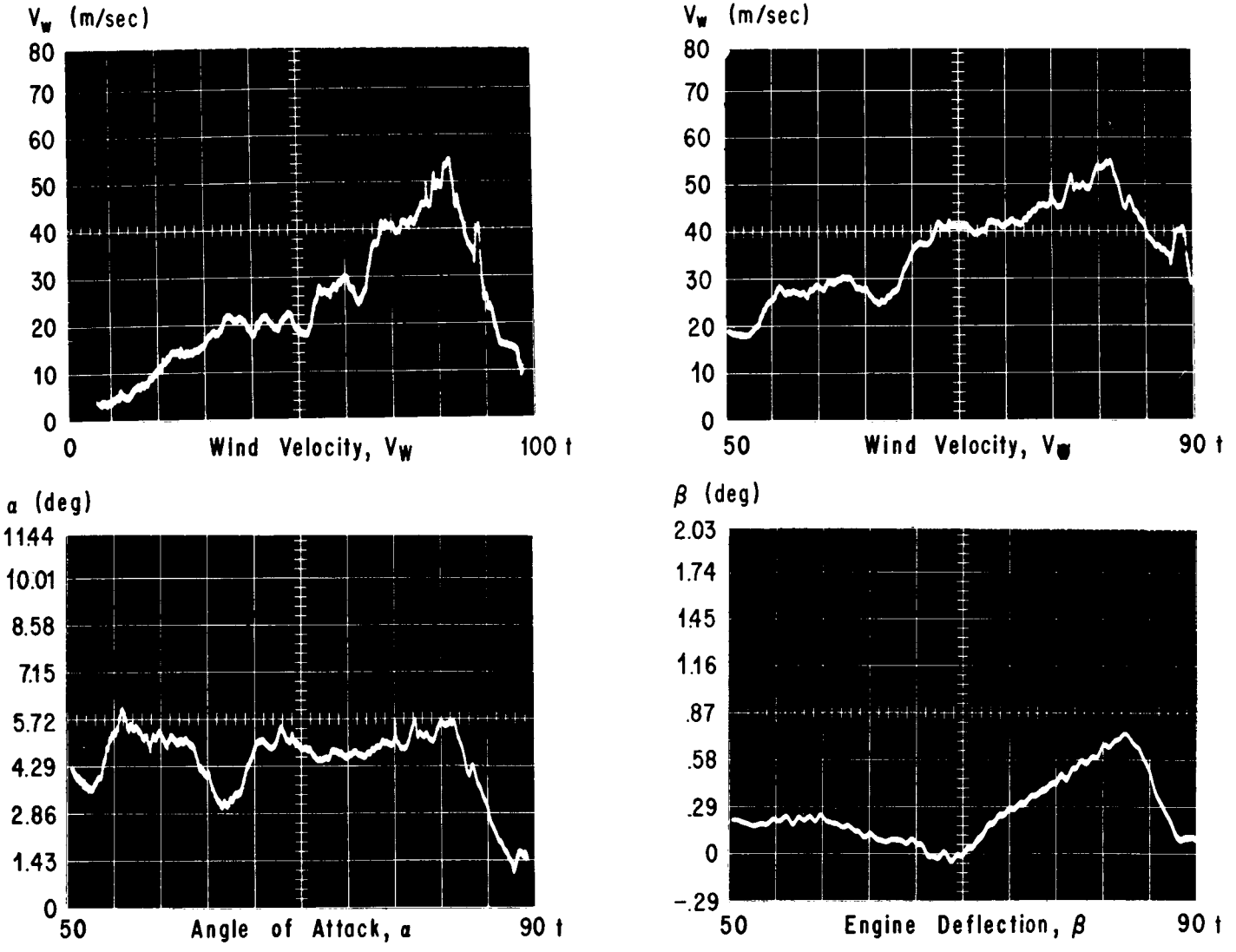

FIG. 21A. VEHICLE RESPONSE FOR WIND (2/24/65 AT 1:00 P.M.)

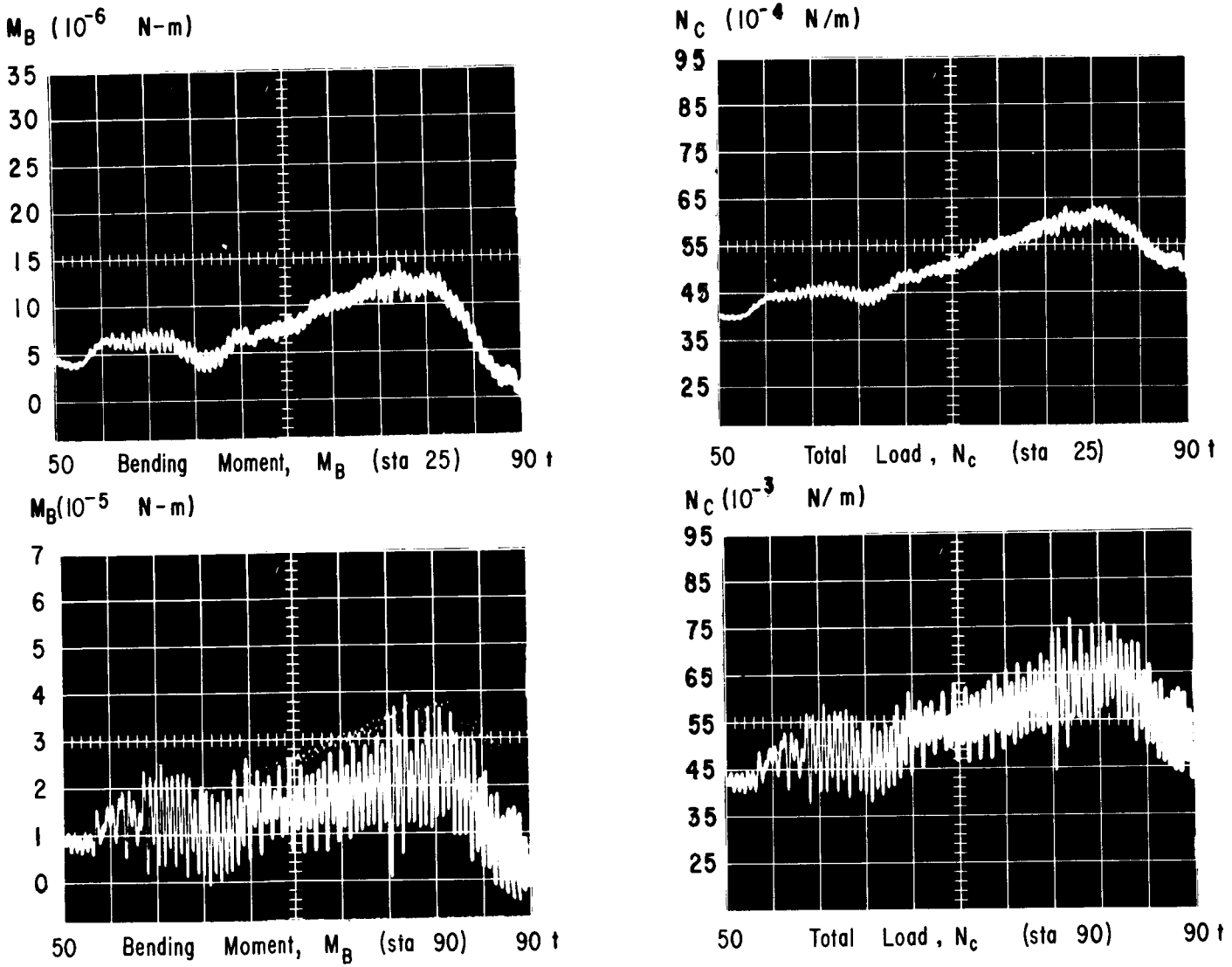

FIG. 22A. VEHICLE RESPONSE FOR WIND (2/24/65 AT 1:00 P.M.)

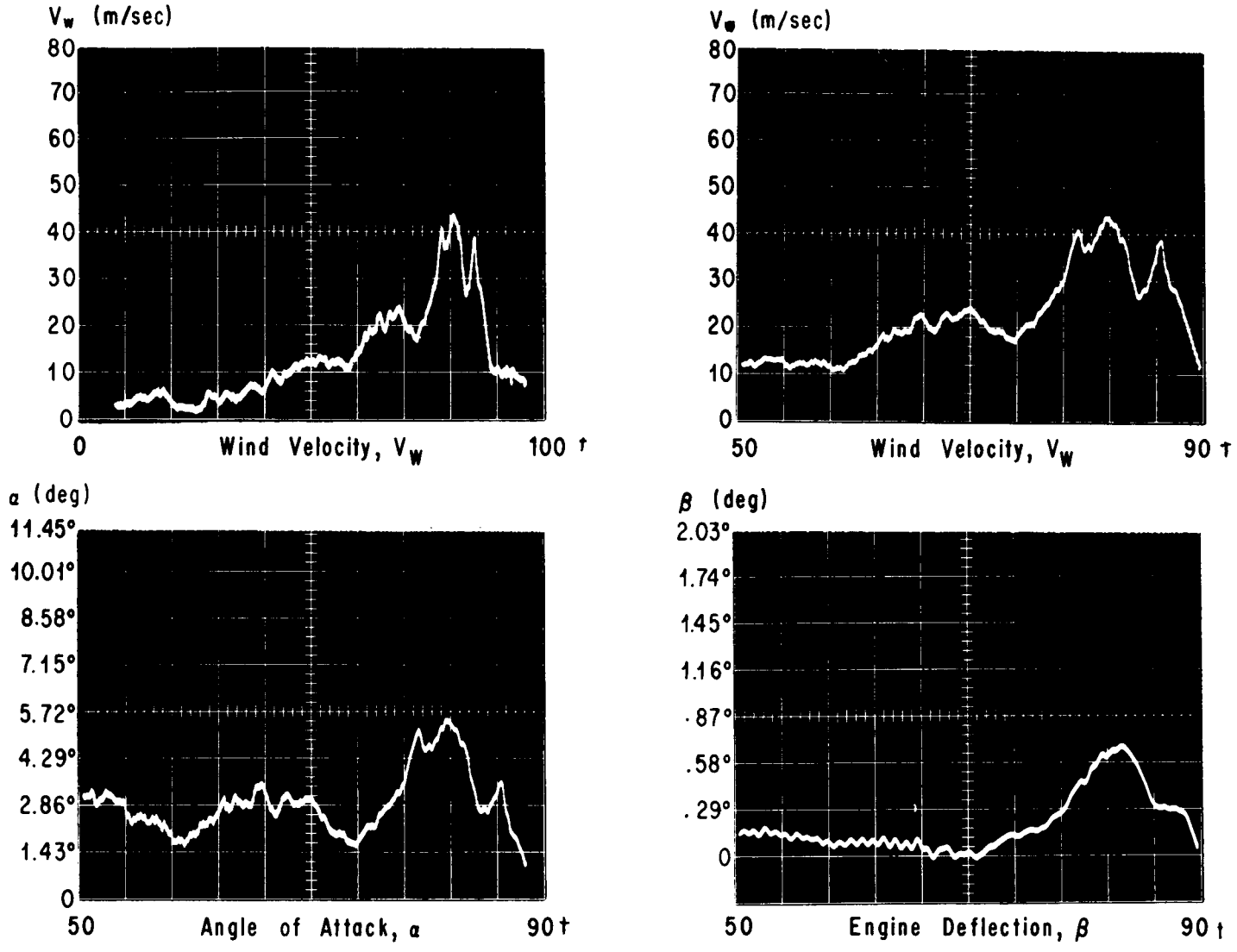

FIG. 23A. VEHICLE RESPONSE FOR WIND (10/19/65 AT 8:30 P.M.)

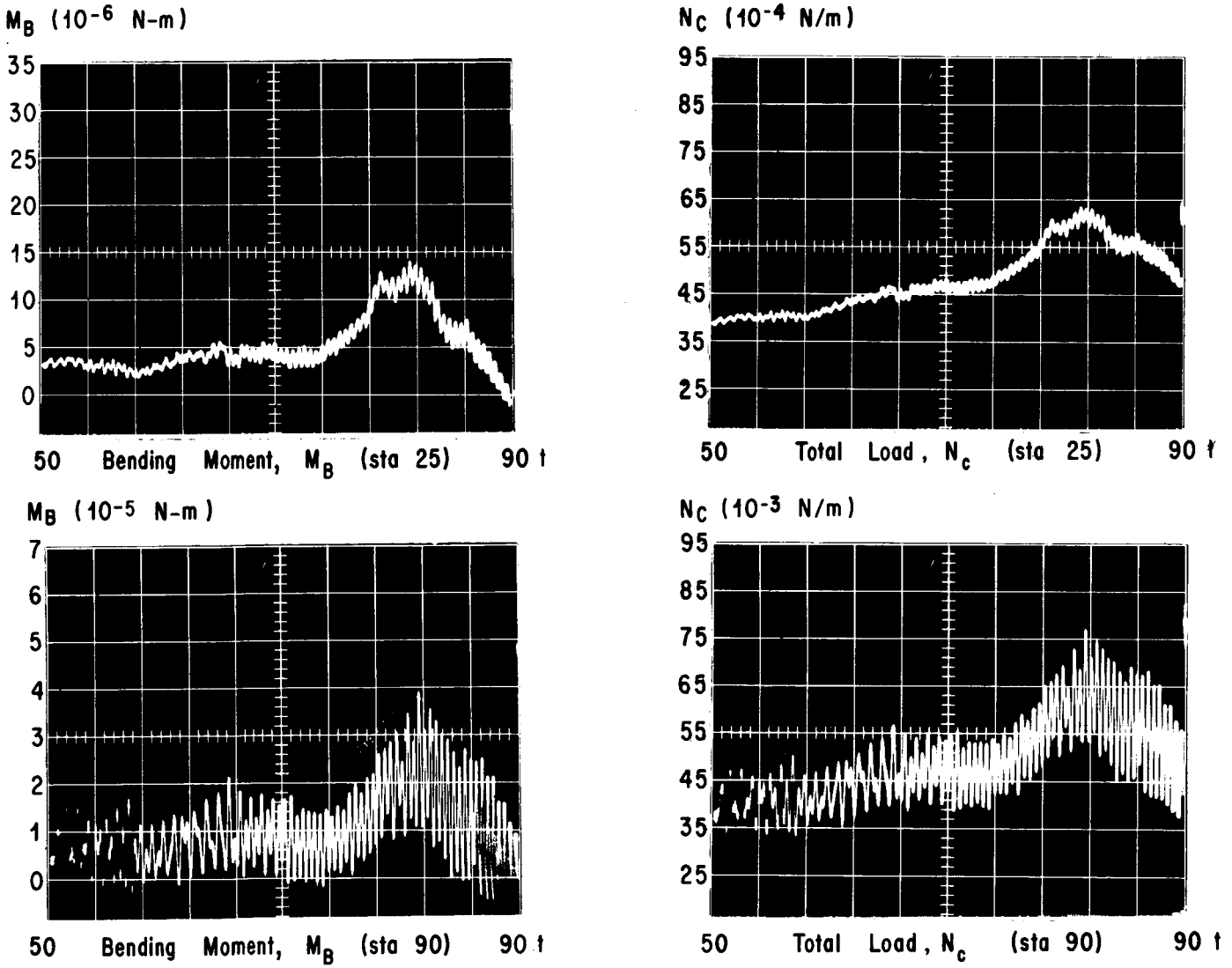

FIG. 24A. VEHICLE RESPONSE FOR WIND (10/19/65 AT 2:15 P.M.)

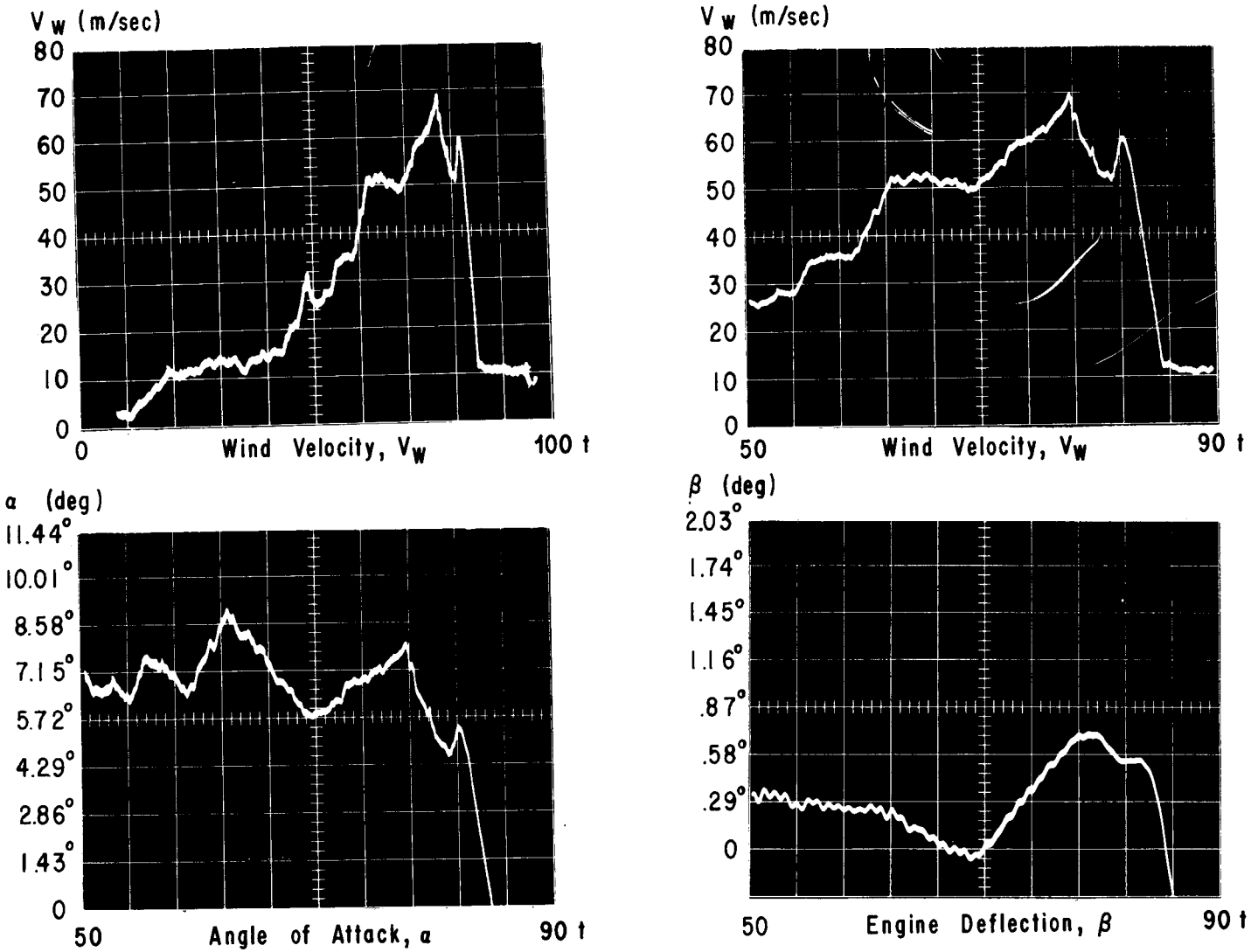

FIG. 25A. VEHICLE RESPONSE FOR WIND (3/10/65 AT 10:01 A.M.)

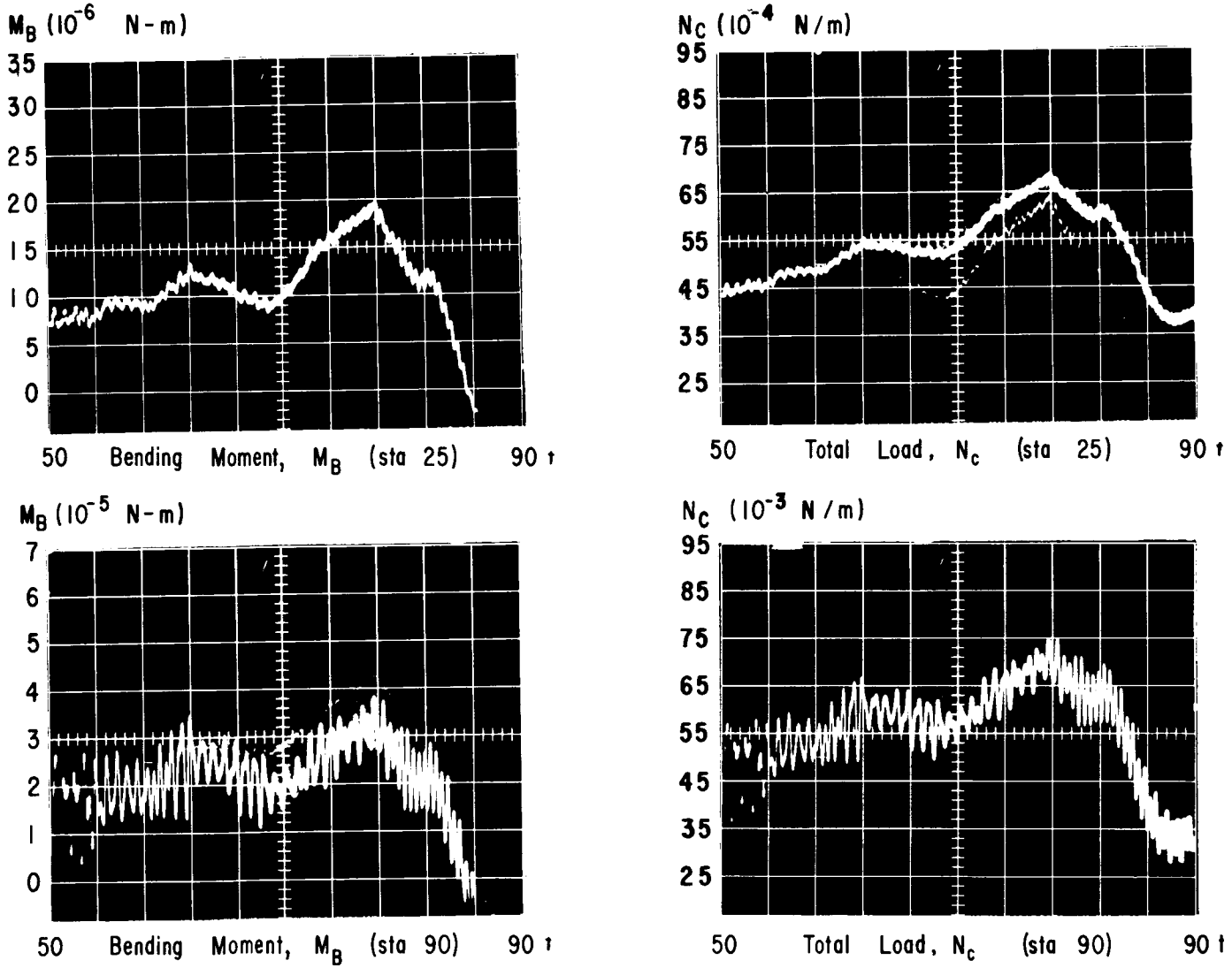

FIG. 26A. VEHICLE RESPONSE FOR WIND (3/10/65 AT 10:01 A.M.)

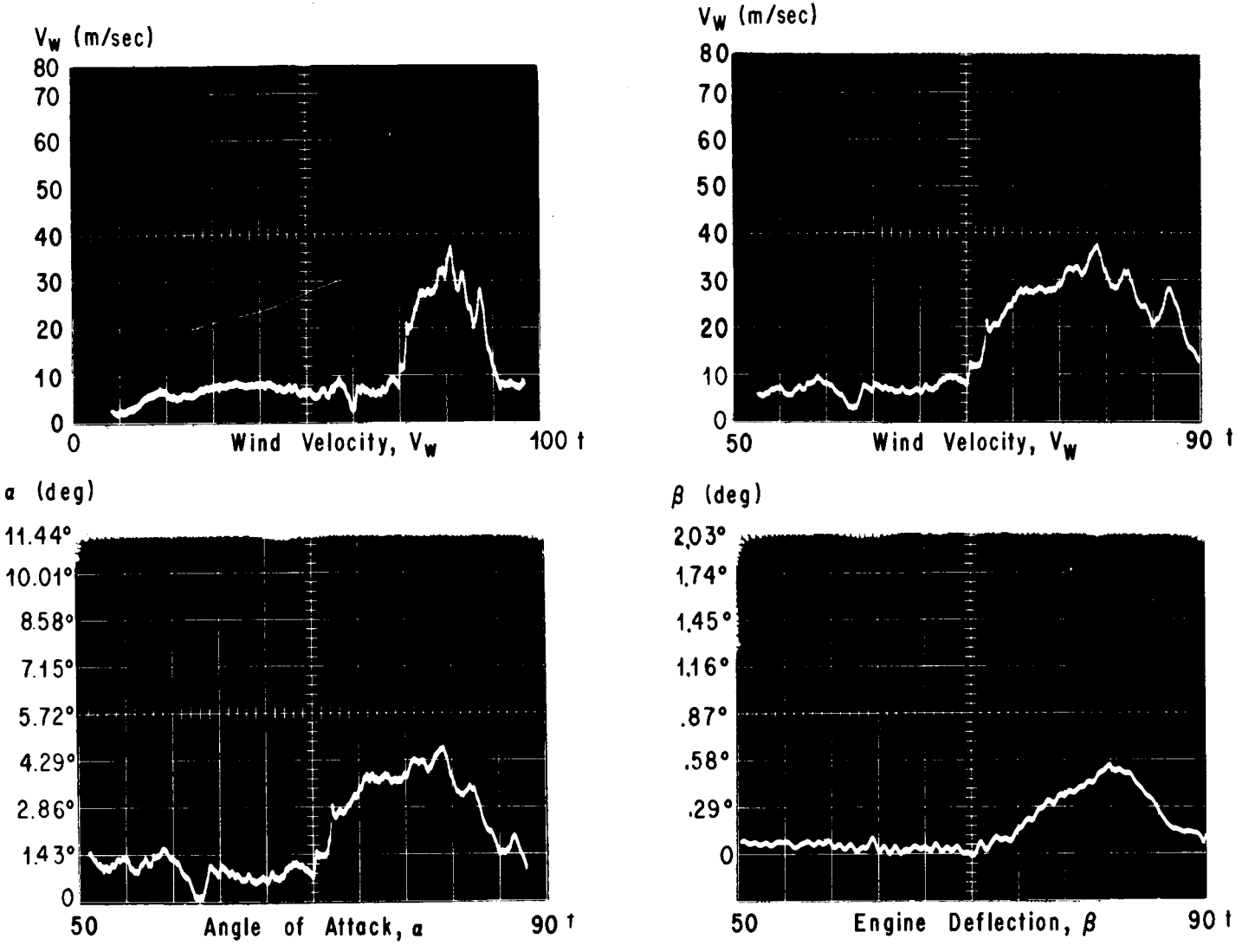

FIG. 27A. VEHICLE RESPONSE FOR WIND (5/4/65 AT 1:00 P.M.)

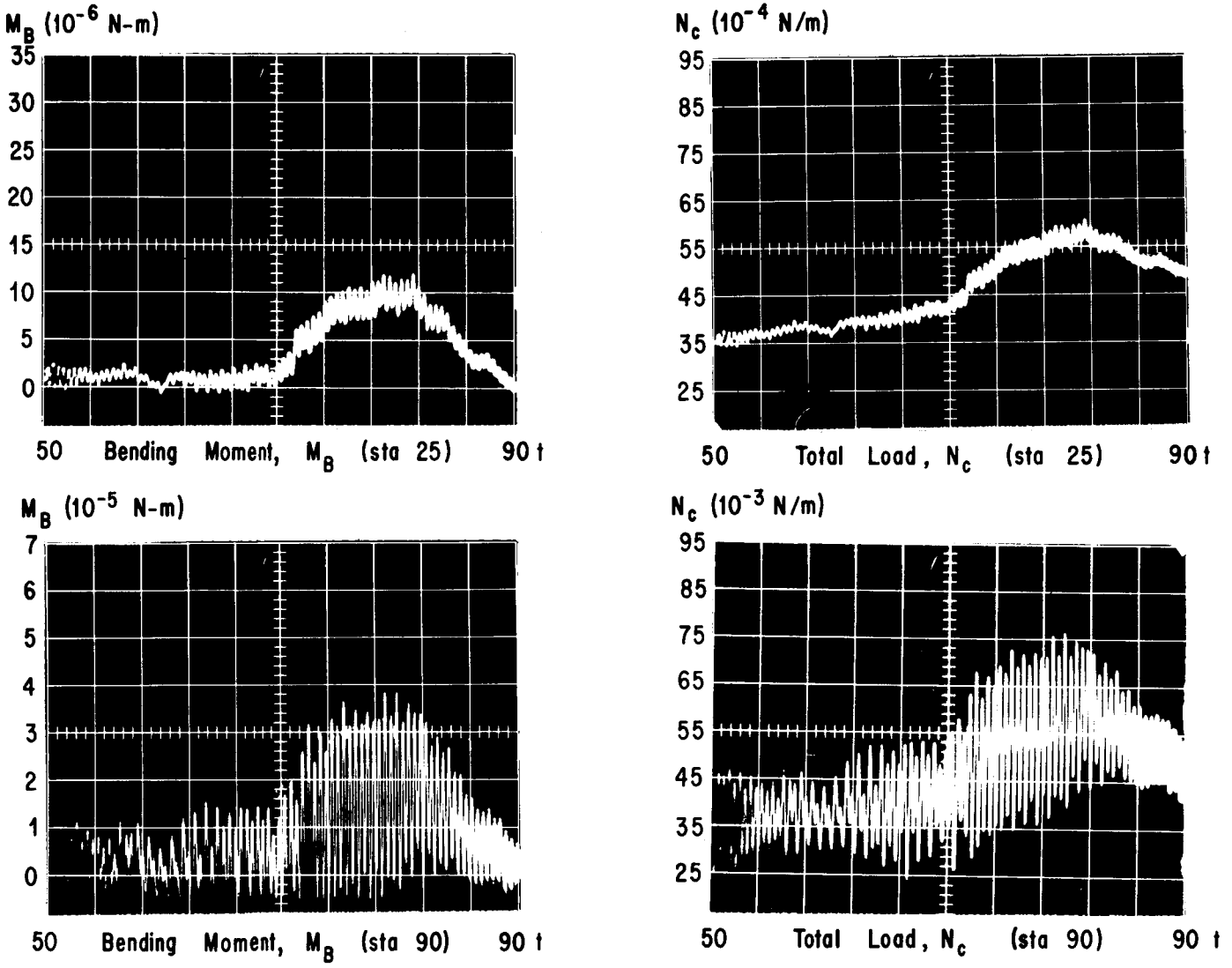

FIG. 28A. VEHICLE RESPONSE FOR WIND (5/4/65 AT 1:00 P.M.)

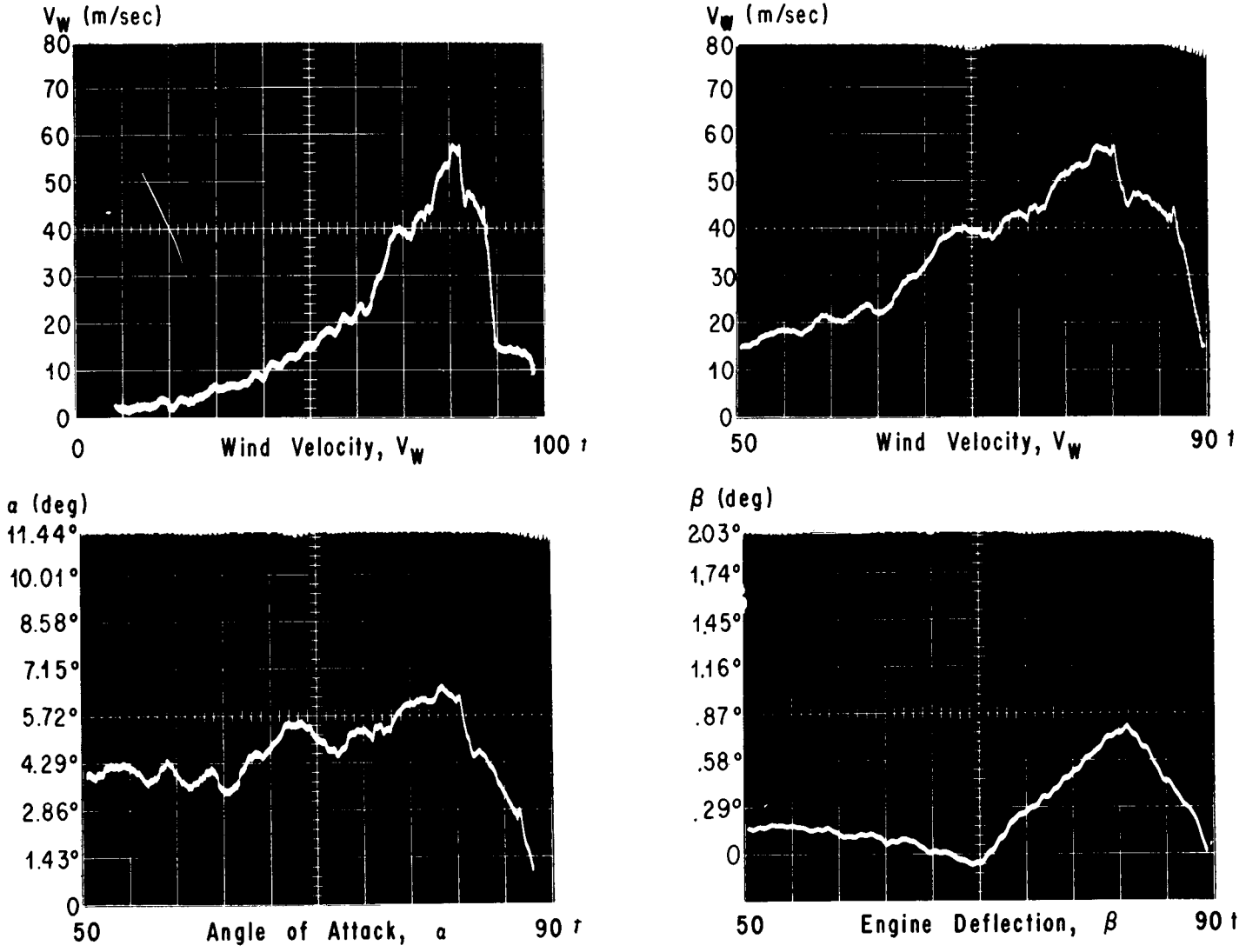

FIG. 29A. VEHICLE RESPONSE FOR WIND (3/23/65 AT 12:12 A.M.)

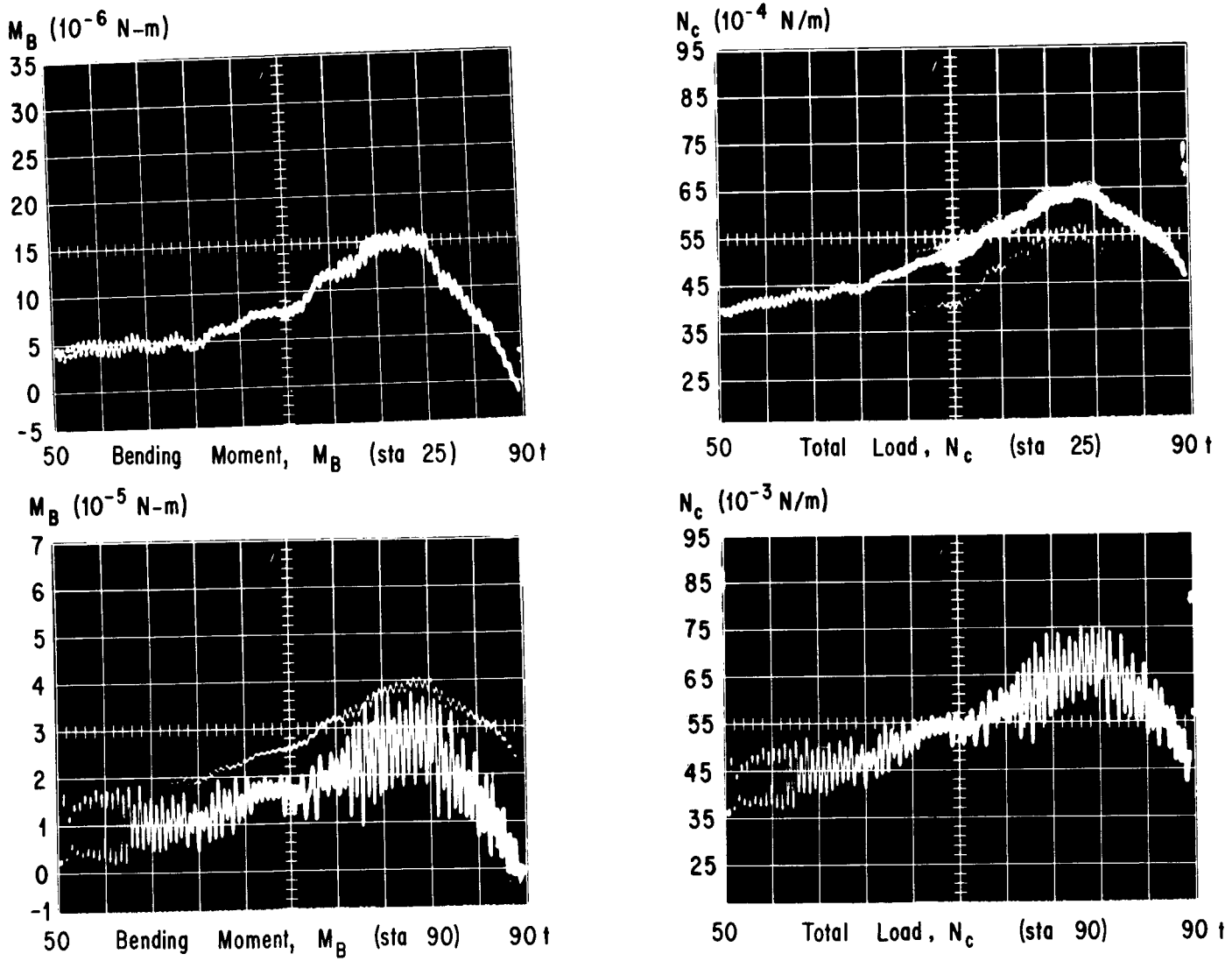

FIG. 30A. VEHICLE RESPONSE FOR WIND (3/23/65 AT 12:12 A.M.)

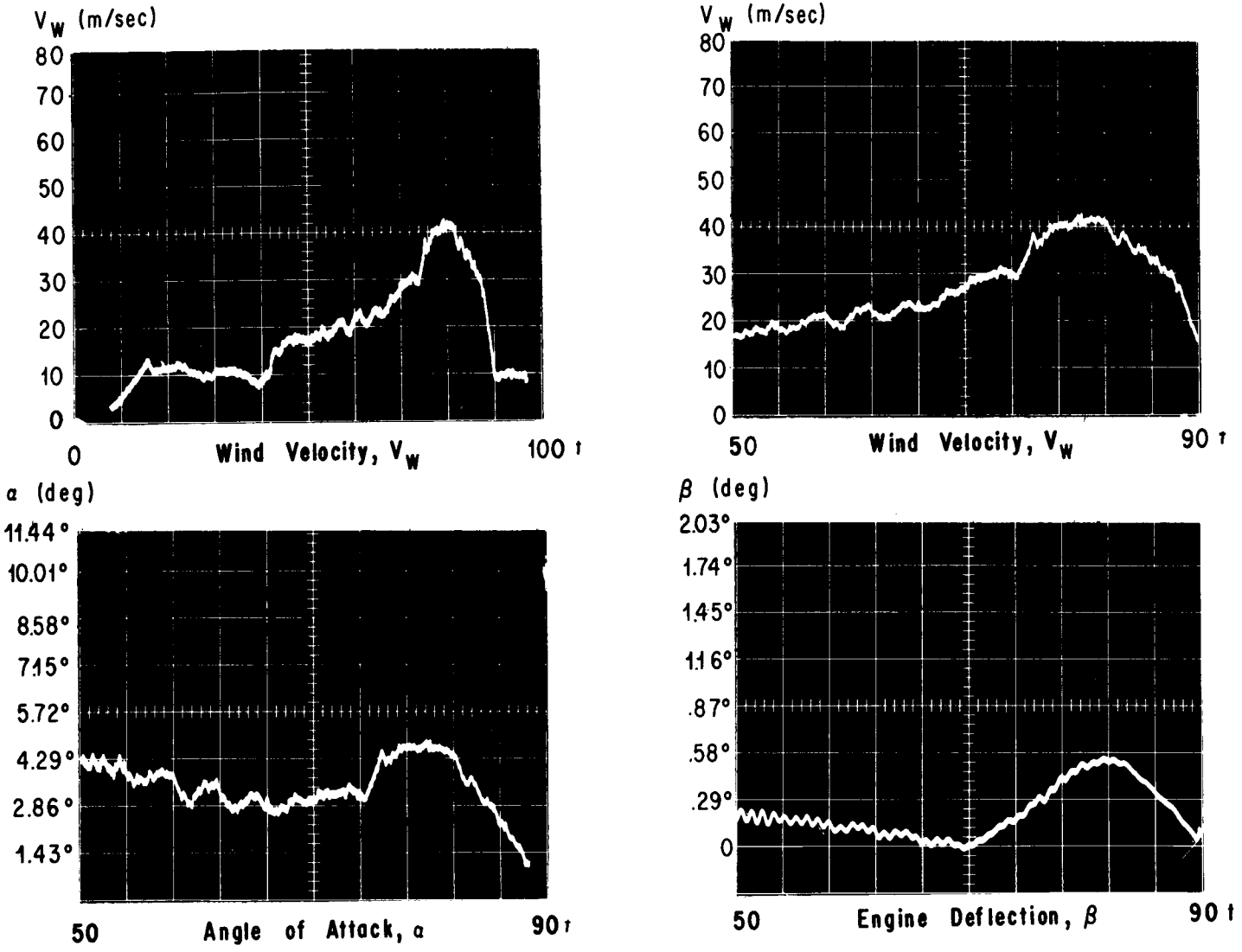

FIG. 31A. VEHICLE RESPONSE FOR WIND (2/16/65 AT 1:00 A.M.)

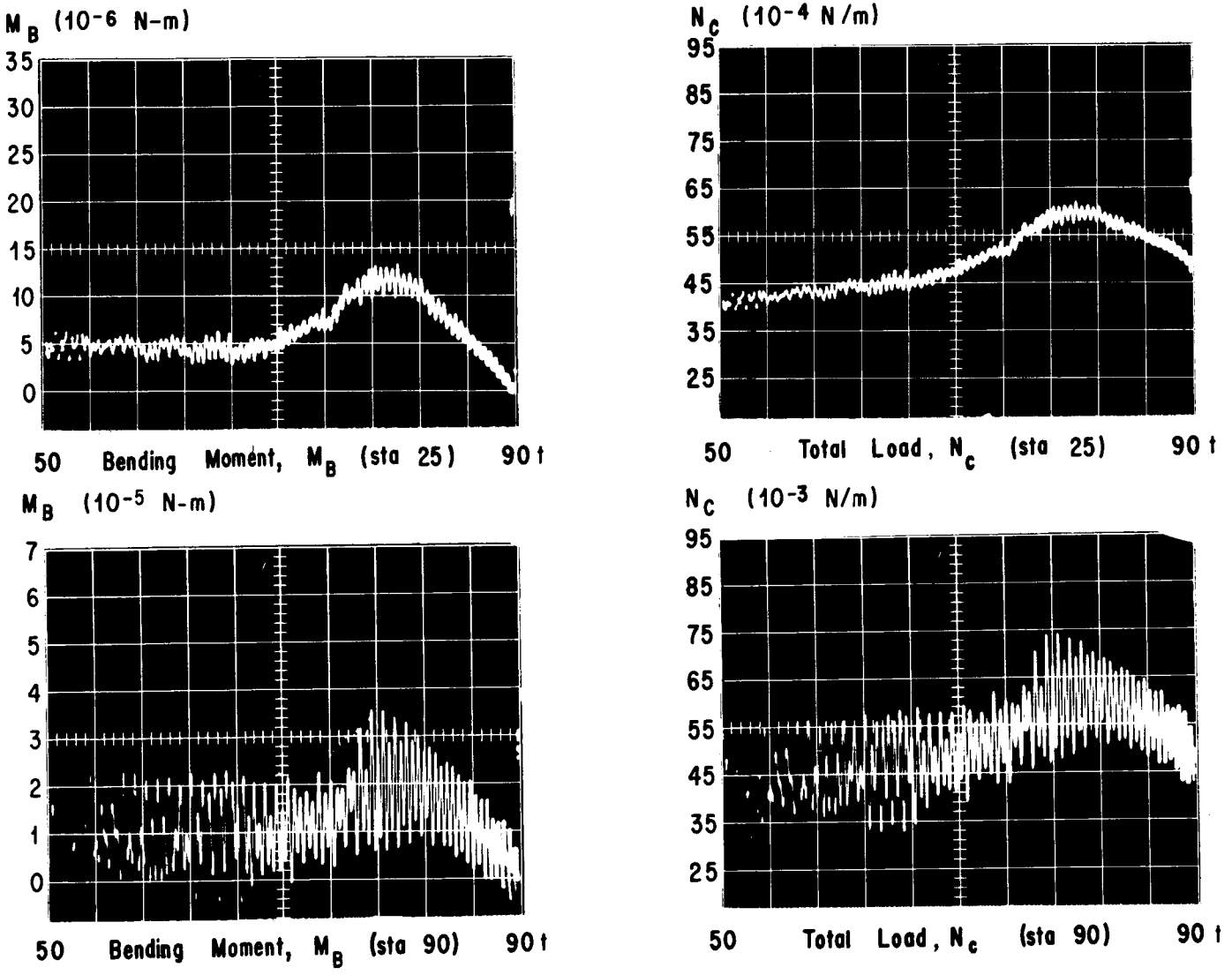

FIG. 32A. VEHICLE RESPONSE FOR WIND (2/16/65 AT 1:00 A.M.)

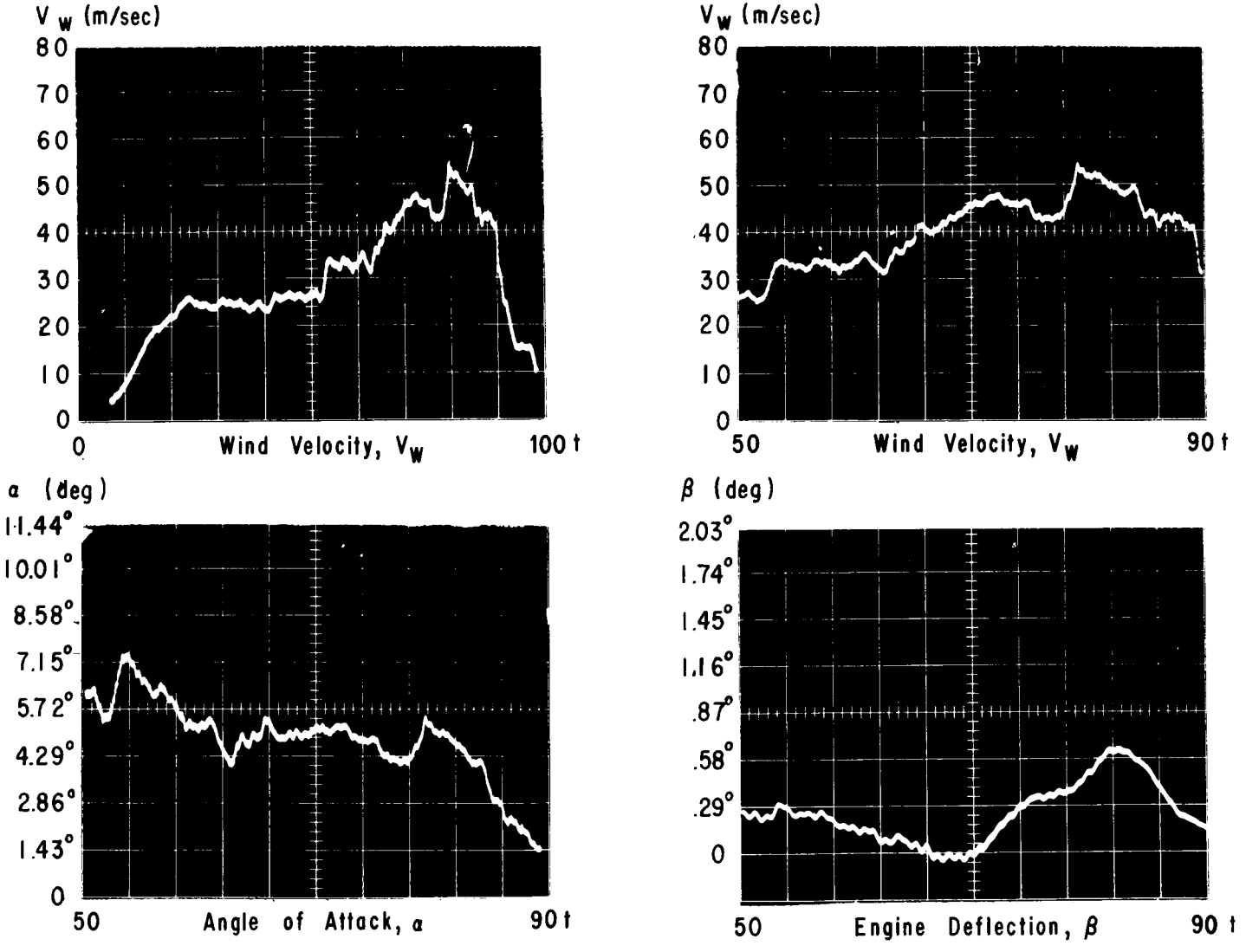

FIG. 33A. VEHICLE RESPONSE FOR WIND (2/25/65 AT 1:44 A.M.)

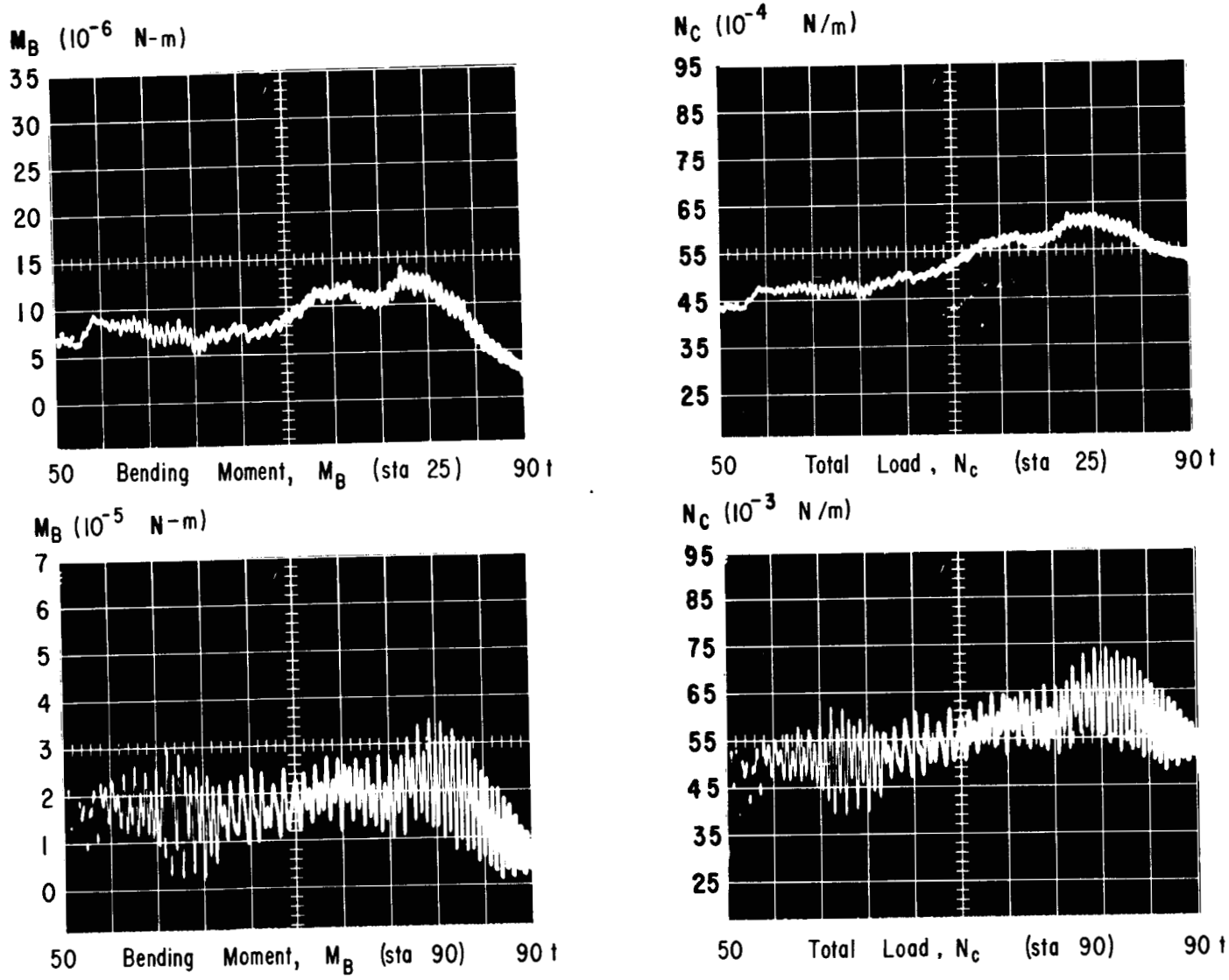

FIG. 34A. VEHICLE RESPONSE FOR WIND (2/25/65 AT 1:44 A.M.)

REFERENCES

1. Townsend, Don, "A Method for the Determination of Control Law Effect on Vehicle Bending Moment," NASA TM X-53077, July 2, 1964, MSFC, Huntsville, Alabama.

2. Scoggins, James R. and Michael Susko, "FPS-16 Radar/Jimsphere Wind Data Measured at the Eastern Test Range," NASA TM X-53290, MSFC, Huntsville, Alabama, 1965.

3. Eckström, Clinton V., "Theoretical Study and Engineering Development of Jimsphere Wind Sensor," Final Report, NASA Contract NAS8-11158, G. T. Schjeldahl Company, Northfield, Minnesota, July 1965.

4. Rogers, R. R. and H. G. Camitz, "Project Baldy, An Investigation of Aerodynamically Induced Balloon Motions," Final Report, NASA Contract NAS8-11140, Cornell Aeronautical Laboratory, Inc., Buffalo, New York, April 1965.

5. Scoggins, James R., "Spherical Balloon Wind Sensor Behavior," J. Appl. Meteor., 4, 1965.

6. Daniels, Glenn E., et al., "Terrestrial Environment (Climatic) Criteria Guidelines for Use in Space Vehicle Development, 1966 Revision," NASA TM X-53328, MSFC, 1966.

7. Ryan, Robert S. and Dieter Teuber, "A Practical Approach to the Optimization of the Saturn V Space Vehicle Control System Under Aerodynamic Loads," NASA TM X-53298, MSFC, July 21, 1965.

8. Lovingood, J. A., "A Technique for Including the Effects of Vehicle Parameter Variations in Wind Response Studies," NASA TM X-53042, May 1, 1964.

THE INFLUENTIAL ASPECTS OF ATMOSPHERIC DISTURBANCES ON SPACE VEHICLE DESIGN USING STATISTICAL APPROACHES FOR ANALYSIS

by Robert S. Ryan and Alberta W. King

The information in this report has been reviewed for security classification. Review of any information concerning Department of Defense or Atomic Energy Commission programs has been made by the MSFC Security Classification Officer. This report, in its entirety, has been determined to be unclassified.

This document has also been reviewed and approved for technical accuracy.

Helmut J. Horn
Chief, Dynamics and Flight Mechanics Division

E. D. Geissler
Director, Aero-Astrodynamics Laboratory

DISTRIBUTION

DIR

DEP-T

R-ASTR
- Dr. Haeussermann
- Mr. Hosenthien
- Mr. B. Moore
- Mr. Blackstone
- Mr. George
- Mr. Mink
- Mr. Clark
- Mr. Seltzer
- Mr. Fisher
- Mr. Nicaise

R-P&VE
- Dr. Lucas
- Mr. Showers
- Mr. Paul
- Mr. Wood
- Mr. Platt
- Mr. Kroll
- Mr. Swalley

R-COMP
- Dr. Hoelzer
- Mr. Lawrence
- Mr. Sutton
- Dr. Polstorff

R-AERO
- Dr. Geissler
- Mr. Horn
- Mr. Dahm
- Mr. Lindberg
- Mr. Baker
- Dr. McDonough
- Mr. Ryan (10)
- Mr. Rheinfurth
- Mr. T. Deaton
- Mr. Hagood
- Mr. Townsend
- Mr. Kiefling
- Mr. Swift
- Mr. Buchanan

R-AERO (Cont'd)
- Mr. Milner
- Mr. Hays
- Mr. Worley
- Mr. Pack
- Mr. Bugg
- Mr. Muller
- Mr. Papadopoulos
- Mr. Billups
- Mrs. King (20)
- Mr. Stone
- Dr. Krause
- Dr. Liu
- Dr. Scoggins
- Mr. W. Vaughan

MS-IP
MS-IL (8)
MS-H
I-RM-M
CC-P
MS-T (6)

Scientific and Technical Info. Facility (25)
P. O. Box 33
College Park, Md.
Attn: NASA Rep. (S-AK/RKT)

Chrysler Corp Space Div.
New Orleans/R. Wells

Boeing
Huntsville, Ala.
Attn: Mr. Haskell
Mr. Rowe

Chrysler (MICHOUD)
Attn: Mr. Wells

Lockheed
Huntsville, Ala.
Attn: Mr. Beiber